DALHOUSIE UNIVERSITY

Department of Earth Sciences
Halifax, Nova Scotia
Canada B3H 4R2
(902) 494-235

A CASE STUDY OF CHROMITE AND ASSOCIATED MINERALS AS INDICATORS OF DIAMOND PRESERVATION IN THE BOTSWANAN ORAPA KIMBERLITE CLUSTER

Eduardo Perez

SUBMITTED IN PARTIAL FULFILLMENT OF THE REQUIREMENTS FOR
THE DEGREE OF BACHELOR OF SCIENCES, HONOURS
DEPARTMENT OF EARTH SCIENCES
DALHOUSIE UNIVERSITY, HALIFAX, NOVA SCOTIA

April 2017

Distribution License

DalSpace requires agreement to this non-exclusive distribution license before your item can appear on DalSpace.

NON-EXCLUSIVE DISTRIBUTION LICENSE

You (the author(s) or copyright owner) grant to Dalhousie University the non-exclusive right to reproduce and distribute your submission worldwide in any medium.

You agree that Dalhousie University may, without changing the content, reformat the submission for the purpose of preservation.

You also agree that Dalhousie University may keep more than one copy of this submission for purposes of security, back-up and preservation.

You agree that the submission is your original work, and that you have the right to grant the rights contained in this license. You also agree that your submission does not, to the best of your knowledge, infringe upon anyone's copyright.

If the submission contains material for which you do not hold copyright, you agree that you have obtained the unrestricted permission of the copyright owner to grant Dalhousie University the rights required by this license, and that such third-party owned material is clearly identified and acknowledged within the text or content of the submission.

If the submission is based upon work that has been sponsored or supported by an agency or organization other than Dalhousie University, you assert that you have fulfilled any right of review or other obligations required by such contract or agreement.

Dalhousie University will clearly identify your name(s) as the author(s) or owner(s) of the submission, and will not make any alteration to the content of the files that you have submitted.

If you have questions regarding this license please contact the repository manager at dalspace@dal.ca.

Grant the distribution license by signing and dating below.

_____ _____

Name of signatory Date

DALHOUSIE UNIVERSITY

Department of Earth Sciences
Halifax, Nova Scotia
Canada B3H 4R2
(902) 494-2358

DATE: 28 April 2017

AUTHOR: Eduardo Perez

TITLE: A case study of chromite and associated minerals as indicators of diamond preservation in the botswanan orapa kimberlite cluster

Degree: B. Sc. Honours Earth Sciences Convocation: May Year: 2017

Permission is herewith granted to Dalhousie University to circulate and to have copied for non-commercial purposes, at its discretion, the above title upon the request of individuals or institutions.

Redacted for Privacy

Signature of Author

Abstract

Kimberlites are deep mantle magmas and the primary source of diamonds. Ilmenite, perovskite, rutile, titanite and spinel group minerals are commonly found in matrixes of kimberlites. Prior research shows that changes in temperature, volatile content, oxygen fugacity, and degrees of country rock assimilation influence what minerals are formed and the textures which are created. Similarly, these processes influence diamond preservation in kimberlites. Presence and abundance of chromite and ilmenite in kimberlites has been long known to correlate with diamond potential. However, the nature of this correlation is not yet understood. In this study we examine assemblages of oxide minerals in different kimberlite facies aiming to constrain crystallisation conditions and their effect on the diamond population.

Two kimberlite bodies positioned in the Botswanan Orapa kimberlite cluster were examined. The first of these kimberlites consists of a single coherent kimberlite pipe, AK-15. BK-1, the second and more complex body is composed of two distinct coherent facies, CK-A and CK-B, with differing origins as well as the volcanoclastic MVK facies. Sixty-seven samples, made up of the 4 kimberlite facies, were investigated using optical microscopy to observe the textures, zoning and phases present in each sample. Twelve thin sections, three from each kimberlite facies, were examined using scanning electron microscope (SEM) with Back Scatter Electron imaging, X-ray mapping and Energy Dispersive Spectroscopic analysis to confirm the presence and relationship between the minerals of interest. CK-A showed heavily altered Ilmenite with clear exsolution textures and reaction products made up of titaniferous magnetite, rutile, and titanite indicating high fluid content which fluctuated during crystallization. Minor chromite was present which also showed exsolution textures and was typically rimmed by titanite. Perovskite was not observed in CK-A implying high silica activity. CK-B contained ilmenite macrocrysts displaying exsolution lamella and typically rimmed by perovskite and titaniferous magnetite. Titanite was often found in microcrysts throughout the sample rimmed by perovskite. Abundant perovskite in the groundmass indicates much lower silica activity than in CK-A magma as well as a much lower fluid content. Chromite and rutile were not observed. In MVK Ilmenite macrocrysts showed exsolution textures and were rimmed by intergrown titaniferous magnetite, rutile and titanite. Chromite was found in low quantities and was heavily altered

and rimmed by titanite. This data is evidence for volatile exsolution and high silica activity possibly due to assimilation of crustal material. AK-15 contained ilmenite typically rimmed by titanite and titaniferous magnetite. Chromite was found throughout with alteration textures and titaniferous magnetite intergrowths. Rutile, perovskite and titanite were also found throughout. We propose that the observed difference in groundmass mineralogy between the four studied kimberlite lithology could be a result of difference in assimilation of crustal material, which would rise silica activity and trigger CO_2 degassing with exsolution of fluid. Absence of fluid in CK-B lithology would explain corrosive surface features and high degree of kimberlitic resorption on CK-B diamonds.

Keywords: kimberlite, chromite, ilmenite, perovskite, titanite, resorption

Table of Contents

Table of Figures

Acknowledgements

Thank you to my supervisor, Yana Fedortchouk. Without her continued guidance and expertise this project could not have been completed. Yana's passion for kimberlite research made the work fascinating and encouraged me to enthusiastically seek out further understanding of this research.

Many thanks to De Beers Group for providing the samples and reports on these kimberlites.

Thanks to Xiang Yang of the Saint Mary's University Electron Microscopy Centre and Daniel MacDonald of the Dalhousie University Robert M. MacKay Electron Microprobe Laboratory for their patience, willingness to teach, and thorough understanding of their labs equipment. Without their assistance, the data for this project would not have been collected.

Many thanks to Ryan Kressall, Rachel Milligan and the Experimental Igneous Petrology Laboratory for their assistance in understanding the morphological intricacies of kimberlites.

Thank you to Djordje Grujic for keeping the project on track and on schedule.

Introduction

Kimberlites are highly potassic ultramafic hybrid rocks which occur in cratons (Winter J. D., 2001). These rocks originate from magmas which are sourced from the deep mantle, and are rich in volatiles, leading to rapid rise of the melt from the mantel and a violent emplacement.

The goal of this study is to investigate how chromite and other oxide minerals can be used as indicators of variability in magmatic conditions, with the ultimate goal of identifying the potential effects of the processes on diamond preservation within diamondiferous kimberlites. In particular, these changes to temperature, volatile content, oxygen fugacity, and degrees of country rock assimilation will be considered with the diamondiferous Kimberlites within the Orapa cluster in northeastern Botswana in mind. Using existing information about the Orapa kimberlite cluster, in combination with other literature on kimberlites as a whole, the study aims to understand and identify characteristic kimberlite features within the various samples. A particular emphasis will understandably be placed on chromites within samples, but to a lesser extent a focus is to be placed on other kimberlite indicator minerals; namely Ilmenite, other Spinels (Magnetite), Hematite, Rutile, Titanite and Perovskite. Through the use of a range of analytical tools, significant features will be interpreted to validate the underlying geological processes and come to the conclusion of identifying the influence of these processes on the preservations of diamond within the kimberlite magma.

Chapter 1: Background

Role of Volatiles in emplacement of Kimberlite Magma

Volatiles play a significant role in the formation of kimberlites as their emplacement and characteristic cone shape (fig. 1) is typically controlled by their presence. Volatiles commonly account for more than 10%wt of melt (Smith, 1996). Volatiles in kimberlites predominantly consist of CO_2 and H_2O which are retained in the melt until emplacement at surface. This behaviour is relatively uncommon among igneous rocks. During crystallization, CO_2 is predominantly incorporated into deuteric carbonate while H_2O is incorporated into serpentine. Furthermore, while high mantle derived volatile content is common, the amount of volatiles present is highly variable; particularly with respect to CO_2. These variations in volatile content are controlled by a number of factors. Firstly, by the amount of volatiles in the original melt. Secondly, by variability in the amount of degassing during the melt's ascent and emplacement, meaning that as the kimberlitic melt is rising to surface, the decrease in pressure permits some of the volatiles in the melt to become gaseous. The rapidly expanding gasses causes the violent and expanding emplacement of the kimberlitic material. The third contributor of volatile variability in kimberlites are other magma interaction mechanisms such as fractionation, meaning crystalized material is separated from the parental melt, or filter pressing, whereby during crystallization a melt will become separated from the crystals as a result of pressure. And lastly, in the case of CO_2 as a result of contamination from carbon containing rocks such a limestone and dolomite. (Smith, 1996).

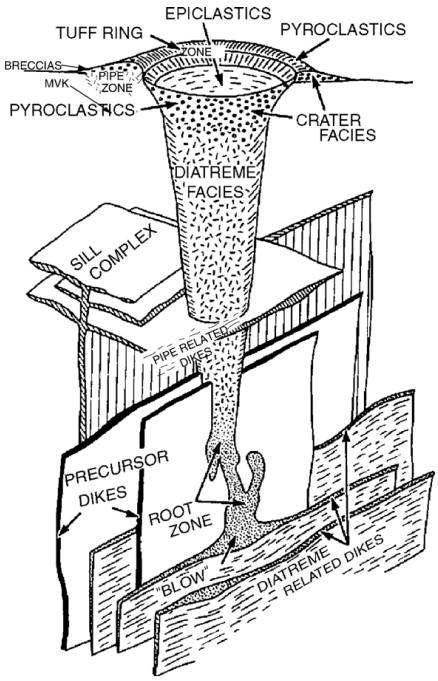

Figure 1. Kimberlite pipe morphology showing dikes and sill related intrusions as well as root zone located at base (Mitchell R. H., 1986).

A significant cause for the variation of kimberlite emplacement processes from other volcanic rocks is the high content of CO_2 and H_2O that remains within the magma on approach to the surface. Additionally, it has been shown that not only are there are typically high CO_2 values among the entirety of the formation but also that CO_2 is mobile. This is an indication that original CO_2 content is likely to be higher than indicated by whole rock analysis (Smith, 1996). Furthermore, Moussallam, Morizet, & Gaillard (2016), show that, due to the decrease in CO_2 solubility with decreasing pressure, major degassing events occur at shallow pressure of about 100MPa in low silicate melts such as kimberlites. Furthermore, the effect of pressure on CO_2 solubility is a strong function of composition with low silica melts retaining a large proportion of their dissolved CO_2 until an abrupt degassing event occurs whereas more silica rich melts show a much more linear relationship between CO_2 degassing and pressure changes. Moussallam, Morizet, & Gaillard go on to suggest that this behaviour is the cause of kimberlites characteristic form (fig. 1) as degassing would lead to strong acceleration of ascending magma which in turn exsolves more CO_2, thereby creating the cone shape (2016). These changes are associated with causing the variation among different kimberlite facies (Smith, 1996).

Chromites as a petrological indicator (Spinel)

Chromite and other spinel group minerals are widely used in the field of petrology, particularly within ultramafic rocks, as indicator minerals. Spinels crystalize over a wide variety of pressure, temperature and compositional conditions and so occur commonly in a wide range of mafic and ultramafic terrestrial rocks. Furthermore, some of the first spinel phases to crystalize from melt are chromites. This, in combination with the mineral's wide solid solution range and resistance to alteration processes relative to other common minerals, make it a useful tool for provenance studies and exploring changes in magmatic systems during the crystallisation (Barnes & Roeder, 2001). Generally, the crystallization spinel crystallization sequence will begin with Chromite crystalizing at higher temperatures with magnetite, ilmenite and titanite following as temperatures decrease. (Railsback, 2006)

Variability in Spinel composition results from varying igneous processes, and in certain instances also metamorphic processes which alter whole rock as well as spinel specific composition from ultimately primitive mantle derived magmas. These primitive, mantel derived magmas are characteristically composed of a mineralogical make up of chromium rich and magnesium rich chromites of which kimberlites are an example (Barnes & Roeder, 2001). However, it is common for chromite to display some extent of re-equilibration as a result of extended cooling periods and metamorphism. Barnes and Roeder outline a variety of geochemical trends including, the Cr-Al trend, the Fe-Ti trend as well as the kimberlitic trend as being indicators of processes occurring in Spinels contained within kimberlites (Barnes & Roeder, 2001).

The Cr-Al trend corresponds to variable Cr/(Cr+Al) proportions with low $Fe^{2+}/(Mg+Fe^{2+})$, Fe^{3+} and TiO_2 concentrations, furthermore, Cr/(Cr+Al) tends to increase with $Fe^{2+}/(Mg+Fe^{2+})$. This is as a result of the spinel equilibrating with olivine of constant temperature and composition (Barnes & Roeder, 2001).

The Fe-Ti trend corresponds to increasing Fe^{3+} and $Fe^{2+}/(Mg+Fe^{2+})$, and typically TiO_2. This behaviour reflects the evolution of spinel compositions during fractional crystallization of olivine or pyroxene from host magma, which will increase the Fe/Mg ration as well as the Ti content within the melt. Variations in $Fe^{2+}/(Mg+Fe^{2+})$ are attributed to two causes; changes in melt compositions throughout crystallization, as well as the exchange of Fe^{2+} and Mg between spinel and surrounding silicates (Barnes & Roeder, 2001).

Barnes and Roeder outline a kimberlite trend which summarizes the compositional changes which the rock's spinels are undergoing within a kimberlitic magma as crystallization occurs (2001). The trend is categorised by increasing Fe^{3+} and TiO_2 while Cr/(Cr+Al) remains constant, furthermore this trend varies from the Fe-Ti trend outlined by the researchers in that $Fe^{2+}/(Mg+Fe^{2+})$ concentrations remain relatively constant for all but large concentrations of Fe^{3+}. These results are caused by the tendency for kimberlitic magmas to contain high Fe^{3+}/Fe^{2+}; the resulting increase in Ti is attributed to the propensity for Ti to become incorporated into Spinels with higher magnetite contents (Barnes & Roeder, 2001).

Due to the violent nature of kimberlitic ascension and emplacement processes, kimberlite characteristics are somewhat contingent on the mantle and lower crustal material which the eruptions sample. Therefore, the spinel composition of kimberlite xenoliths is an important aspect of kimberlite research. In general kimberlite xenoliths show a strong Cr-Al trend displaying high pressure Mg-Al spinel, extending to low Fe^{3+} chromites; this tendency can be explained as a high to low pressure trend resulting from Al exchange with surrounding pyroxenes (Barnes & Roeder, 2001). Furthermore, low Cr/(Cr+Al) may be found in some samples and is attributed to the reaction whereby subsolidus equilibration of clinopyroxene-spinel occurs resulting in aluminous spinel (Barnes & Roeder, 2001). Another important characteristic of xenoliths in kimberlites, particularly from an economic geology perspective is the presence of high Chromium chromites, as they are associated with diamonds. These chromites, which historically have been found as inclusions in diamonds, have notably high Cr/(Cr+Al) content, low Fe^{3+} and low TiO_2. This characteristic composition is attributed to equilibration with Cr-garnets at high pressure (Barnes & Roeder, 2001).

Oxidation of spinels in kimberlites is commonly observed and is believed to result from volatile evolution mechanisms and oxidation once the melt is introduced into the crust. Alternatively, the oxidation may be attributed to the effect that alkalis have on the ferric/ferrous iron ratios of basic melts, leading to higher ferric iron content (Barnes & Roeder, 2001).

Kimberlite Mineralogy

Kimberlite mineralogy reflects the process of rapidly changing crystallization conditions reflecting the movement of the melt from upper mantle through to the upper crust (Mitchell R. H., 1986). This is further complicated by the addition of crustal interaction predominantly in the form of mantle derived xenocrysts. This process begins crystallization of olivines and spinels at close to 1200°C and continues to below 600°C where hydrous and carbonatitic minerals crystalize (Roeder & Schulze, 2008).

Ilmenite [$(Fe,Mg,Mn,Ti)O_3$]

Ilmenite, particularly the magnesian variety is generally found in kimberlites. While commonly used as a Kimberlite Indicator Mineral, ilmenite content can vary widely from kimberlite to kimberlite, from different facies of a kimberlite complex, and even within different areas of the same kimberlite (Mitchell R. H., 1986). Furthermore, kimberlitic ilmenites show a wide range of paragenetic forms.

Macrocrysts:

Ilmenite may be found as rounded macrocrysts typically coated with perovskite and leucoxene, an alteration product composes of titanium dioxide (predominantly rutile and anatase phases) (Mitchell R. H., 1986). Large macrocrysts grains tend to become fragmented and heavily altered by perovskite and spinel reactions, as such it is difficult to definitively distinguish from groundmass ilmenite. Additionally, macrocryst ilmenite textures vary considerably and include banded, porphyroclastic and granoblastic textures. Porphyroclastic examples typically exhibit rimming by spinel group minerals such as magnetite which are interpreted as resulting from high temperature deformation, crystallization and annealing (Mitchell R. H., 1973). Mitchell states that these styles of ilmenites form a solid solution

between ilmenite ($FeTi0_3$), geikielite ($MgTi0_3$), and hematite (Fe_20_3) (1986). Compositional variability is common in macrocryst ilmenite and if occurring within a single kimberlite can occur when compositionally zoned ilmenite cumulates become fragmented and subsequently undergo random mixing during transport (Mitchell R. H., 1986). Furthermore, several trends are regularly observed within this variety of ilmenite; the magmatic trend of increasing MgO and Cr_2O_3 in combination with decreasing or constant Fe_2O and the Kimberlite reaction which is less common. The magmatic trend reflects the process whereby ilmenite macrocrysts attempt to equilibrate with newly introduced melt as the composition is similar to that of ilmenite found in groundmass. The magmatic magnesium trend appears to result from a reaction caused by a decrease in pressure, which results in a decrease in oxygen fugacity which ultimately decreases Fe_2O_3 content of the rim (Mitchell R. H., 1986). Another trend, opposite to the magnesium enrichment trend, called the Manganese-Enrichment trend which is characterized by increasing MnO and FeO, and decreasing Fe203 and MgO relative to the core of the grain. This trend is attributed to commencement of carbonate immiscibility late in the crystallization of kimberlitic magma.

Intergrowth relations:

Occurrences of ilmenite within kimberlites commonly manifest themselves in various manifestations and with varying textural elements along with other minerals. One such instance is the ilmenite-clinopyroxene lamellar intergrowths. These ilmenite intergrowths generally trend in a single orientation intersecting pyroxene at 60 and 120 degrees with a typically graphic intergrown texture (Mitchell R. H., 1986). Additionally, their composition tends to be more magnesium rich, similar to that of magnesium rich macrocrysts.

Ilmenites are fairly common within the groundmass of kimberlites, these grains tend to be anhedral, monocrystalline, and zonation free. It is also typical to find these grains in complexes, intergrown and/or rimmed by perovskite and spinel, as well as included within macrocrysts of olivine and phlogopite. An important note is that, generally, groundmass ilmenite composition and the composition of ilmenite rims tend to be very similar (fig. 2) which indicates the occurrence of equilibration processes between melt and macrocrystal ilmenite.

Figure 2 also shows how ilmenite inclusions in olivine exhibit similarities in composition to the iron enriched groundmass examples. This is indicative of early ilmenite crystallization where Mg would be preferentially incorporated into olivine. In contrast in the later stages of crystallization magnesium rich ilmenites would become more common as crystallization of olivine comes to a stop.

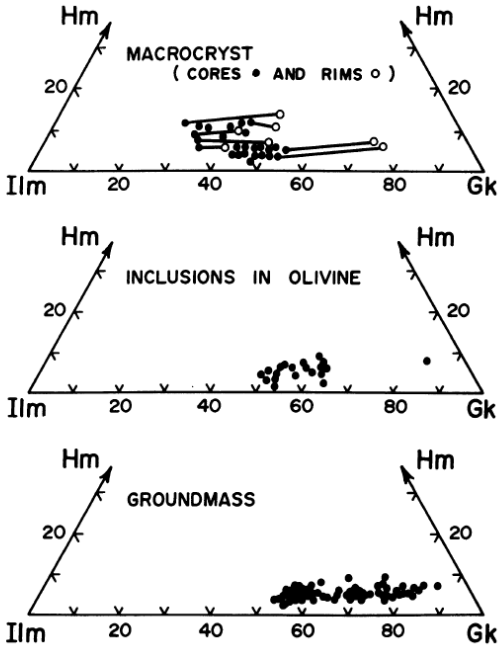

Figure 2. Variability in Ilmenite composition based on crystallization stage (Mitchell R. H., 1986).

Similar to the ilmenite-pyroxene intergrowths, ilmenite-spinel intergrowths are also quite common in kimberlite suites. These rod like lamellar inclusions of spinel are largely parallel to the ilmenite macrocrysts they occur in. Furthermore, the fringes of these ilmenite grains tend to contain abundant spinel grains. This reaction is widely attributed to a combination of changes in temperature and oxygen fugacity. Whereby a decrease in either of these parameters results in a sub-solidus reaction which causes a homogenous ilmenite macrocryst to exsolve spinel minerals of which titanian chromites and aluminous magnesian ulvospinel-magnetites commonly appear. Mitchell states that the composition of both original ilmenite macrocrysts and the exsolved spinel constituents are fairly variable. Furthermore, there are other forms of spinel ilmenite intergrowths which do not result form subsolidus reduction. Instead, this mineralization pattern results from unstable oxygen fugacities which in

turn change the bulk composition of the magma shifting to and from the ilmenite decomposition loop as seen in figure 3.

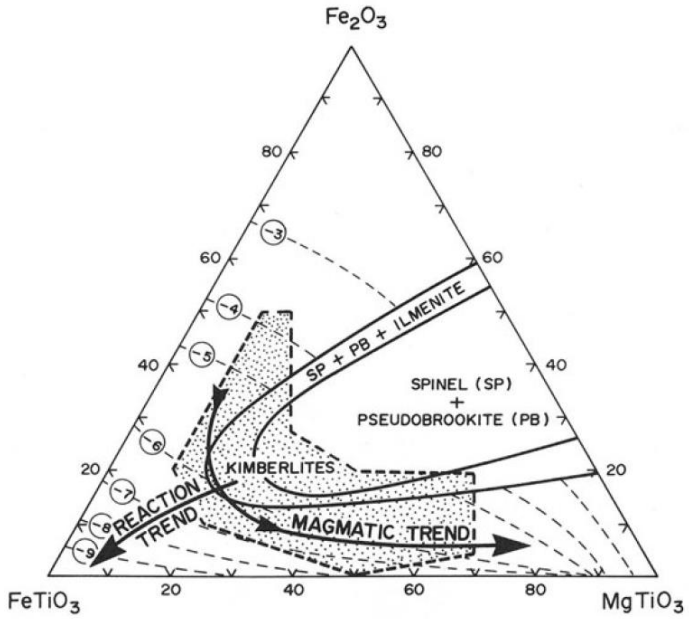

Figure 3. Relationship between spinel end member composition. Dashed lines indicate contours of oxygen fugacity at 1300 degrees Celsius (Mitchell R. H., 1986).

A similar but distinct lamellar interaction is observed by Cr enriched ilmenite macrocrysts containing lamellar segregations of Cr-spinels and Cr-rutile. The presence of rutile suggests that these phases result from the disintegration of Cr rich titanite and would form at higher temperature and lower oxygen fugacity values than the that of the ilmenite spinel interactions.

Silica activity and oxygen fugacity of kimberlite magmas

The association between the minerals observed in a sample and the implications this has for conditions during crystallization is significant. Broadly speaking, the type of mineralization which is to occur is dependent on the pressure, temperature and composition of the melt during crystallization. However, in reality this is a complex reaction involving several different considerations. One such parameter is oxygen fugacity which in chemical thermodynamics is used to better approximate the chemical potential of a real gas. This

parameter is typically constrained by considering mineral assemblages as buffers in the crystallization reaction with respect to temperature (Lindsley, 1991). More simply the oxygen fugacity describes the willingness for oxygen within the melt to become incorporated into a certain phase. Another important parameter in kimberlite petrology is the silica activity which describes the proportion of silica with respect to the melt. Variations in these parameters result in differences in the type of mineralization which occurs. Therefore, by evaluating the connection between different minerals in a sample it is possible to make inferences about the state of the system throughout the crystallization period.

One method for doing this involves studying the interaction of Fe-Ti oxides. The relationship between Fe-Ti oxides has been extensively studied and analyses involving these minerals are commonly used to understand rock forming conditions, particularly those pertaining to geothermometry and geobarometry (Lepage, 2003). Understanding the phase-equilibrium conditions within the FeO-Fe_2O_3-TiO_2 system allows for the calculation of geothermometry and oxygenbarometry parameters. This thermometer and oxygen barometer system is based on the composition of hematite and magnetite. Hematite forms a solid solution into ilmenite, and magnetite forms a solid solution into ulvospinel as seen in figure 4, which describes the phases present in the FeO-Fe_2O_3-TiO_2 system. The composition of these solid solutions in mutual equilibrium is dependent on both temperature and oxygen fugacity (Buddington & Lindsley, 1964). Therefore, if the compositions of the ilmenite-hematite ($FeTiO_3$-Fe_2O_3) and ulvospinel-magnetite (Fe_2TiO_4-Fe_3O_4) minerals is known, it is possible to determine the temperature and oxygen fugacity parameters. Moreover, if compositions are known quantitatively, these parameters can be calculated with certainty. However even if this information is not known for a set of samples, it is possible to estimate these parameters in relative terms and deduce which kimberlite facies have more oxidizing conditions and which facies have more oxidizing conditions.

Data gathered experimentally indicates that the solubility of ilmenite in magnetite is not significant. Furthermore, Ilmenite ($FeTiO_3$) occurrences in the form of lamellar structures in magnetite-ilmenite intergrowths are thought to result from the subsolidus oxidation of ulvospinel (Fe_2TiO_4) in the magnetite-ulvospinel solid solution. This indicates that exsolution into lamellar ilmenite is simultaneous with the oxidation of ulvospinel (Fe_2TiO_4).

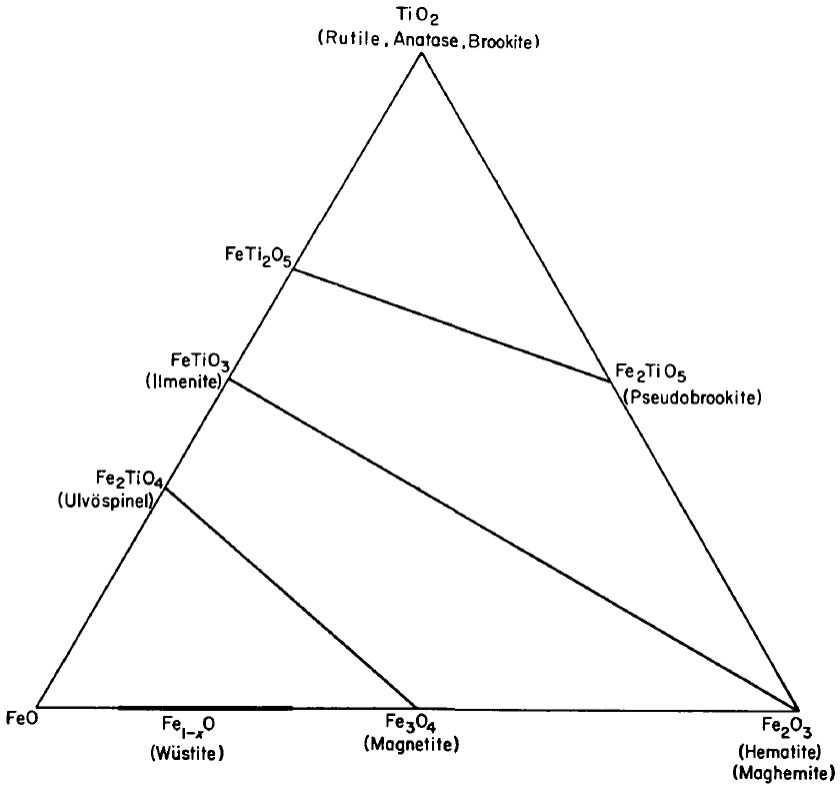

Figure 4. Major solid solution series of the FeO-Fe_2O_3-TiO_2 system between magnetite-ulvospinel and hematite-ilmenite (Buddington & Lindsley, 1964)

Estimates of fO2 and SiO2 activity in kimberlite magma have been well constrained. Using the thermal effects associated with the intrusion of kimberlites the temperature and pressure at the time of groundmass crystallization can be estimated. By associating the intrusion of kimberlite deposits into other bodies such as coal, hydrocarbon reservoirs and salt deposits temperature at the time of emplacement has been roughly constrained to 600 degrees centigrade. (Mitchell R. , 1973). Furthermore, studies on fluidization in kimberlites have demonstrated a depth of emplacement of typical kimberlites to be around 2km, with this in

mind, taking the average crustal density the load pressure can be accounted for as well as any additional affects put in place by retained fluid. Furthermore, silica activity can be used to determine oxygen fugacity parameters if the iron-titanium oxide geo-barometer cannot be used. Therefore, the perovskite-titanite buffer can be used to estimate the maximum silica activity in the kimberlite groundmass. With the diopside-akermanite buffer used to derive and estimate of the minimum activity of silica. With this in mind, silica activity at typical kimberlitic conditions (600 degrees Celsius and 0.5kb) is constrained to within $10^{-1.63}$ and $10^{-2.41}$ (Mitchell R. , 1973). These low values of silica activity accentuate the silica under saturated nature of kimberlite magmas. Next, by using the silica activity of the fluid which formed the groundmass the oxygen fugacity of the groundmass forming fluid can be computed using the quartz-magnetite-fayalite buffer. At a pressure of 0.5kb and 600 degrees Celsius oxygen fugacity of kimberlite groundmass has been constrained to between $10^{-18.79}$ $10^{-21.11}$. In a similar way, silica activity and oxygen fugacity can be calculated at the diamond formation stage using various buffer reactions and making a set of assumptions. These assume that the magma is oxidized to a point that pure magnetite is stable in order to constrain maximum oxygen fugacity. Secondly it is assumed that the magma is so reduced that metallic iron is stable which allows for the derivation of the minimum limit of oxygen fugacity. These relatively low oxygen fugacity values demonstrate the tendency for kimberlite magmas to be highly reduced. (Mitchell R. , 1973)

Chapter 2: Geological Setting

Botswanan geology, particularly in the northeast of the country, is dominated by basement rocks of Archean age (Schluter, 2006). These Archean rocks are made up of the Lobatase and lower Transvaal group to the west as well as the Zimbabwe Craton to the east. The Zimbabwe Craton is lithologically similar to the Kapvaal Craton but varies in its structure and geological history. These cratons are constructed of complex assemblages and include a varied array of lithologies such as migmatites, porphyric granites, metasedimentary rocks, amphibolites, meta-intrusive rocks, gabbroic anorthosites and gneissic granites. The Paleoproterozoic Limpopo Belt is also located in northeastern Botswana and can be seen in figure 5 (Schluter, 2006). These belts are overlain by the Karoo super group which young to the west of the country. The Karoo Supergroup was deposited within the Kalahari basin and have been interpreted to represent the breakup of Gondwana (Schluter, 2006).

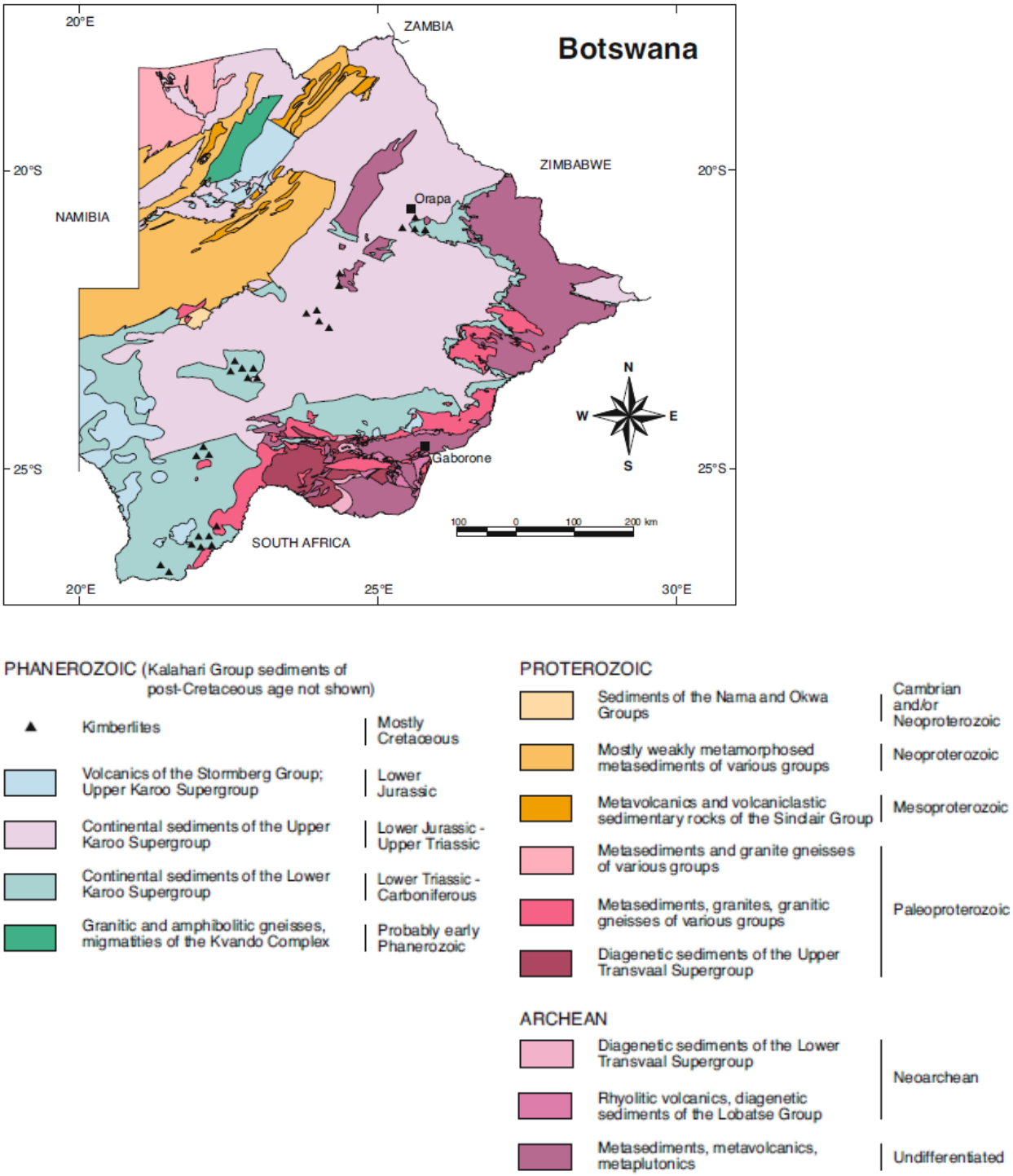

Figure 5. Geological Map of Botswana (Schluter, 2006)

Kimberlite suites occur relatively frequently in Botswana and over 200 Kimberlites have been discovered in the nation. These kimberlites are most commonly cretaceous in age. The BK01 and AK15 kimberlites follow this tendency and belong to the cretaceous Orapa kimberlite cluster, which is emplaced between the Archean Zimbabwe craton and the Limpopo Belt. These Archean basement rocks are overlain by the Karoo Supergroup which, in the Orapa area, is comprised of siliciclastic siltstones and mudstones of the Mosolotsane Formation belonging to the Lebung Group. The Mosolotsane is overlain by the calcareous Aeolian sandstones of the Ntane formation which also belongs to the Lebung Group. The area is then overlain by the Stromberg formation's amygdaloidal basalts; however, these deposits are very thin at the BK01 kimberlite. So much so that the kimberlite pipe is essentially exposed with only a thin calcrete cover. The AK15 kimberlite is partially overlain by tholeiitic basaltic deposits and up to 50m in thickness (Simelane, 2012).

Diamond data and petrography of AK-15 and BK-01 kimberlites

BK-01 Kimberlite

The BK-01 kimberlite consists of four distinct kimberlite facies. These are outlined in table 1 however only samples from the CK-A, CK-B and MVK facies were provided for the study and as such these were the only facies examined. The BK-01 kimberlite contains 2 separate lobes, the coherent CK-B kimberlite to north and, another coherent body, CK-A to the south. These kimberlite pipes are spanned by a volcanoclastic facies, MVK, which is similar to CK-A in the composition of its chromite as well as the style of diamond resorption (Figure 6).

Table 1. Classification scheme used for the BK1 kimberlite complex

BK-1 Lithological Classification		
Facies Classification	Facies Sub-classification	Description
CK-A	CK-A	Coherent Kimberlite
	CKA-CRB	CK-A and Ntane sandstone contact breccia
CK-B	CK-B	Coherent Kimberlite
	CK-B_a	Altered CK-B
RVK-A		Resedimented Volcanoclastic, large basalt xenoliths, high basalt dissolution
MVK	MVK	Massive volcanoclastic Kimberlite
	MVK-CRB	MVK and Ntane sandstone contact breccia

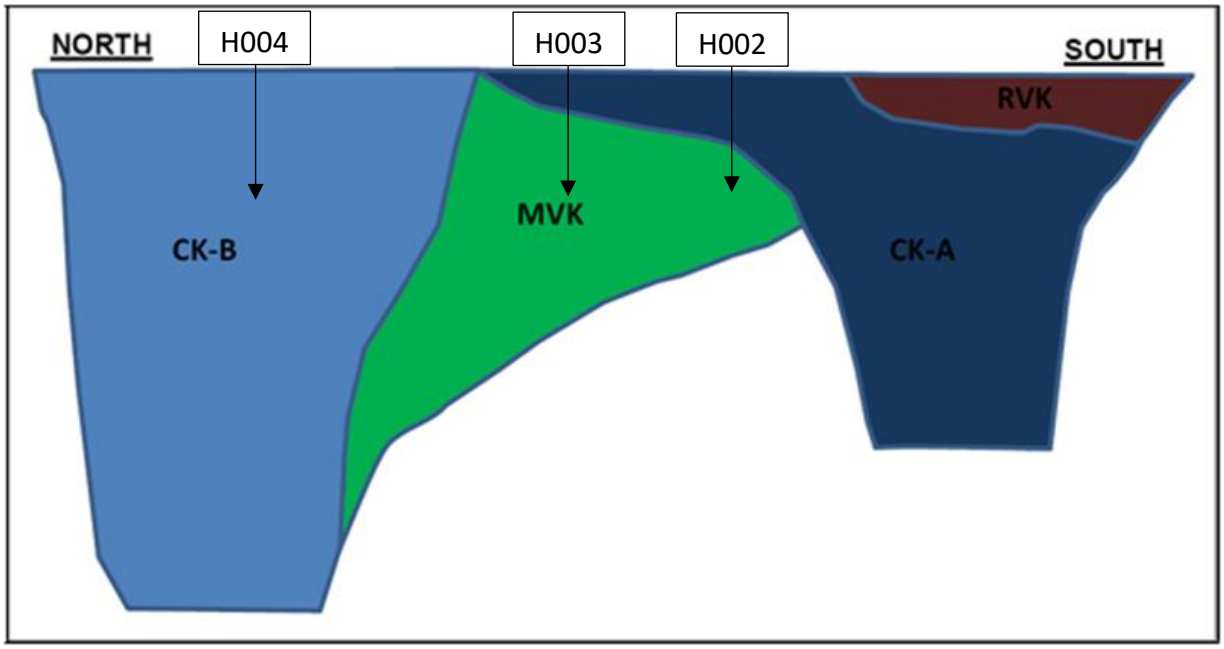

Figure 6. Cross sectional model of the BK1 kimberlite pipe outlining approximate borehole locations (Simelane, 2012)

Ingrid Chinn indicates that data collected from groundmass spinel show significant petrographic differences between the CK-B facies and the CK-A and MVK facies, this can be attributed to differing origins which is supported by the data collected from geophysical surveys (Chinn, BK1 Kimberlite notes for Yana, 2013). In contrast, CK-A and MVK show very similar groundmass spinel data, which is an indication that the two facies are cogenitic. Therefore, the BK-1 kimberlite appears to be a kimberlite complex made up of two different superimposed

kimberlite pipes with at least two independent feeder dike systems. Moreover, this is supported by geophysical data which indicates that there is a body of massive material, likely CK-A, to the south of the known kimberlite (CK-B) are two massive bodies (Winter, Henning, & Munyawiri, 2012).

MVK diamonds show resorption features which are indicative that resorption occurred in the presence of fluid. This is to be expected as, being a pyroclastic kimberlite, the melt would have had a high fluid content in order to produce a sufficiently violent emplacement to fragment the rock (Kopylova, 2016).

Petrography

The CK-A kimberlite has a predominantly segregationary texture, with local development of magmaclasts. Furthermore, extensive serpentine segregations were identified which are identified by their irregular and wormy shape. Olivine has mostly been replaced by carbonate and serpentine. These olivine macrocrysts now show a carbonate or serpentine core with a rim of serpentine around the entirety of grains. Groundmass mineralogy is made up of predominantly serpentine as well as spinel and carbonate. Lastly, several veins cut through the kimberlite and are filled with a combination of talc, carbonate and serpentine. (Kopylova, 2016)

The CK-B kimberlite facies is made up of a high proportion of olivine macrocrysts. These grains show alterations to serpentine with the smaller grains being completely serpentinized and the large grains only showing partial alteration. Furthermore, these facies show a small proportion of crustal xenoliths interpreted to have originate from the karoo basalts. These can be identified as areas of groundmass containing serpentine but no groundmass spinel. Within this facies the groundmass is made up of mostly serpentine with smaller proportions of carbonate, phlogopite, perovskite and spinel.

The MVK facies shows features consistent with a kimberley type pyroclastic kimberlite. Samples show segregational textures which vary into kimberly pyroclastic textures. Samples show small oval magmaclasts as well as serpentinized olivines, with ilmenite macrocryst also present. Magmaclasts display serpentine cores with clinopyroxene rims. Clinopyroxene is fairly

abundant within this facies and the mineral is commonly observed mantling xenoliths. (Kopylova, 2016)

AK-15 Kimberlite

The same diamond resorption features found in the CK-B facies are also present within the magmatic AK15 kimberlite. This is somewhat unexpected as high fluid content is associated with pyroclastic kimberlites and not the magmatic variety. However, this could result from the kimberlite being much larger and much more eroded in such a way that the samples were exclusively taken from the root zone of the kimberlite. In effect this would mean that the AK15 kimberlite would be positioned higher relative to the BK-01 kimberlite (Chinn, AK15 Kimberlite notes for Yana, 2013).

Petrography

The AK15 kimberlite shows substantial influence from crustal material. Samples are composed of predominantly olivine and phlogopite macrocrysts. The smaller olivine grains tend to be angular/euhedral, furthermore all olivine grains show nearly complete replacement by serpentine. Similarly to the BK01 kimberlite, this kimberlite shows a segregationary texture and a groundmass mineralogy made up of mostly serpentine with a smaller proportion of phlogopite and carbonate. Other, less abundant groundmass constituents include clinopyroxene, spinel and perovskite. Lastly, in some instances remnants of the karoo basalt can be observed in the form of assimilated xenoliths. These xenoliths are typically accompanied with clinopyroxene coronas. (Kopylova, 2016)

Chapter 3: Methods

Approach of this study

The aim of this study is to investigate how various Fe & Ti oxides (spinel and rhombohedral oxides) among other minerals can be used as an indicator of diamond preservation in Diamondiferous Kimberlites. Therefore, it is essential to first accurately recognize and correctly interpret mineral grains and related petrographic features. This is to be completed primarily using the petrographic microscope, the scanning electron microscope and wavelength dispersive spectroscopy on the electron microprobe analyzer. Firstly, the samples were all thoroughly inspected under both reflected and cross polarized light in order to get an understanding of the general petrography. Subsequently, the samples were analyzed from a depth perspective in order to identify any gradational trends resulting from samples proximity to other facies. With these factors in mind, the opaque minerals were analyzed under reflected light in an attempt to identify unaltered chromite grains of sufficient size (in the order of 1mm - 0.1 mm). Next, 12 samples were selected out of the 67 provided which were identified as being representative of the four respective facies as a whole, while maintaining a range of samples coming from across as many varied sampling depths as possible. Depth to borehole information for the set of samples was not complete however available information (figure 7) was correlated with sample information to provide approximate distribution of samples with depth and distance from contacts.

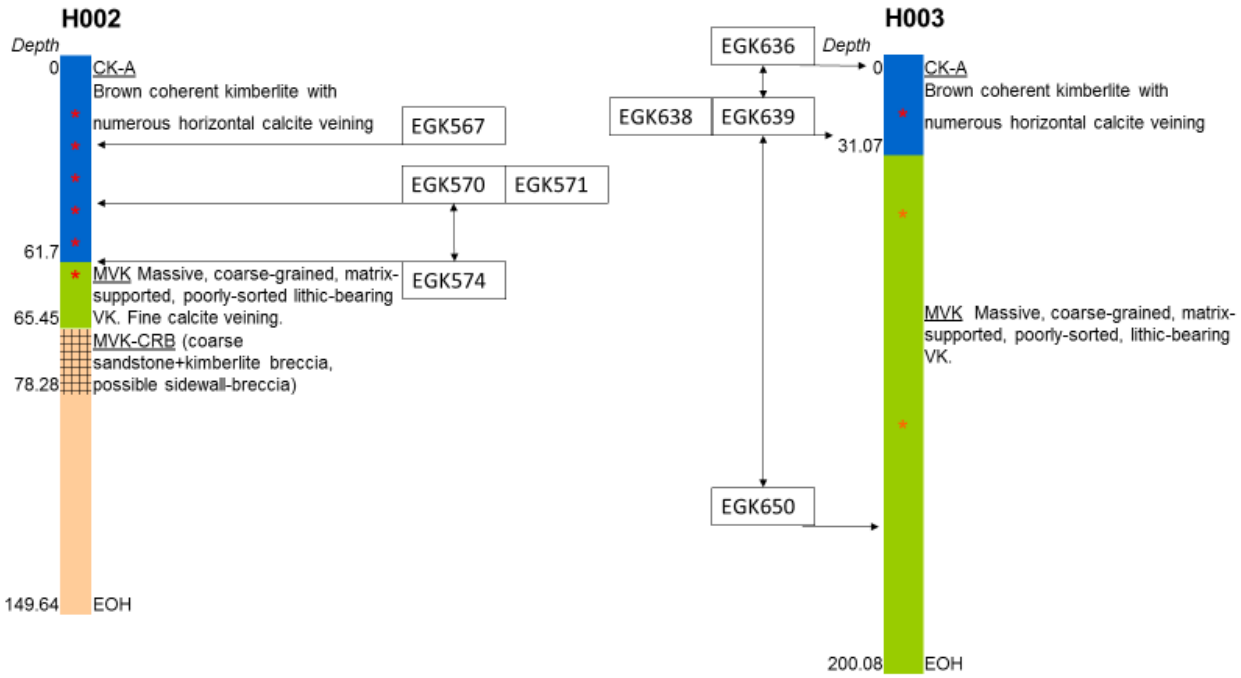

Legend	
	CK-A = Grey, inequigranular, massive, macrocrystic coherent kimberlite contains completely metasomatised country-rock. Comprises coarse, macrocrystic and megacrystic olivine. Traversed by numerous horizontal calcite veins. Found in H001, 002 and 003
	MVK = Massive, poorly-sorted, matrix-supported, coarse-grained volcaniclasitc kimberlite. Found over a short interval in H002 below CK-A and to greater depth in H003.
	MVK-CRB = Coarse breccia made up of sandstone and kimberlite. Poorly-preserved.

Figure 7. BK01 boreholes H002 and H003 showing sample depth information,with red dots outlining aproximate location of samples studied under SEM.

With a representative subset of samples, an SEM analysis of 15 samples was conducted to validate the composition of the opaque minerals identified during the microscopic analysis and study replacement assemblages and textures. During this analysis and emphasis was placed on identifying chromite and ilmenite macrocrysts, oxide inclusions within olivine, as well a groundmass composition. Other minerals analyzed were magnetite, rutile, perovskite and titanite. The presence, relative abundance, relative stability and any interactions with other surrounding minerals were noted with respect to these minerals. In addition to this, textural variations across samples were noted, while paying close attention to alterations, stability of different phases, as well as intergrowth and zoning features. Furthermore, any down section variation across the same kimberlite facies was noted. Lastly, in four instances, one for each

kimberlite facies, an element mapping analysis was taken in order to provide information on the compositional variation of the groundmass of the samples. Next, the samples underwent a microprobe analysis. The Ilmenite, chromite and oxide inclusions in olivine were analyzed. If grains were of sufficient size and showed some form of zoning, multiple point analyses were taken. Otherwise, only one compositional analysis was recorded.

SEM method

The Scanning Electron Microscope (SEM) is commonly used tool for providing highly magnified and highly resolved images of the surface analyzed. The SEM method uses a focused beam of electrons aimed at the sample to generate signals termed electron-sample interactions. These signals are the product of collisions between the electrons and sample which excites the electrons contained within the sample being imaged. This results in the samples electrons dropping into a lower energy state which results in the release of secondary electrons which are then read by the different detector tools that make up the SEM system (Swapp, 2013). The energy/electrons emitted during a collision is proportional to the atomic number of the elements present. Therefore, heavier elements will release more electrons and therefore appear to be brighter in a BSE image.

The SEM system located in Saint Mary's University's Electron Microscopy Centre was use to asses the textures present throughout the kimberlite samples. The majority of the analysis was done using the backscattered electron detector, which measures the backscattered electrons leaving the surface of the sample, to survey the sample area. The analyses were conducted using a 20kV electron beam with a 158uA beam current. Furthermore,

EDS Analysis

While conducting the SEM analysis where textures of particular interest were observed the Saint Mary's INCA X-max 80mm 2 Energy Dispersive Spectroscopy system was used to provide semi-quantitative elemental information about the sample. This technology functions by using a crystal contained within the tool which absorbs the incoming x-ray produced through electron surface interactions as electrons drop to a lower valance shell. As the x-rays reach the crystal the energy is transferred into the crystal in the form of a charge which is proportional to

the type of emission being measured. Meaning that a measurable charge is produced depending on the nature of the emission from different energy level shells in different elements. (Swapp, 2013).

Once a particular area of a sample was deemed to require further investigation due to the presence of an unknown or interesting texture/assemblage the EDS was used to quickly confirm the presence of reaction products along grain boundaries. Particularly in areas made up of complex intergrown secondary textures. The EDS system is commonly used because while not producing quantitative data or maintaining high precision at small elemental abundancies the tool is able to take a full compositional measurement in seconds.

Elemental X-ray Maps

In addition to the analysis of single points, maps of elemental composition can be constructed using the same SEM and EDS tools as were used in the SEM analysis. This tool is useful for determining the spatial distribution of elements in a sample as well as to aid in the identification of mineral phases by assessing the similarities in distribution of elements contained in a certain mineral phase. Using software, a raster graphic or grid, of EDS analysis points is programmed which when executed shows readings for a specific element in counts made by the detector for each point in the raster file thereby creating a map of elemental composition. These raster files can then be rendered as images showing the relative proportion of an element in the sample, with higher counts corresponding to higher abundances of a particular element.

WDS Analysis

When more accurate and precise measurements are required, wavelength-dispersive spectrometer may be used at the expense of more time per analysis. The technology is based off of the same principles as SEM and EDS whereby as an electron beam interacts with a sample x-rays are generated which are proportional to the elemental composition of the sample. However the WDS technique differs in how these x-rays are measured (Henry & Goodge, 2013). Crystals are used to pick up the x-ray signal. The crystal-samples geometry can be altered so that x-rays meet the crystal at an angle Θ, in such a way that only x-rays that satisfy Bragg's Law

are reflected. A single wavelength is then passed to the detector, meaning that the tool is limited to analyzing one element concentration at a time. (Henry & Goodge, 2013)

Single point microprobe analyses were conducted on 10 samples (table 2) with an emphasis on taking compositional measurements of chromite and ilmenite macrocrysts. If these macrocrysts were of sufficient size, or had during previous analyses appeared to be zoned, both core and rim measurements were taken. Where oxide inclusions in olivine were found, measurements were taken as well. Lastly, groundmass minerals which during the SEM analysis were identified to be chromite and ilmenite in stable form were also analyzed. The microprobe analysis was conducted at Dalhousie University's Robert M. MacKay Electron Microprobe Laboratory using the labs JEOL JXA-8200 WD/ED Combined Microanalyzer using the standards and analyzing conditions outlined in table 3.

Table 2. List of samples used in SEM analysis.

Depth from (m)	Depth to (m)	Hole	Kimberlite	Facies	Sample
56.16	56.26	NA	AK15	-	EGR665
98.48	98.59	NA	AK15	-	EGR683
151.7	151.83	NA	AK15	-	EGR705
18.29	18.53	H003	BK1	CK-A	EGK637
34.53	34.7	H002	BK1	CK-A	EGK567
36.7	36.9	H002	BK1	CK-A	EGK568
40.78	41.01	H002	BK1	CK-A	EGK569
42.74	42.96	H002	BK1	CK-A	EGK570
NA	NA	H004	BK1	CK-B	EGK619
NA	NA	H004	BK1	CK-B	EGK627
NA	NA	H004	BK1	CK-B	EGK634
45.65	45.85	H003	BK1	MVK-A	EGK641
50.41	50.64	H002	BK1	MVK-A	EGK571
54.33	54.48	H002	BK1	MVK-A	EGK572
124.41	124.65	H003	BK1	MVK-A	EGK648

Table 3. Analyzing conditions and list of standards used in Micro Probe analysis.

Element	Standard Used	Peak Count Time (s)	Background Count Time (s)
Cr, Mg, Al, Fe	Chromite	20	10
Mn	Pyrolusite	20	10
Ca	Kakanui (Kaersutite Amphibole)	20	10
V	Vanadium Metal	40	20
Na	Jadeite	20	10
Si	Sanidine	20	10
Ni	Nickel Metal	40	20
Nb	Columbite	40	20
Ti	Rutile	20	10
Zr	Cubic Zirconia	40	20
Zn	Sphalerite	20	10

Analyzing Conditions	
Voltage	20 kV
Current	$2.00X10^{-8}A$
Beam Size	1 um

Image processing

The groundmass mineralogy of each kimberlite facies was approximately determined by taking element maps of a section of each sample's groundmass. The elemental maps were taken during SEM sessions and the procedure involved in their capture is, for the most part, identical to the SEM method described earlier. However, the process varies in that the software's settings must be changed such that machine takes composition points in a grid format for the area outlined for all elements specified by the user. The elemental maps can then be rendered as an image file reporting the content of a single element per image, in terms of counts.

These elemental mapping images were rendered for all relevant elements. Then, using ImageJ, the originally RGB formatted maps were converted to an 8-Bit file. The threshold was then adjusted to differentiate between areas which were considered to contain the element in

question and areas which did not contain the element. The output of this process is a binary file with areas containing the element in question taking a value of 255 and areas not containing the element taking a value of 0.

With this process completed for all elements in each sample image, the image calculator tool was used to output an image which displayed the area with a combination of elements corresponding to a certain mineral assemblage with a value of 255, and the remaining area which did not contain the mineral assemblage taking a value of 0. This process was then done for each sample and each mineral assemblage of interest. The mineral assemblages used, and the image calculator operations done to result in the output can be seen in table 4.

Table 4 Image calculator operations used to represent various mineral assemblages.

Mineral	Mineral Formula	Image Calculator Operation
Chromite	$FeCr_2O_4$	Cr Multiply Fe
Ilmenite	$FeTiO_3$	Fe Multiply Ti
Titanite	$CaTi(SiO_4)O$	Ca Multiply Ti Multiply Si
Perovskite	$CaTiO_3$	(Ca Multiply Ti) Subtract (Ca Multiply Ti Multiply Si)
Rutile	TiO_2	Ti Subtract Si Subtract Fe Subtract Ca
Magnetite	Fe_3O_4	Fe Subtract Cr Subtract Ti

With this step completed, there were six different images corresponding to each of the six minerals of interest for each of the four kimberlite facies samples imaged. Next, quantitative abundancies of the mineral assemblages in each sample were measured. First, the scale bar, found at the bottom of each image by default, was outlined and using the fill command was set to a value of 0. Next, using the threshold tool, which presents the user with the percentage of the image's area above or below the threshold value, was used to select the proportion of the total image area covered by the mineral. However, the value stated in the tool is not the true proportion of the mineral in the sample, as the area which corresponds to the scale bar was also used in the calculation. Consequently, the scale bar was again selected, and using the

invert tool, was set to a value of 255. The threshold tool was then used again, in the same way as previously discussed, resulting in a new value corresponding to the area of both the scale bar and the mineral. The difference in these values, corresponding to 7.4% of the image area was then used to normalize all values to that of only the sampled area and not the total image area. This process was then repeated for all six minerals in all four samples.

Next, the images were reclassified so that cell values were no longer 255 for areas with the mineral present and 0 for the rest of cells. The range of possible values, 0 – 255, were split into 6 and one of these values was used to reclassify each image such that a different cell value corresponded to a different mineral assemblage.

After this was completed for each mineral and sample the different mineral images were added to each other using the image calculator tool such that, for each sample, each of the six minerals corresponded to a different value and the remaining area was assigned a value of 0. This results in an image containing areas with different shades of grey, each of which correspond to a different mineral. Next, a lookup table was applied to assign a unique RGB colour to each mineral's cell value as seen in table 5. This results in an image with each mineral represented as a different color allowing the different assemblages to be more easily distinguished.

It is important to note that, as the image files report elemental abundance in terms of counts, this analysis is by no means comprehensive. In addition, the range of counts observed in a given sample varied widely by element. Attempts to compensate for this were made by selecting a threshold value which included a narrower band of the spectrum in cases were ranges were low, and picking a broader spectrum range in cases were the range of counts recorded were large. However, this technique is not accurate and as the threshold value is arbitrary and the relationship between counts and actual elemental abundance is more complex. Additionally, this procedure does not account for the compositional complexities present in most minerals particularly in situations relating to minerals which form a solid solution. For example, titaniferous magnetite, ulvöspinel and ilmenite would all be recorded as

ilmenite using this method. Another such example is any iron oxide mineral such as magnetite and hematite which would appear only as magnetite in this analysis.

Table 5. Look up table cell value and color scheme used.

Mineral	Assigned Cell Values	Colour Assigned
Chromite	43	
Ilmenite	85	
Titanite	170	
Perovskite	128	
Rutile	213	
Magnetite	32	

Chapter 4: Results

Textural and Compositional Variation

The SEM analysis showed evidence of textural and mineralogical variation across a single kimberlite facies throughout the depth of a single kimberlite facies. Typically, this is observed as a gradual change with more drastic changes from shallow to deep depths with a gradual change between these two end member at transition depths. Samples showed minor variations in the amount of macrocrysts present in each slide with a slight correlation with depth. In AK-15 sample and CK-B sample there was no observed change in macrocryst presence however texture did vary with depth in these samples. In the case of CK-A and MVK-A macrocryst minerals present change with depth, however this is not a case of a gradual transition from one set of minerals to another. Relic mineral assemblages show a similar pattern whereby the set of minerals making up the relic textures in samples do not show a gradual change with depth and instead show more complex variation. In contrast, secondary mineral assemblages show a much more gradual trend with depth and in all samples, with the exception being CK-B, there is a distinct assemblage present at shallow depths and a distinct assemblage present at deep depths with a gradual change which contains elements of each end member.

BK-1 Kimberlite

CK-A

Chromite:

In the CK-A facies chromite is present in low quantities as macrocrysts. These macrocrysts show evidence of alteration, with exsolution products composed predominately of intergrowths of titanite, with minor magnetite and rutile. Furthermore, chromite is not found within the groundmass or as olivine inclusions. These chromite macrocrysts generally show a heavily fractured and anhedral habit as can be seen by figure 8 and 9.

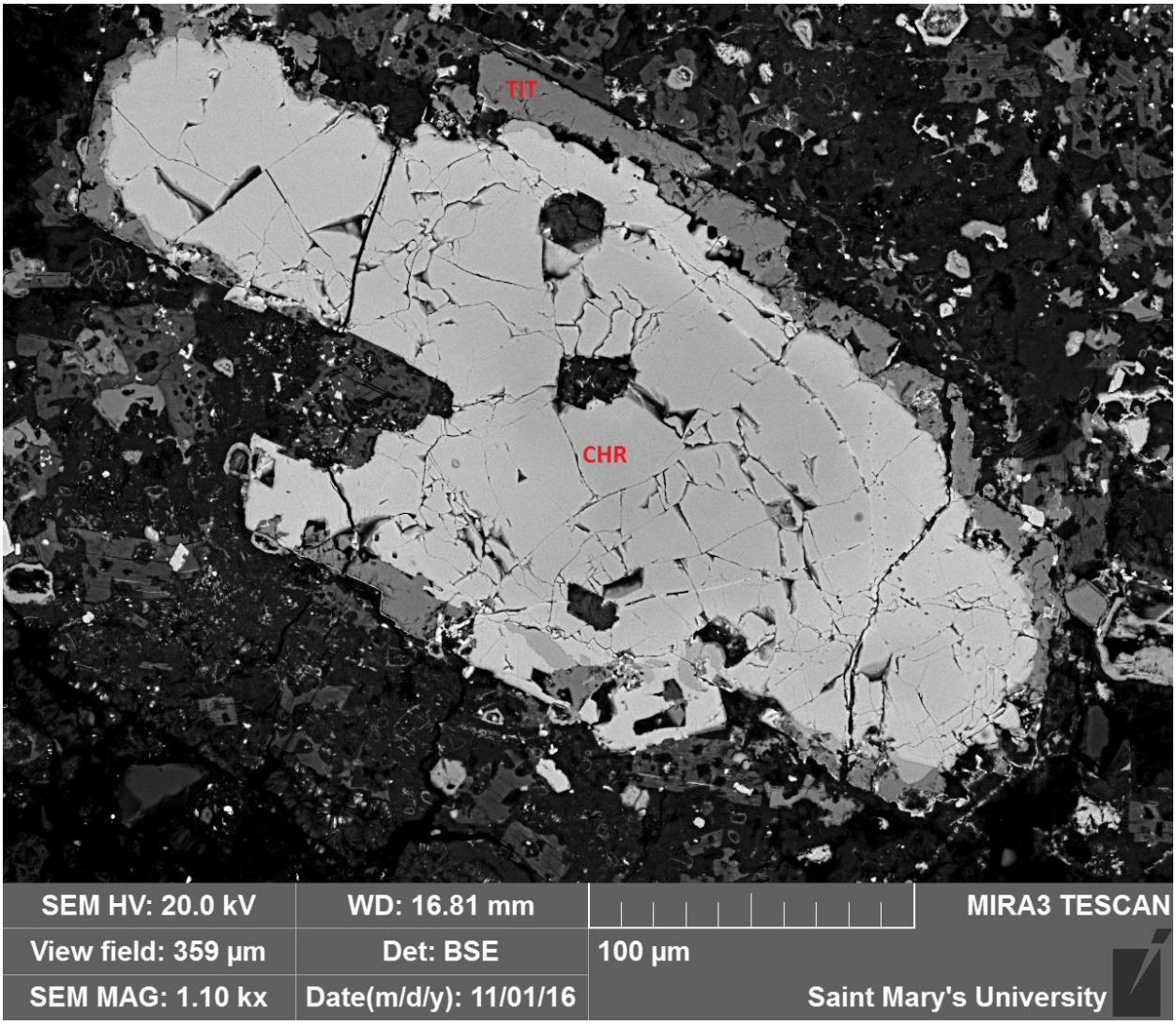

Figure 8. Back scattered electron image of sample EGK637 of the BK01 kimberlite and CKA facies displaying chromite macrocryst

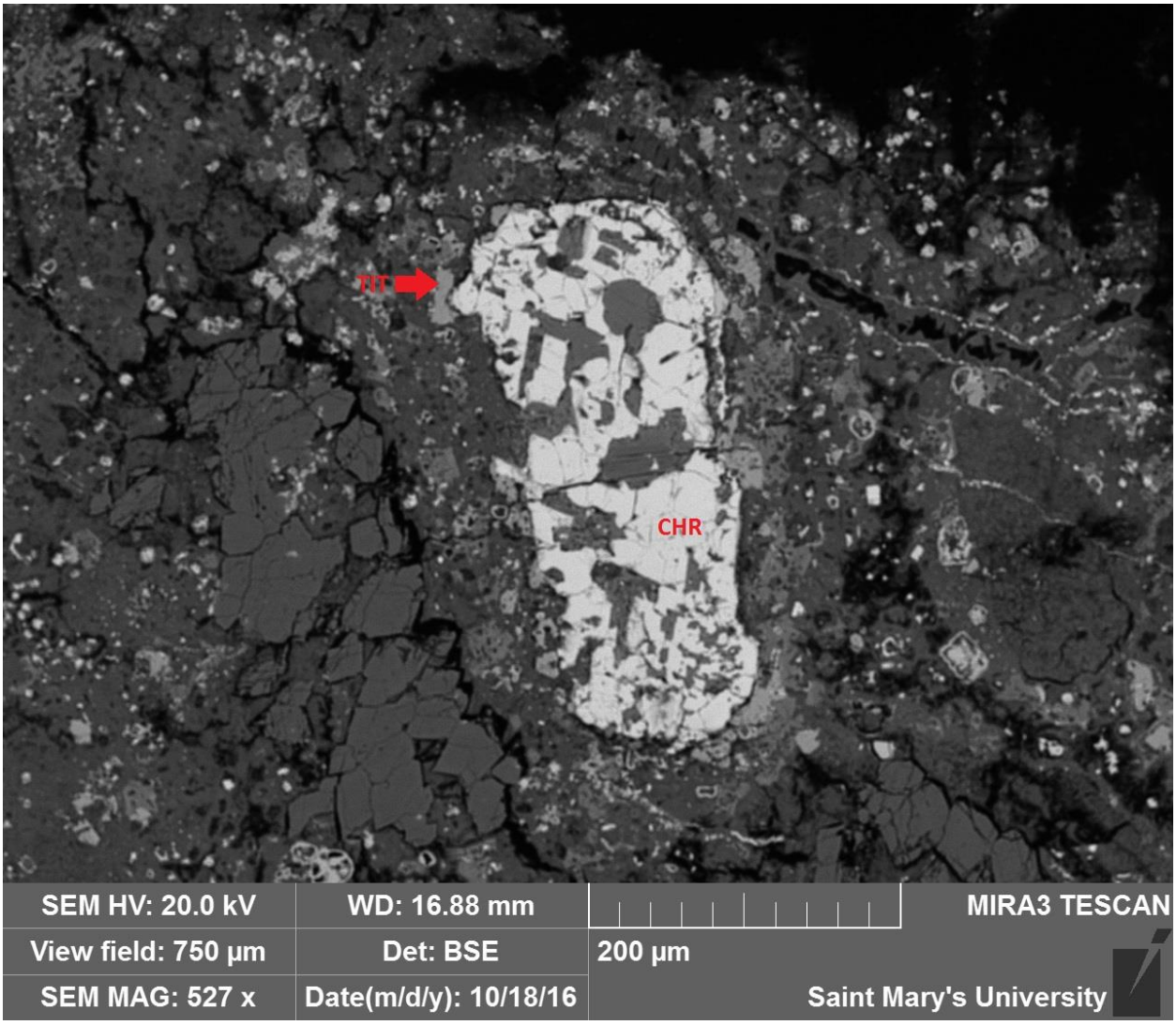

Figure 9. Back scattered electron image of sample EGK637 of the BK01 kimberlite and CKA facies displaying chromite macrocryst

Ilmenite:

Ilmenite is abundant throughout all CK-A samples as macrocrysts. These ilmenite grains show evidence of significant alteration in the form of exsolution textures made up of rims of intergrown magnetite and titanite surrounding ilmenite grains (figure 10, 11, 12). Ilmenite does not appear in the groundmass of CK-A. The degree of alteration of these ilmenites varies widely from grain to grain. Certain grains show a minute amount of alteration along grain edges while others will be almost entirely altered (figure 10, 11, 12). Furthermore, different boundaries of the same grain show differences in the amount of alteration. In many cases this is clearly a result of fracturing, however there are examples where this does not hold true. One such

example can be seen in figure 10, 11, 12 where the band of alteration is slightly thicker on the left edge of the grain than on the right. However, it is important to note that this grain also shows a significant amount of fracturing.

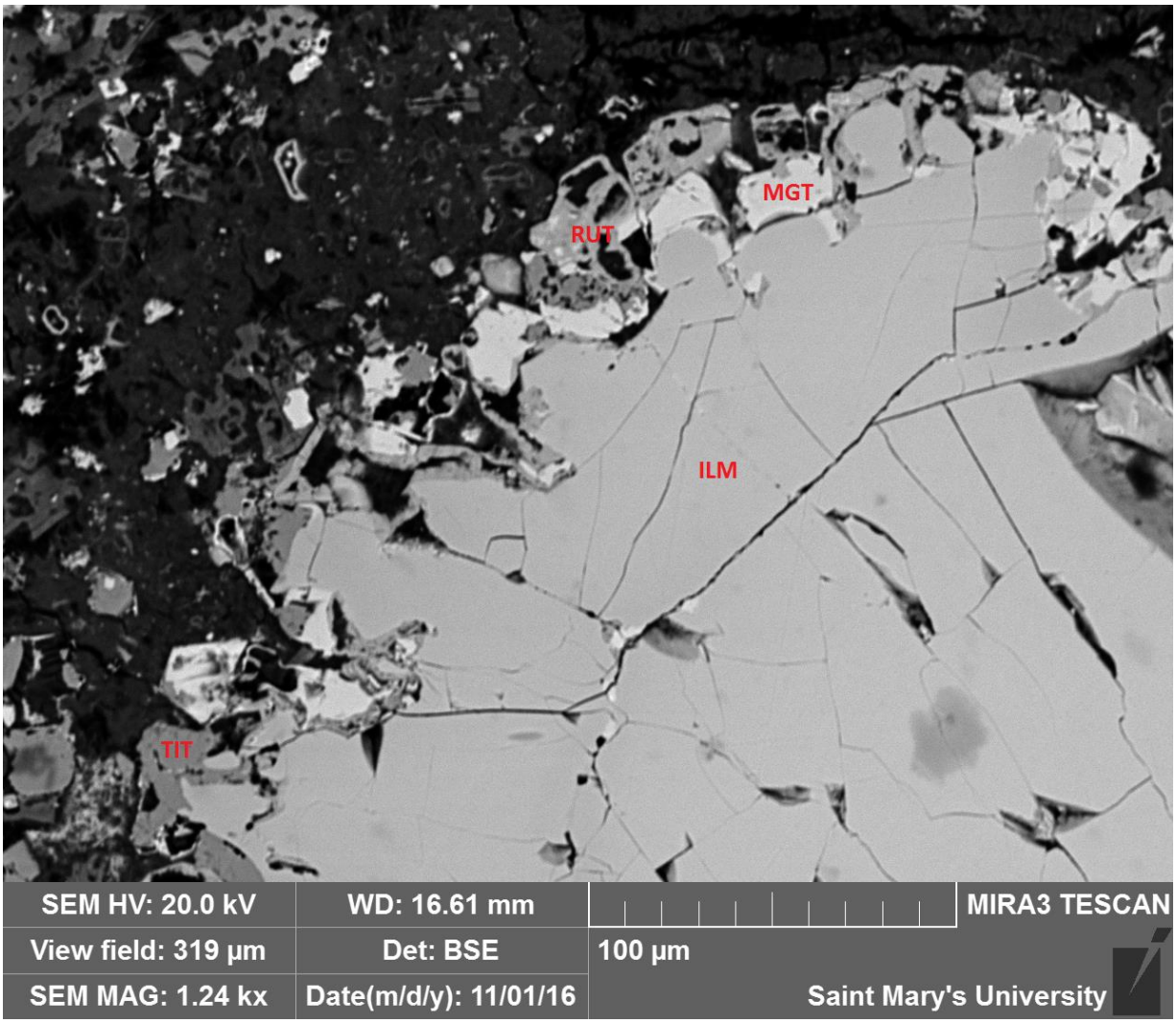

Figure 10 . Back scattered electron image of sample EGK637 of the BK01 kimberlite and CKA facies displaying ilmenite macrocryst and magnetite, titanite and rutile alteration

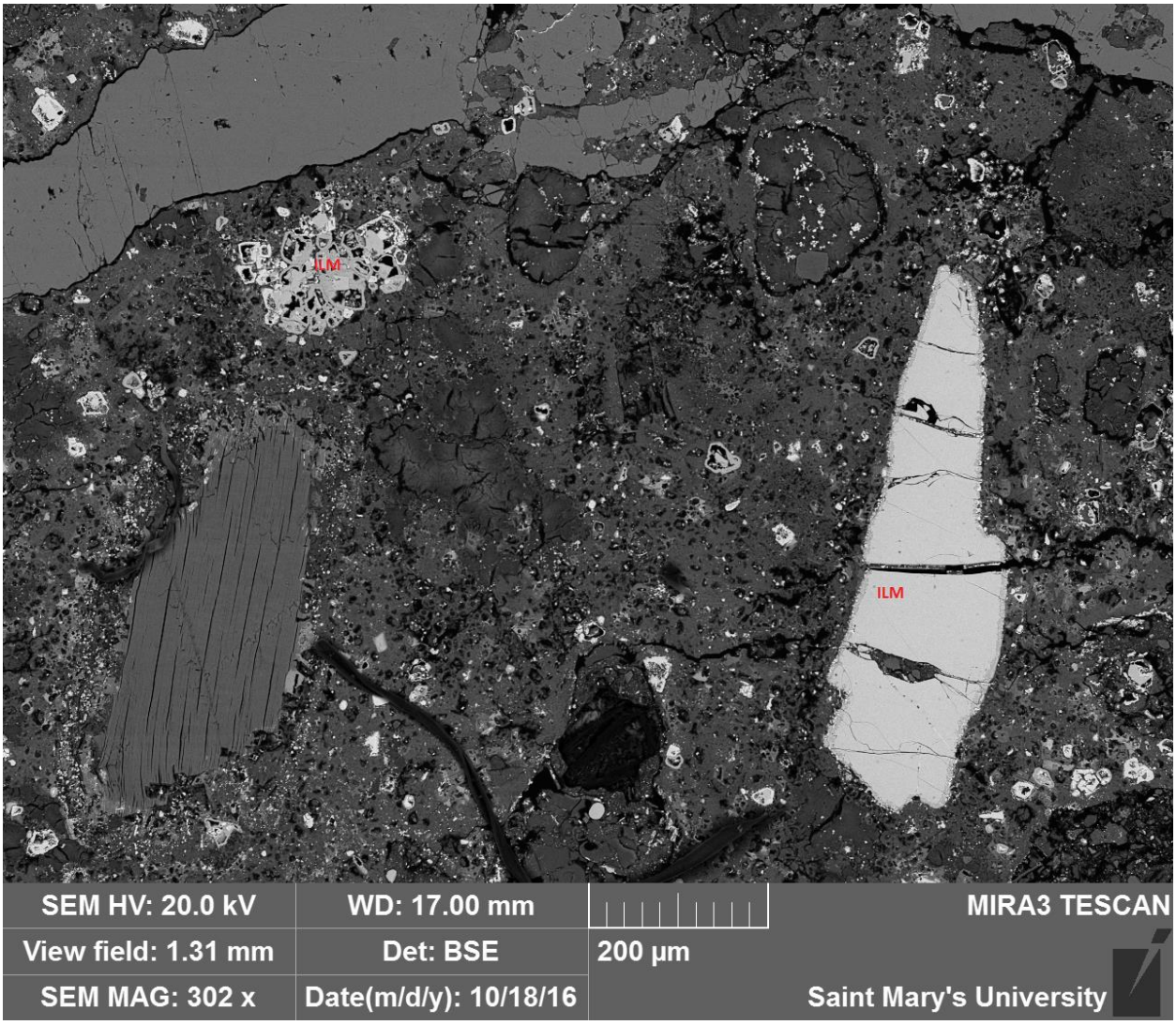

Figure 11 . Back scattered electron image of sample EGK637 of the BK01 kimberlite and CKA facies displaying ilmenite macrocrysts showing varied amounts of alteration

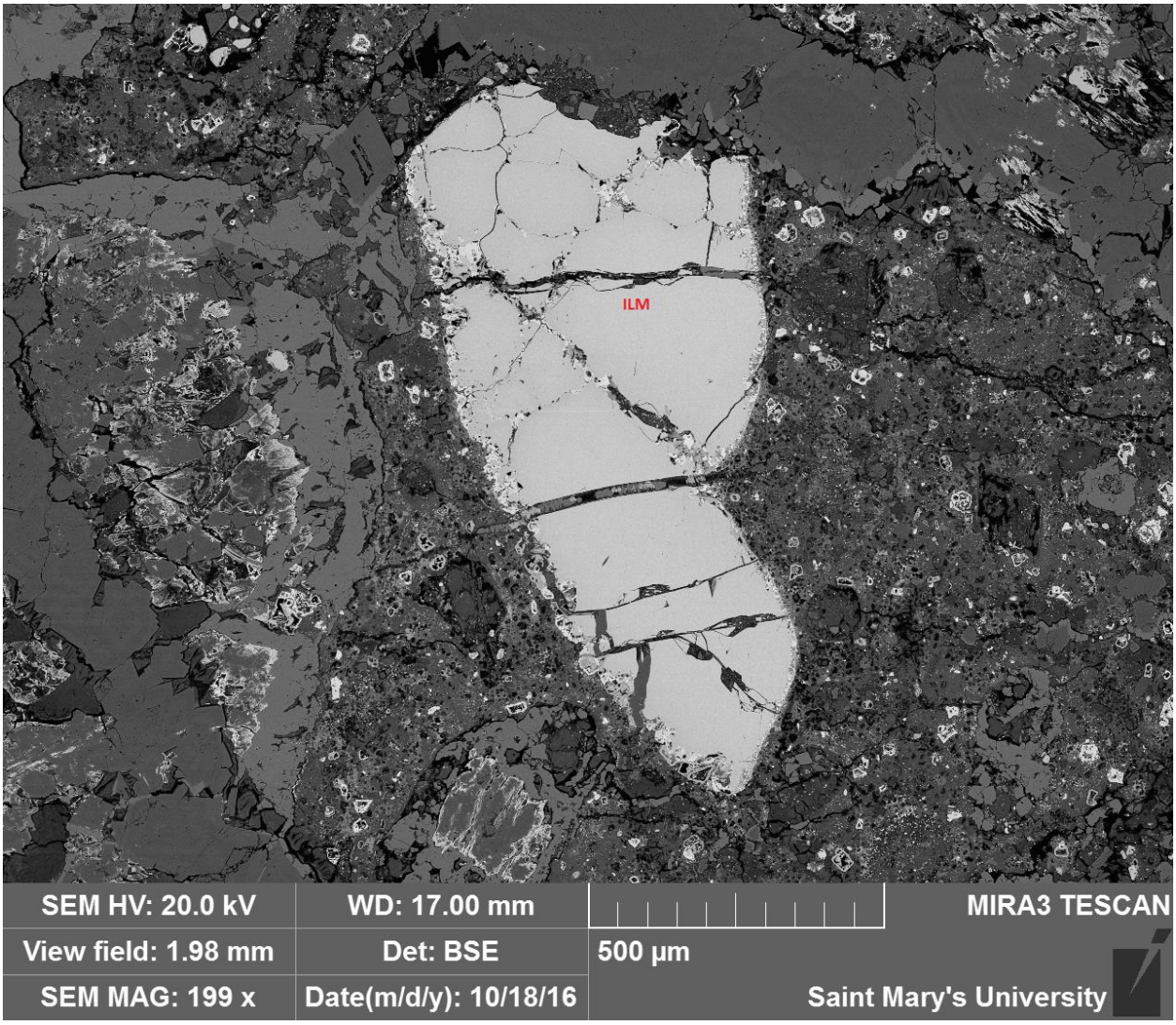

Figure 12 Back scattered electron image of sample EGK637 of the BK01 kimberlite and CKA facies displaying ilmenite macrocryst showing varied amounts of alteration

Groundmass:

Titanite and rutile occur commonly throughout the sample as alteration products of chromite and ilmenite as well as throughout the groundmass as euhedral grains figure 14. Other minerals which make up the groundmass include magnetite apatite and phlogopite. Perovskite is not found in CK-A in major quantities. Several samples are crosscut by 1-2mm thick veins composed primarily of dolomite with a small proportion of REE minerals.

Quantitative mineral abundancies corresponding to the area observed in figure 14 and 15 show that chromite occurs only as macrocrysts and is not present in any extent as a groundmass mineral. The large chromite grain shows intergrowths around the rim of the grain made up of perovskite and titanite, as well as Fe_xO_x and $Fe_xTi_xO_x$ which appear to be magnetite and titaniferous magnetite respectively. Minor titanite and perovskite occur together in the groundmass. Fe_xO_x, most likely magnetite occurs abundantly throughout the groundmass. $Fe_xTi_xO_x$ is moderately common in the groundmass and is typically found intergrown with rutile, however some examples of these $Fe_xTi_xO_x$ grains appear to be composed of ilmenite. Rutile also occurs commonly independently as subhedral grains with a wide range in size.

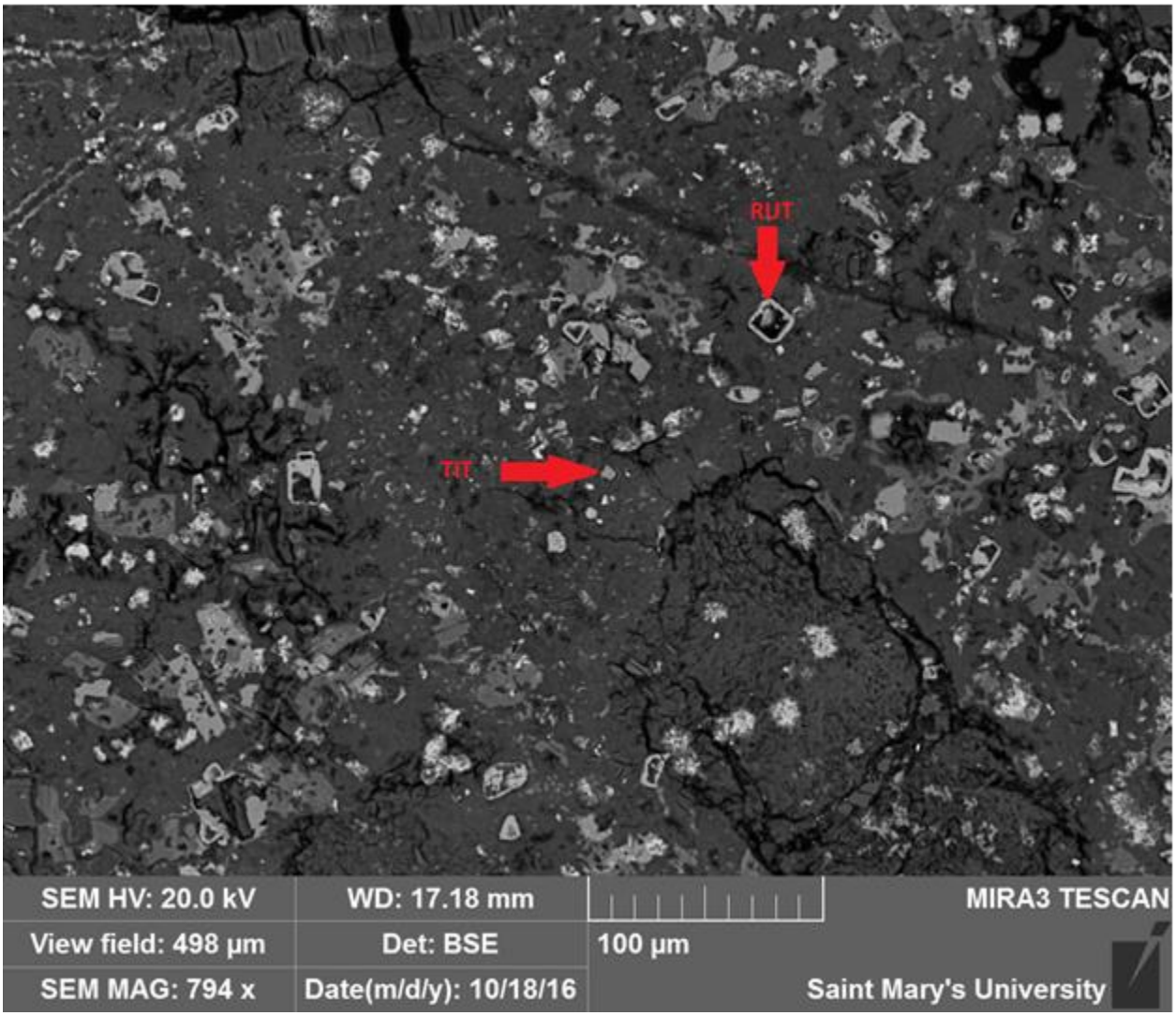

Figure 13 Back scattered electron image of sample EGK637 of the BK01 kimberlite and CKA facies showing groundmass mineralogy composed of predominantly titanite and rutile

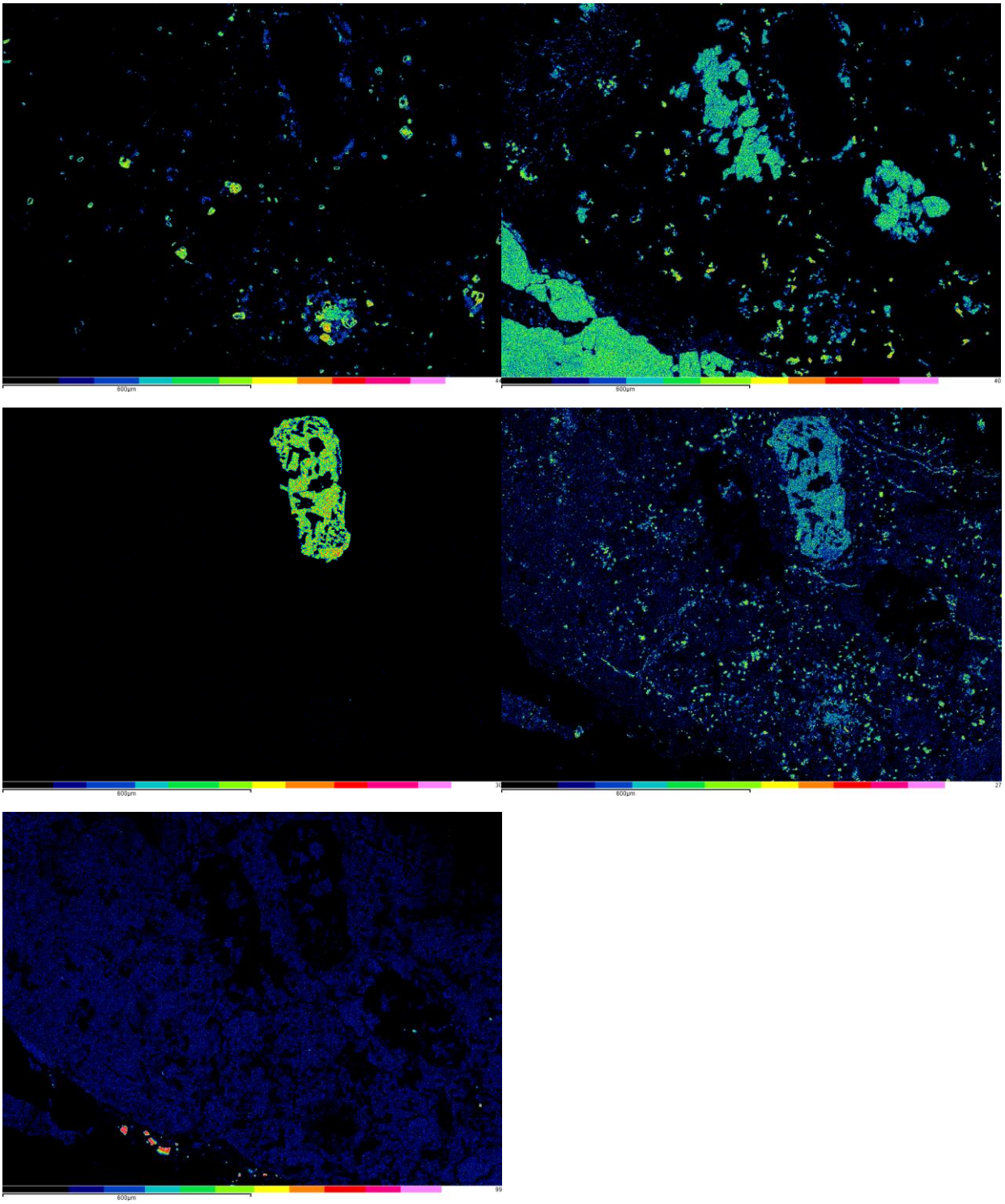

Figure 14 EDS elemental X-ray maps of EGK637 groundmass of the BK01 kimberlite and CKA facies showing Ti (upper left), Ca (upper right), Cr (middle left), Fe (middle right) and Si (bottom left) elemental abundancies

Variation with depth:

CK-A macrocrysts show little variation with depth, ilmenite macrocrysts are present throughout all depths. Chromite macrocrysts are present in only EGK637 and EGK569 samples. However, the low quantities observed may be the cause of the lack of chromite in other samples as those samples may have not sampled an area with chromite even though the mineral was present in the area. CK-A shows clear variation in its secondary mineralogy where secondary titanite is present at shallow depths, secondary rutile at transitional depths and secondary perovskite is present at the deepest depths. Furthermore, secondary magnetite is present in all samples with the exception of EGK570 which is a deep sourced sample. Groundmass mineralogy shows similar results, where both deep and shallow sourced samples show groundmass compositions of titanite and magneite and transitional depths show only magnenite with minor rutile present in the upper transitional EGK567. Relic textures in CK-A samples are more varied in shallow depths relic mineralogy is composed of chromite ilmenite and rutile whereas in deep sourced samples the primary relic mineral is titanite.

CK-B

Chromite:

Chromite macrocrysts were not found within any CK-B samples analyzed.

Ilmenite:

Ilmenite macrocrysts within the CK-B facies show complex intergrowth assemblages. The grains indicate the complete dissolution of ilmenite macrocrysts into a composite assemblage of secondary minerals made up of magnetite and perovskite. These grains show a lamellar texture within the core (figure 15 and 16), with intergrowths of the same composition and relative proportions along the rims of the grain. Magnetite is also observed concentrated into larger anhedral grains within the core of macrocrysts while perovskite tends to be found only as lamellar bodies. The majority of lamella are generally orientated in a single direction,

however this is not consistent across the grain and orientation vary widely. Furthermore, these grains typically show a higher proportion of perovskite than of magnetite.

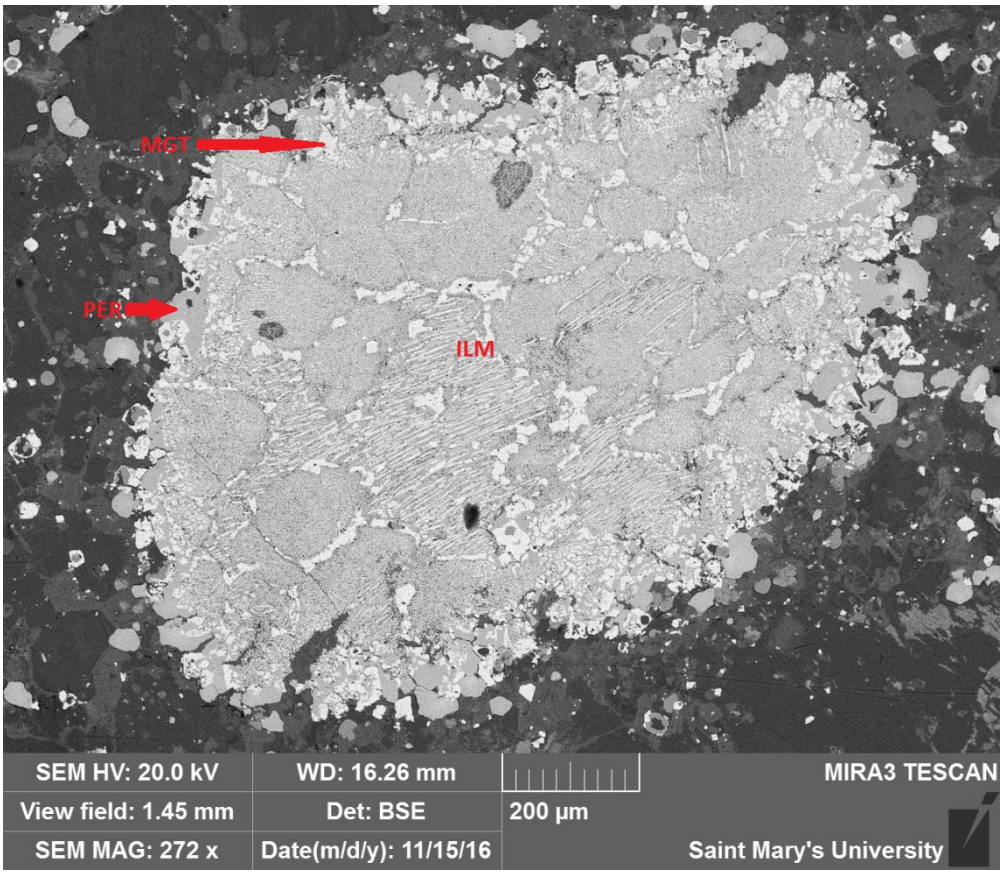

Figure 15. Back scattered electron image of sample EGK627 of the BK01 kimberlite and CKB facies displaying ilmenite macrocryst with symplectitic magnetite and perovskite alteration

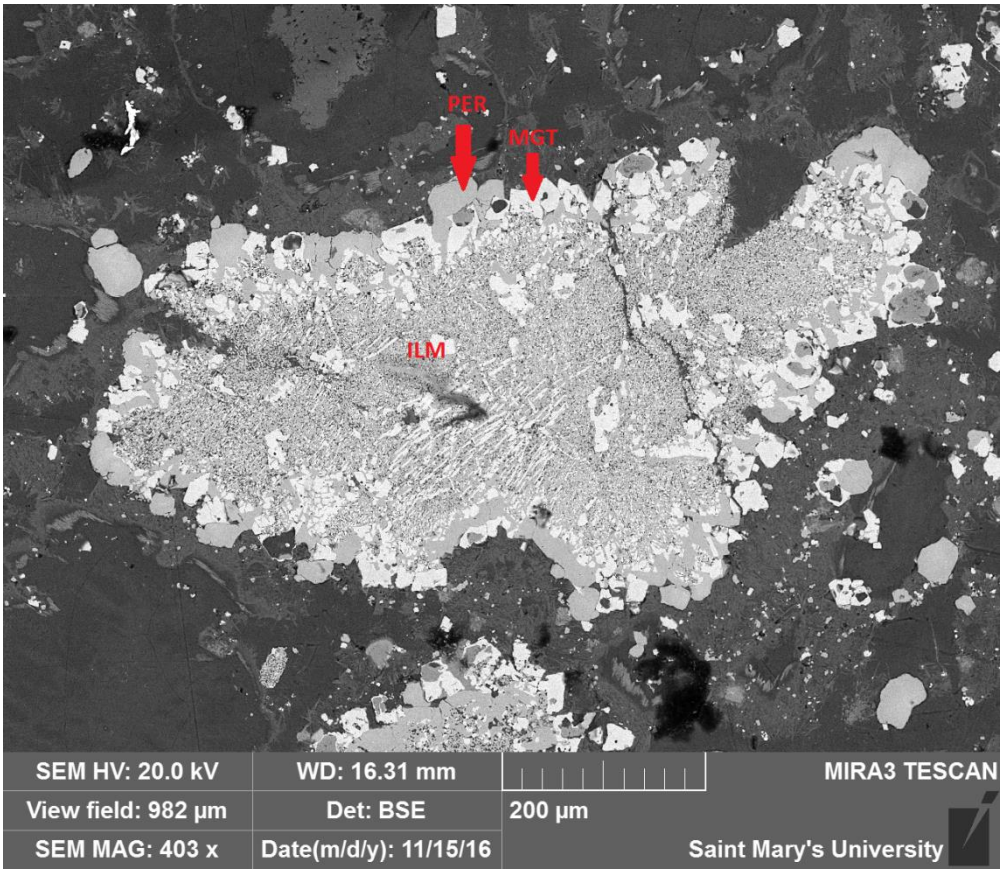

Figure 16 Back scattered electron image of sample EGK627 of the BK01 kimberlite and CKB facies displaying ilmenite macrocryst with symplectitic magnetite and perovskite alteration

Groundmass:

Chromite is found in the groundmass of CKB as anhedral crystals in very small quantities. Perovskite and titaniferous magnetite occur abundantly throughout the groundmass (Fig. 17). Titanite is found in moderately low quantities throughout the groundmass of CKB while rutile and ilmenite was not observed.

Quantitative mineral abundancies corresponding to the area observed in figure 18.

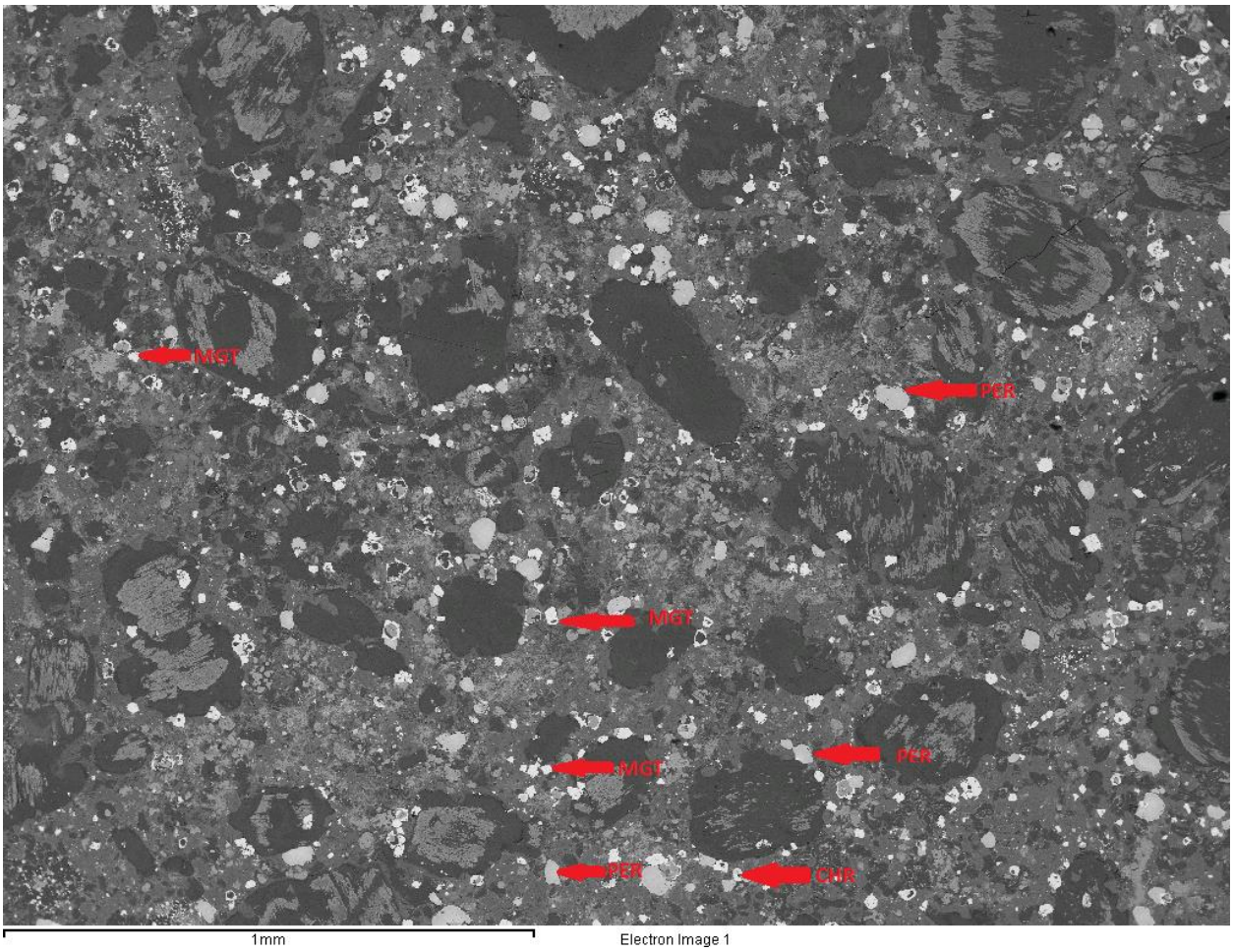

Figure 17 CKB Groundmass back scattered electron image of sample EGK627 of the BK01 kimberlite and CKB facies showing groundmass mineralogy composed of magnetite, perovskite and minor chromite

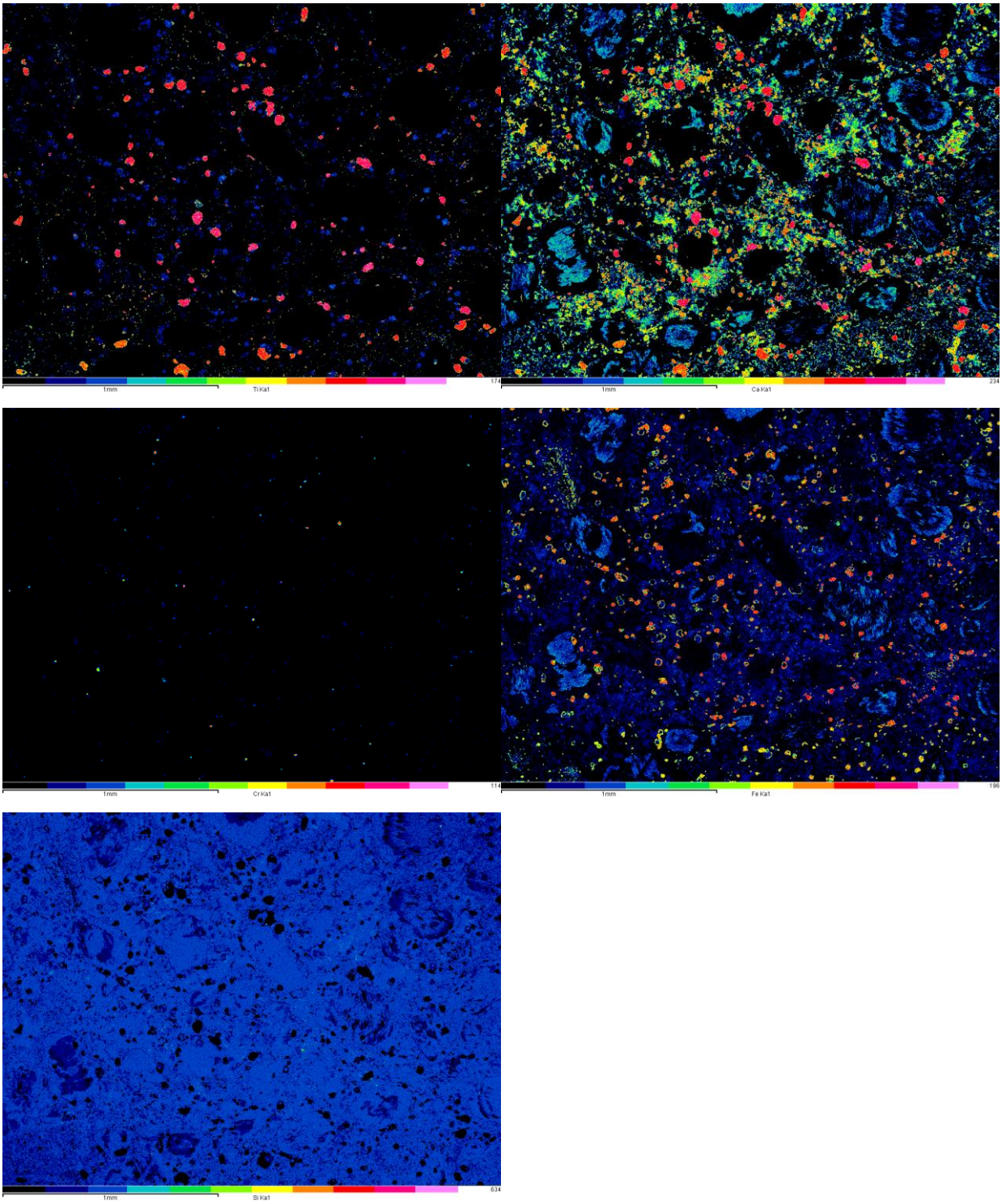

Figure 18 EDS elemental X-ray maps of EGK627 groundmass of the BK01 kimberlite and CKB facies showing Ti (upper left), Ca (upper right), Cr (middle left), Fe (middle right) and Si (bottom left) elemental abundancies

Variation with depth:

CK-B does not show any variation with depth in terms of its macrocrystal mineralogy. These samples all show abundant ilmenite with no presence of chromite across all depths sampled. Furthermore, all ilmenite macrocrysts show alteration to grains showing symplectitic texture made up of secondary magnetite and perovskite. This is consistent across secondary mineralogical compositions as well. Secondary mineralogical assemblages are made up of perovskite and magnetite regardless of the depth sampled. Groundmass mineral assemblages show slight variation, all samples show assemblages made up of perovskite and magnetite, however samples taken from shallow to transitional depths show presence of groundmass chromite. Slight variation is also present in the relic mineralogy where titanite is seen in shallow and transitional samples but not found in deep sourced samples.

MVK-A

Chromite:

Within the MVK-A facies chromite was found as macrocrysts in small quantities. These chromite grains exhibit anhedral grain boundaries with clear exsolution textures throughout. In some cases, these chromite grains are rimmed by silicates and high Al and K mica intergrowths. These silicates also appear as vug and rod-like intergrowths within grains as in figure 19. These silicate minerals have an olivine like composition however the shape and crystal habit are not consistent with olivine. All grains observed, however, show intergrown perovskite and titanite with small amounts of rutile as seen in figure 20.

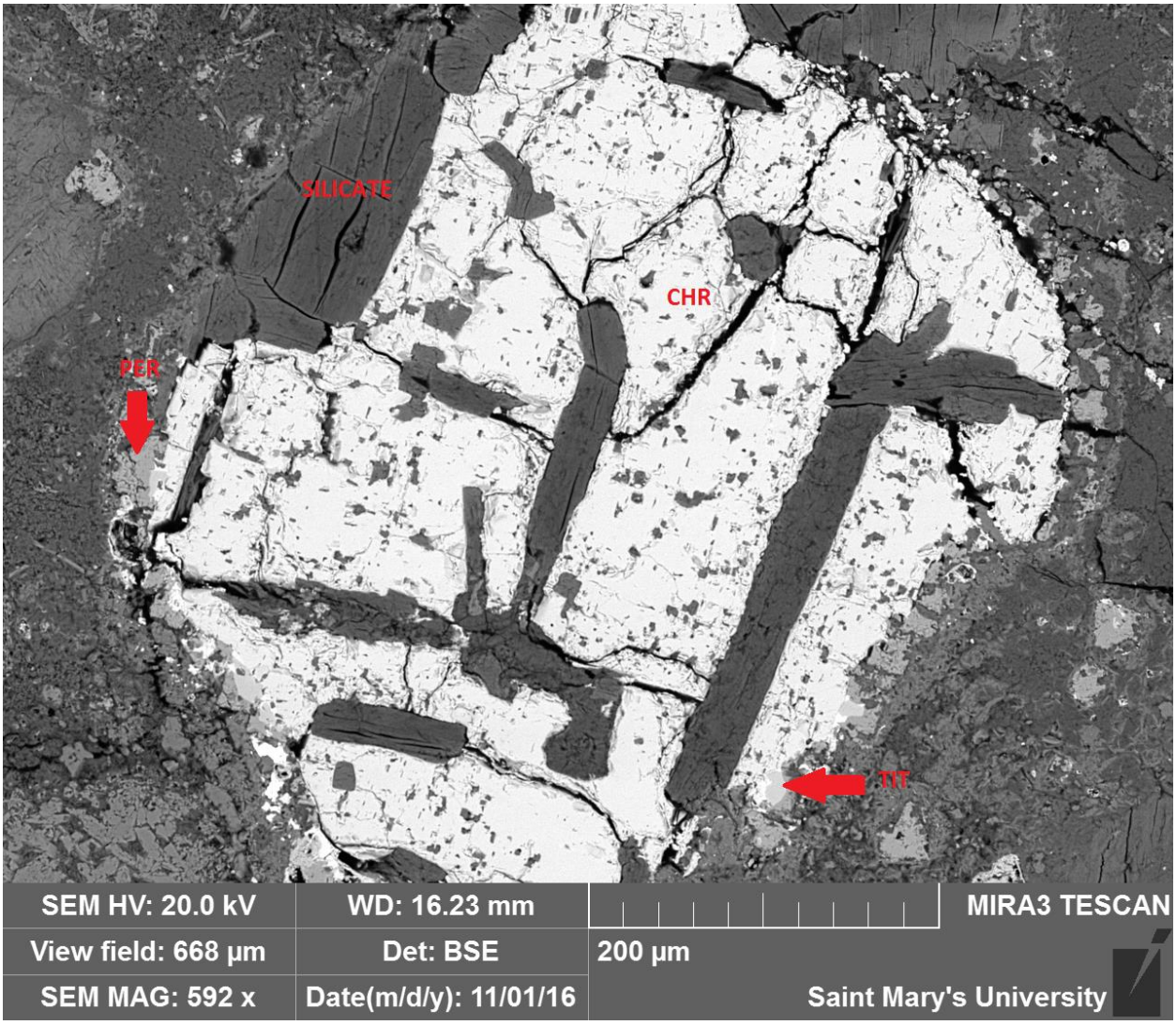

Figure 19 Back scattered electron image of sample EGK641 of the BK01 kimberlite and MVK-A facies displaying chromite macrocryst with titanite and perovskite alteration

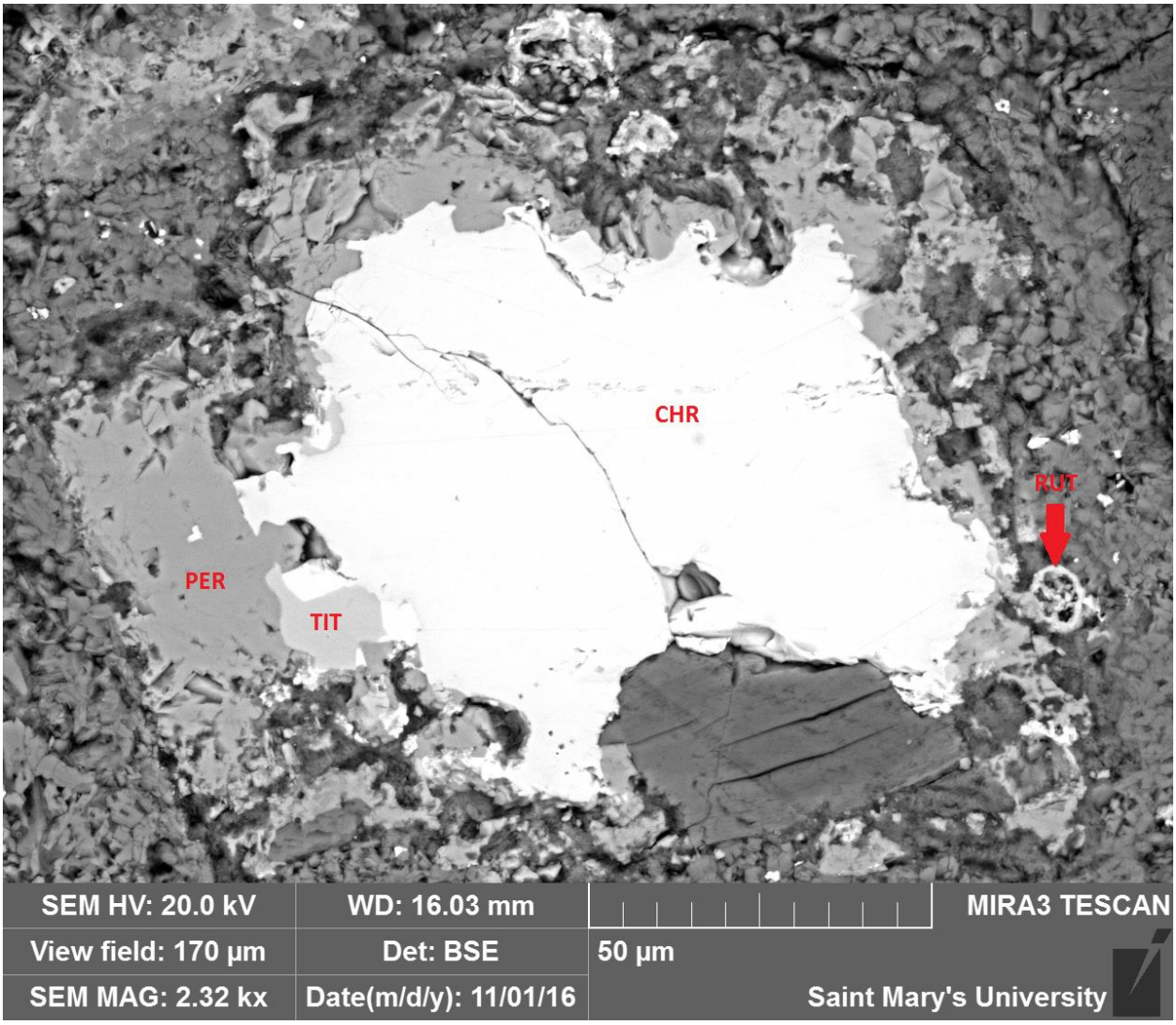

Figure 20 Back scattered electron image of sample EGK641 of the BK01 kimberlite and MVK-A facies displaying chromite macrocryst with titanite and perovskite alteration

Ilmenite:

Ilmenite macrocrysts are commonly found across all MVK-A samples analyzed. These grains show active exsolution, particularly along grain boundaries as in figure 21 and 22. These alterations are composed predominantly of titanite with some Ti-magnetite present as well. Furthermore perovskite is typically observed alongside titanite in these alteration rims, generally closer to the fringes of the grain with titanite closer to the interior of the grain. Moreover, as can be seen in figure 23 the ilmenite grain shows differential alteration across the whole grain. The alteration consists of a thicker more rounded alteration band across the

majority of the grain and a thinner but similarly structured band across the stepped and fractured areas of the grain through the upper right side of the mineral. This differentially altered assembly is commonly found within this facies. The interior of the ilmenite grains tend to be cohesive and unaltered. However, in rare cases the interior of the Ilmenite-titanite-magnetie assemblages show heavy exsoloution. Here the ilmenite is exsolving magnetie as can be seen in figure 23.

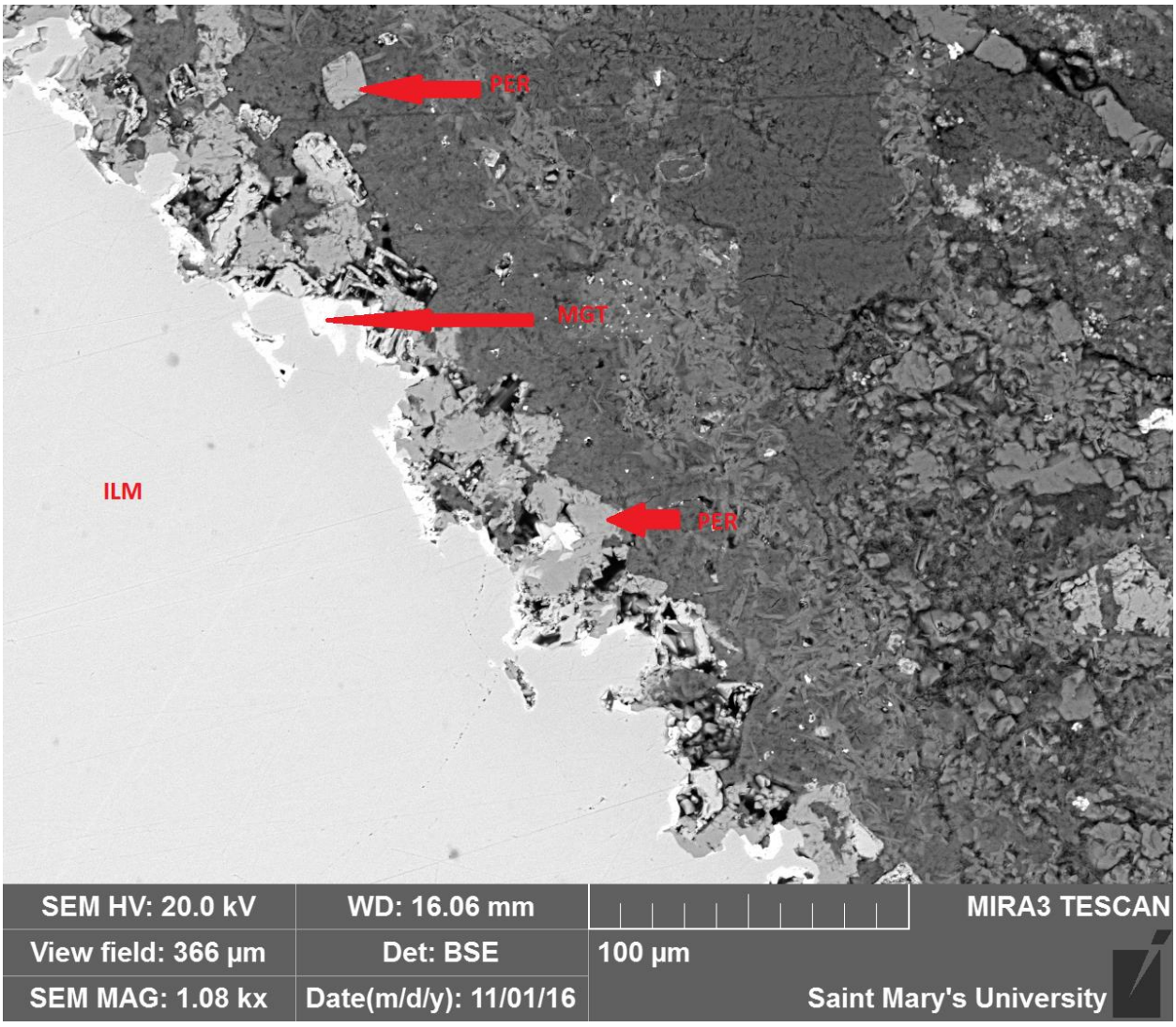

Figure 21. Back scattered electron image of sample EGK641 of the BK01 kimberlite and MVK-A facies displaying ilmenite macrocryst with magnetite and perovskite alteration

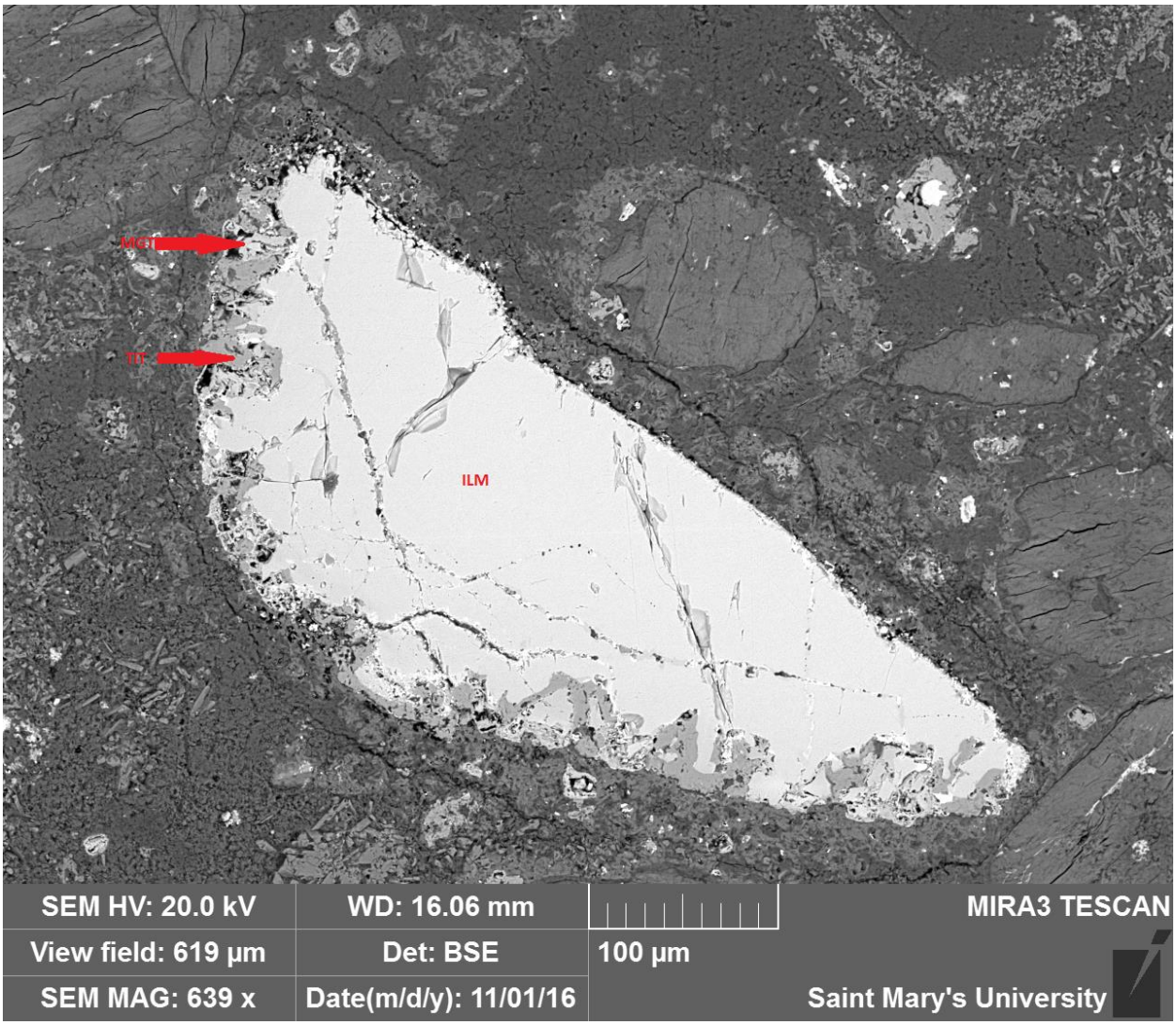

Figure 22. Back scattered electron image of sample EGK641 of the BK01 kimberlite and MVK-A facies displaying ilmenite macrocryst with magnetite and perovskite alteration

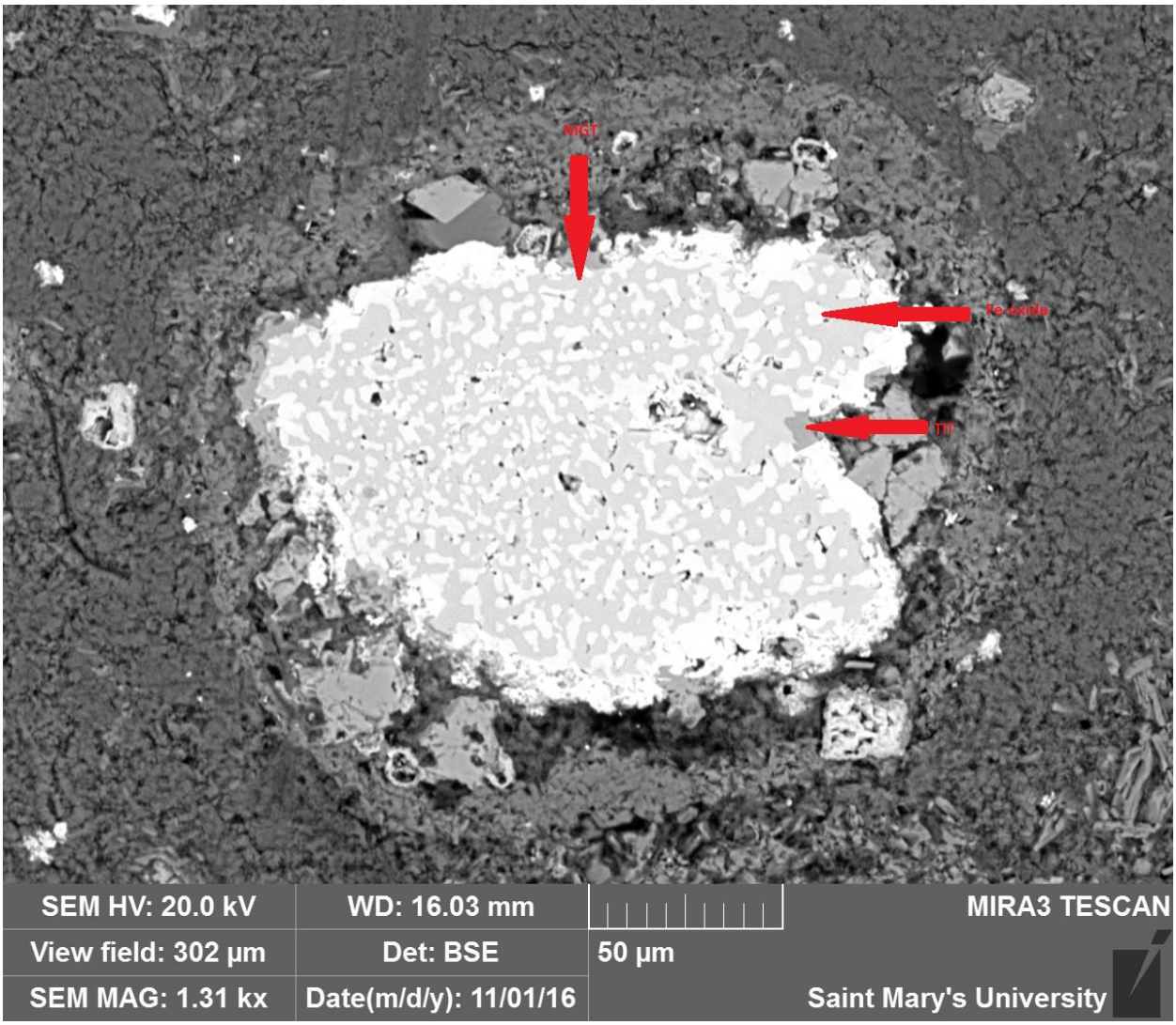

Figure 23. Back scattered electron image of sample EGK641 of the BK01 kimberlite and MVK-A facies displaying ilmenite macrocryst with symplectitic texture consisting of magnetite and perovskite alterations

Groundmass:

Within the groundmass of MVK, samples show subhedral perovskite grains with thin rims composed of rutile. Magnetite is also very commonly found in the groundmass. Additionally, perovskite and titanite interactions are seen within the groundmass in the form of small titanite intergrowths on grains boundaries of perovskite as can be seen in figure 24 and 25. Furthermore, titanite is regularly found independently within the groundmass, though the size of these titanite grains tend to be much smaller, in line with the size of independent magnetite grains and smaller than perovskite grains. Perovskite grains show an anhedral habit

while the perovskite and magnetite grains are much more euhedral. Rutile appears within the groundmass as anhedral grains and show rims composed of Ti-magnetite as in figure 26.

Quantitative mineral abundancies corresponding to the area observed in figures 27.

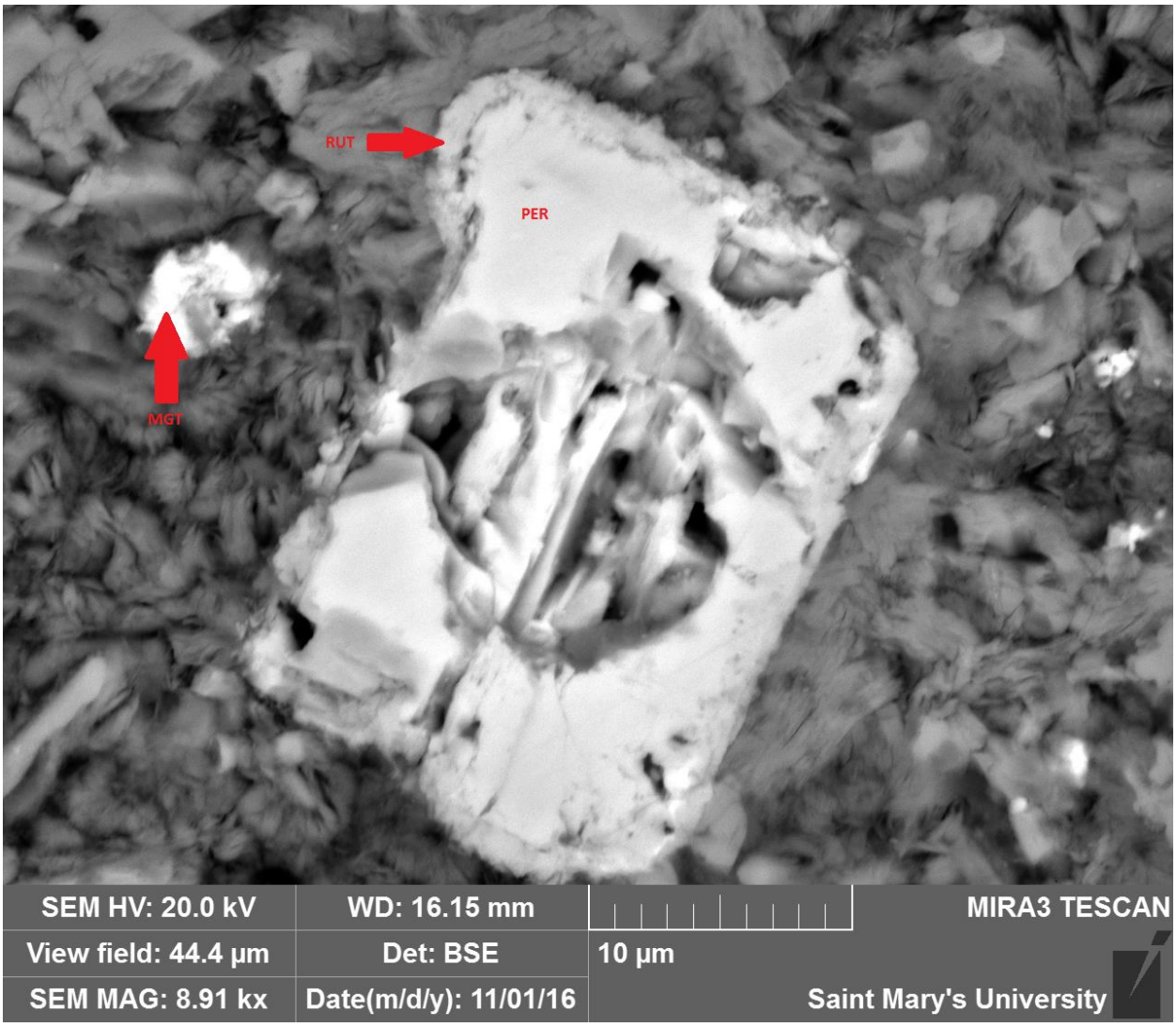

Figure 24 Back scattered electron image of sample EGK641 of the BK01 kimberlite and MVK-A facies displaying a perovskite groundmass grain showing alteration rim of rutile, with small magnetite groundmass grain also present

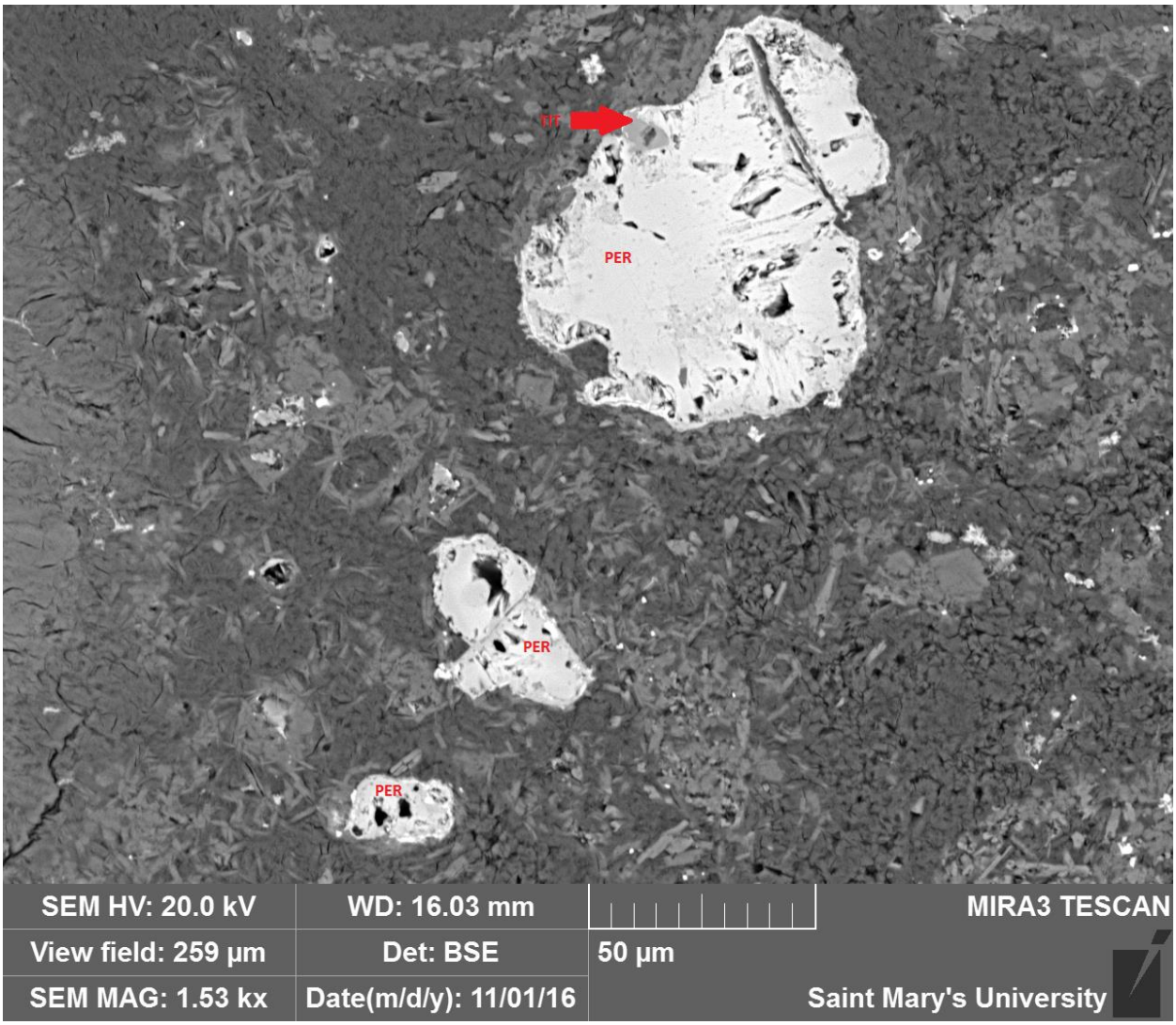

Figure 25. Back scattered electron image of sample EGK641 of the BK01 kimberlite and MVK-A facies displaying a perovskite groundmass grains with small relic titanite present

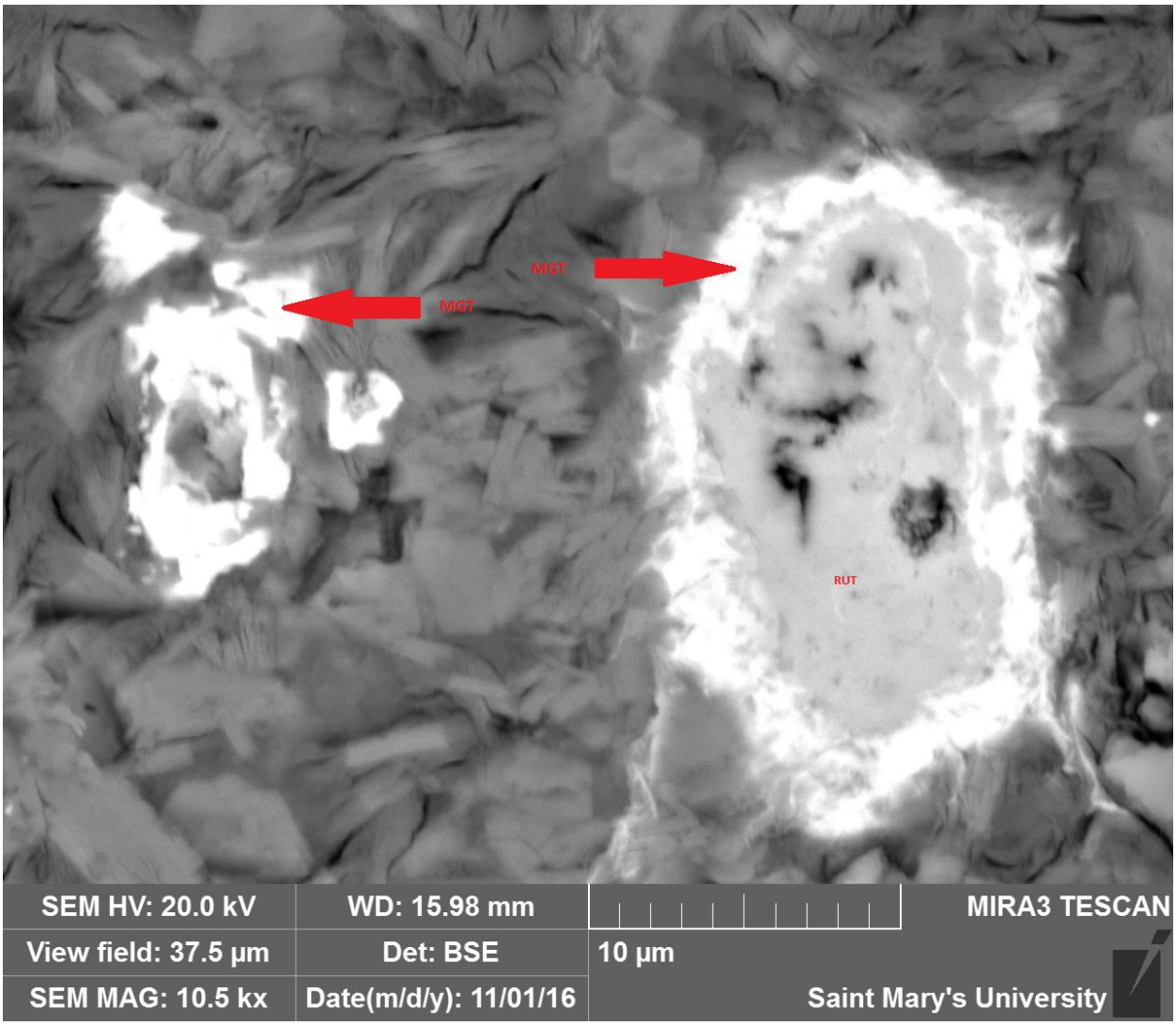

Figure 26. Back scattered electron image of sample EGK641 of the BK01 kimberlite and MVK-A facies displaying a rutile groundmass grain with magnetite alteration rim

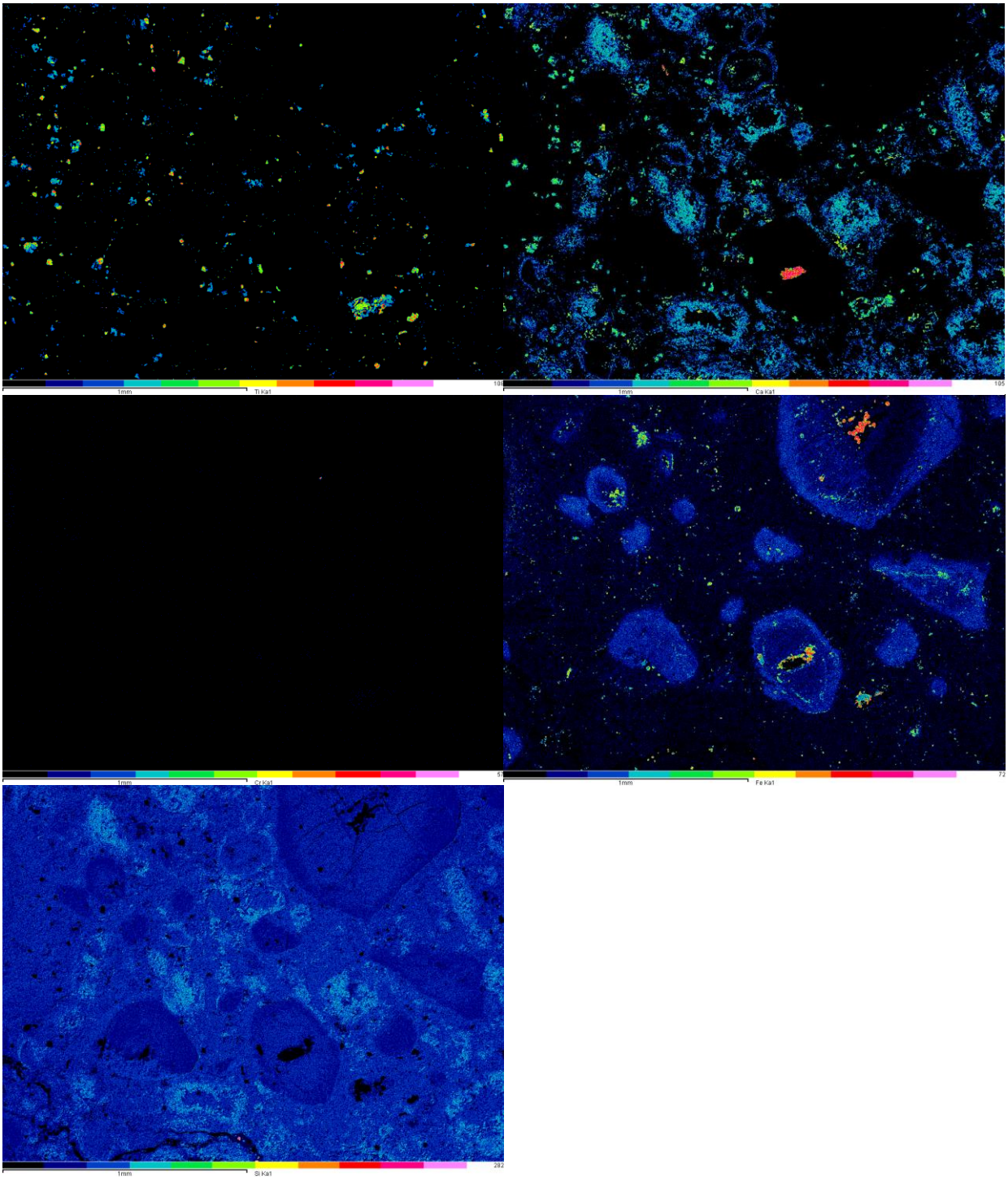

Figure 27 EDS elemental X-ray maps of EGK641 groundmass of the BK01 kimberlite and MVK-A facies showing Ti (upper left), Ca (upper right), Cr (middle left), Fe (middle right) and Si (bottom left) elemental abundancies

Variation with depth:

MVK macrocrysts show distinct variation with depth. Ilmenite macrocrysts are present across the entirety of samples with the exception of the deep transitional EGK572 sample. Furthermore, the shallow sourced EGK641 shows a single example of a symplectitic ilmenite made up of secondary magnetite and perovskite. Relic mineralogy is variable in MVK with shallow samples made up of relic ilmenite, titanite and rutile. Transitional and deeply sourced samples only contain titanite as a relic phase. Secondary phases are relatively continuous as well, magnetite and perovskite are present across all depths. One slight variation is the presence of secondary rutile in upper transitional EGK571. Lastly, within the groundmass of MVK, mineralogy is highly variable. Shallow sourced samples contain perovskite and magnetite while deep sourced samples contain magnetite and chromite.

AK-15 Kimberlite

Chromite:

AK-15 displayed chromite macrocrysts in very small quantities. However, unlike the other kimberlite facies, these chromite grains show minor alteration around the core of the grain. These chromite grains also show a much more euhedral habit than those of the other kimberlite facies as seen in figure 28 and 29. In areas were alteration is present, chromite is overgrown by perovskite as well as titanite, magnetite and minor rutile.

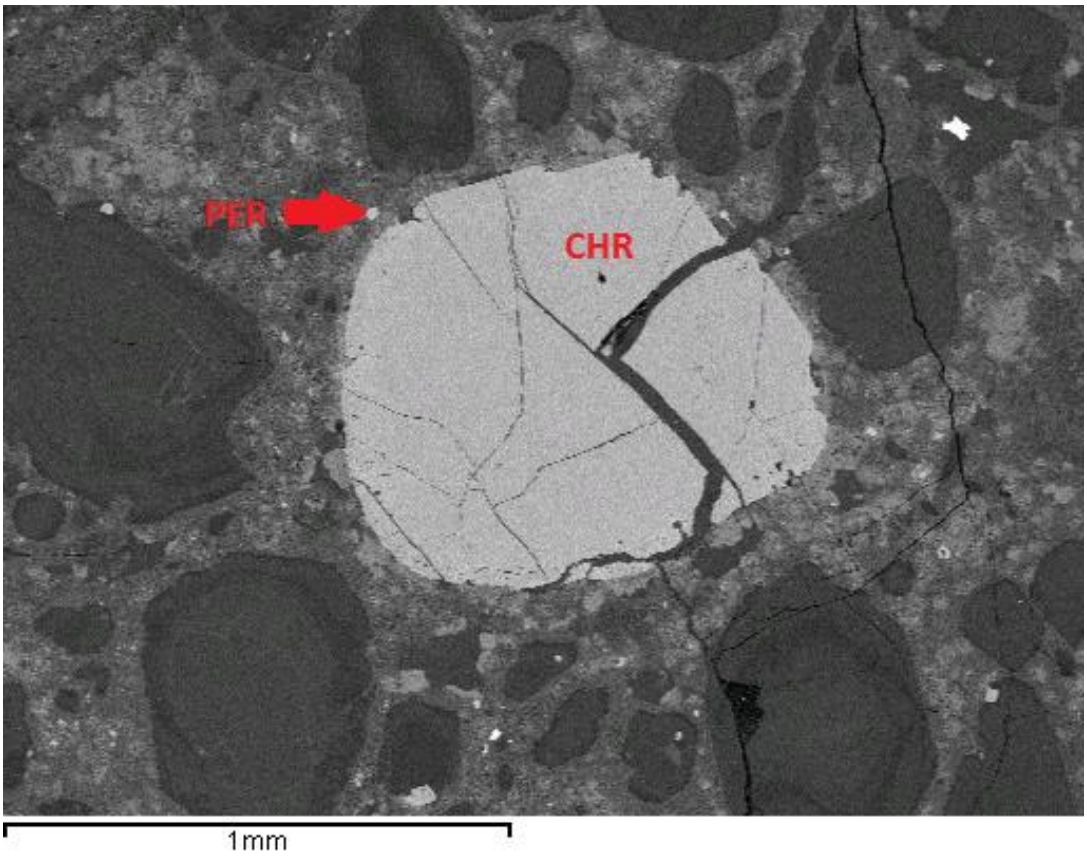

Figure 28 Back scattered electron image of sample EGR705 of the AK15 kimberlite displaying chromite macrocryst and proximal perovskite groundmass grain

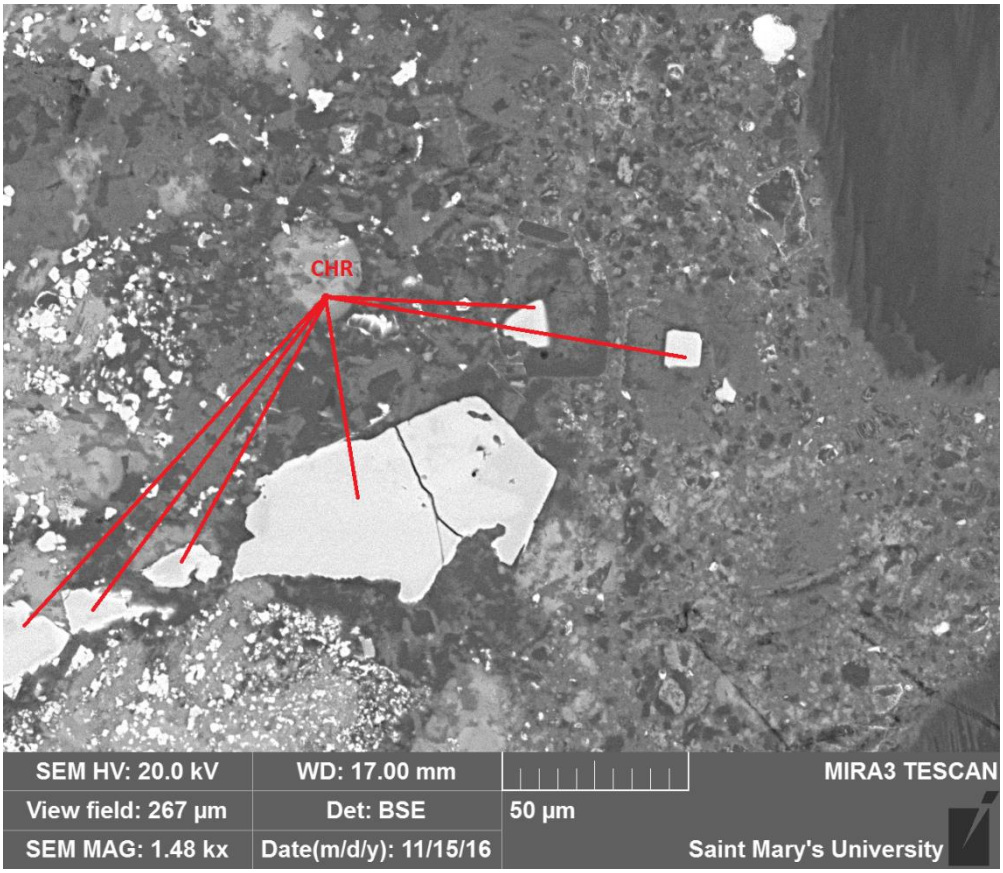

Figure 29 AK15 Back scattered electron image of sample EGR683 of the AK15 kimberlite displaying chromite macrocrysts

Ilmenite:

Ilmenite macrocrysts were not observed in the AK15 kimberlite, however it is present in small quantities within the groundmass. Grains similar to those observed in CKB were present. These grains, which while not showing any ilmenite, may be the alteration products of a grain which at one point was composed of ilmenite Fig. 30. These grains show a lamellar and orientated texture with a composition made up of perovskite and titaniferous magnetite. These grains also show the similar intergrown texture around grain rims observed in CKB.

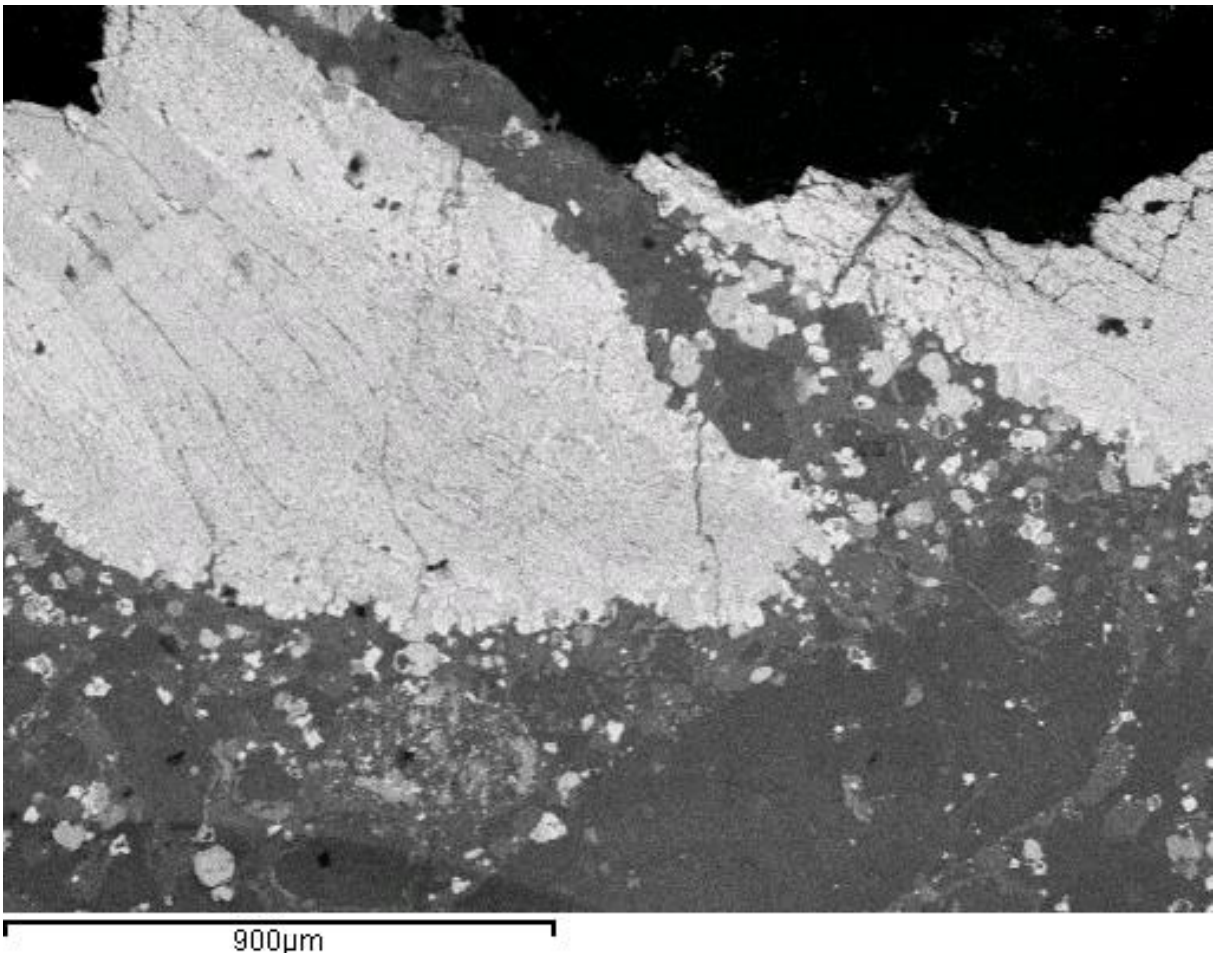

Figure 30 AK15 Back scattered electron image of sample EGR705 of the AK15 kimberlite displaying an ilmenite macrocryst showing symplectitic perovskite and magnetite alteration

Groundmass:

Within the groundmass of AK15, samples show subhedral, heavily zoned, perovskite grains which vary widely in size as seen in figure 31 and 32. Titanite also appears frequently in the groundmass of AK15 as subhedral grains. Magnetite is commonly found in the groundmass. Rutile appears within the groundmass as anhedral grains and is commonly observed in the rims of titanite grains. Ilmenite and chromite are also found in the groundmass in relatively low proportions.

Quantitative mineral abundancies corresponding to the area observed in figures 33.

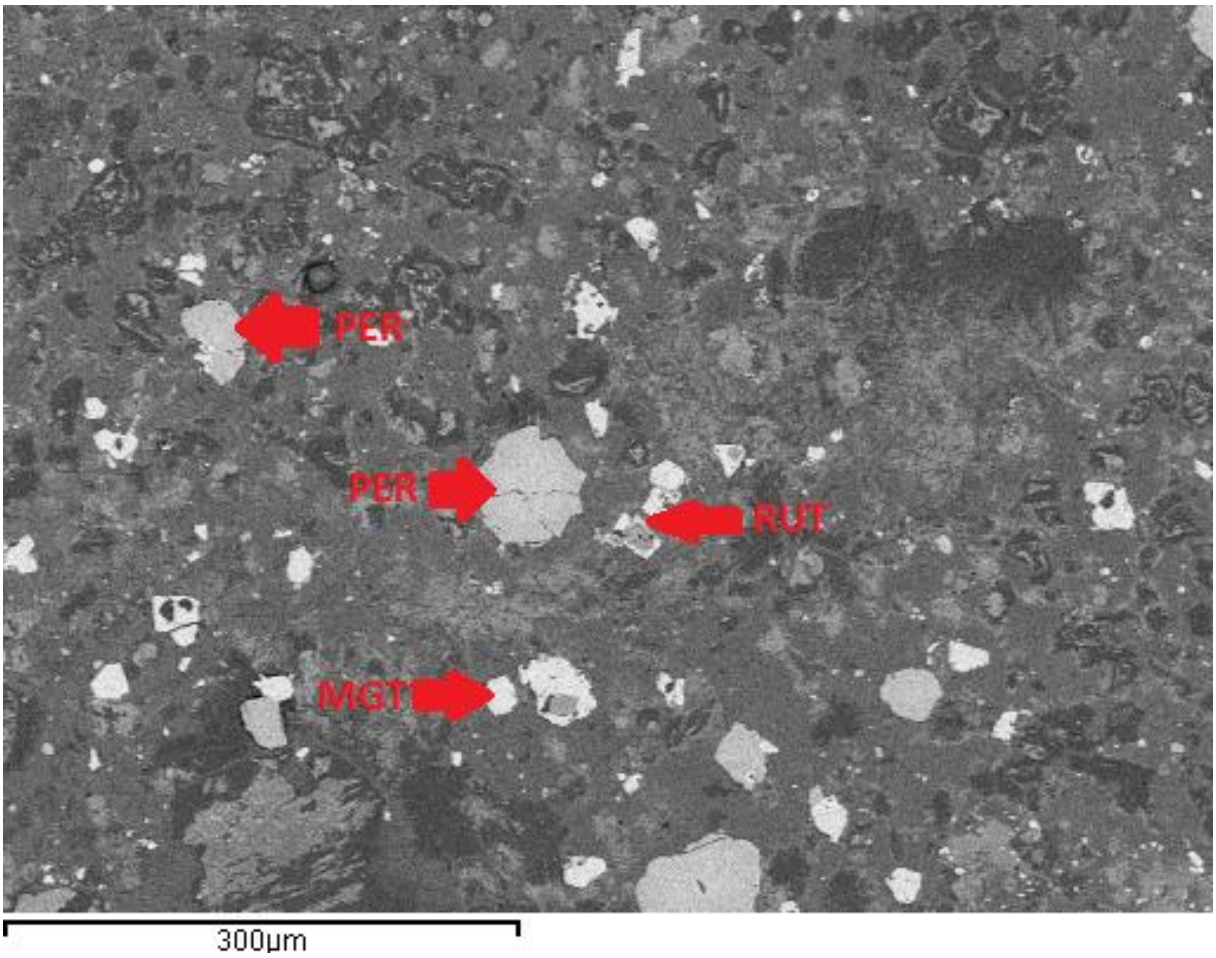

Figure 31 Back scattered electron image of sample EGR683 of the AK15 kimberlite showing groundmass mineralogy composed of predominantly perovskite magnetite and rutile

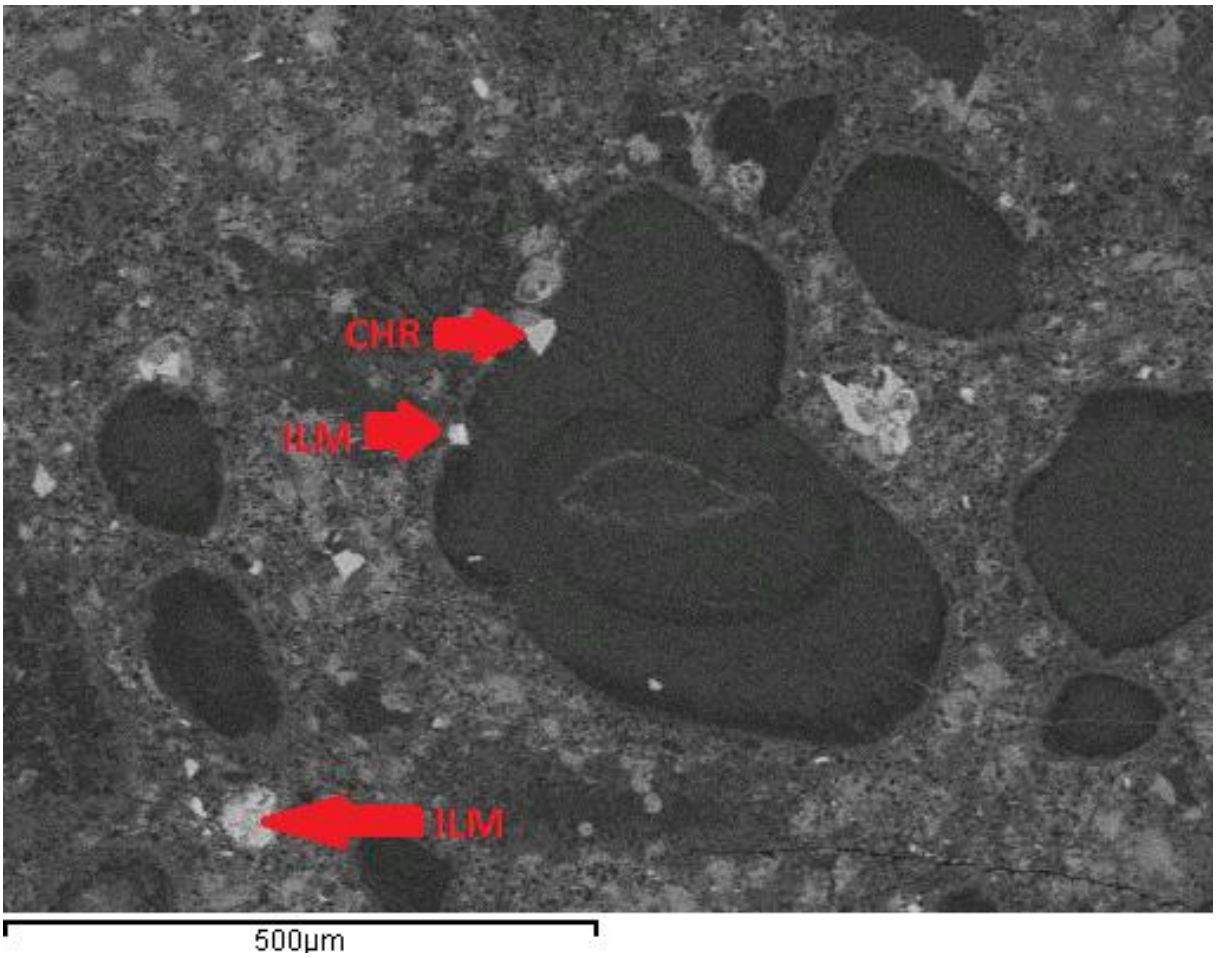

Figure 32 Back scattered electron image of sample EGR705 of the AK15 kimberlite showing groundmass mineralogy containing chromite and ilmenite

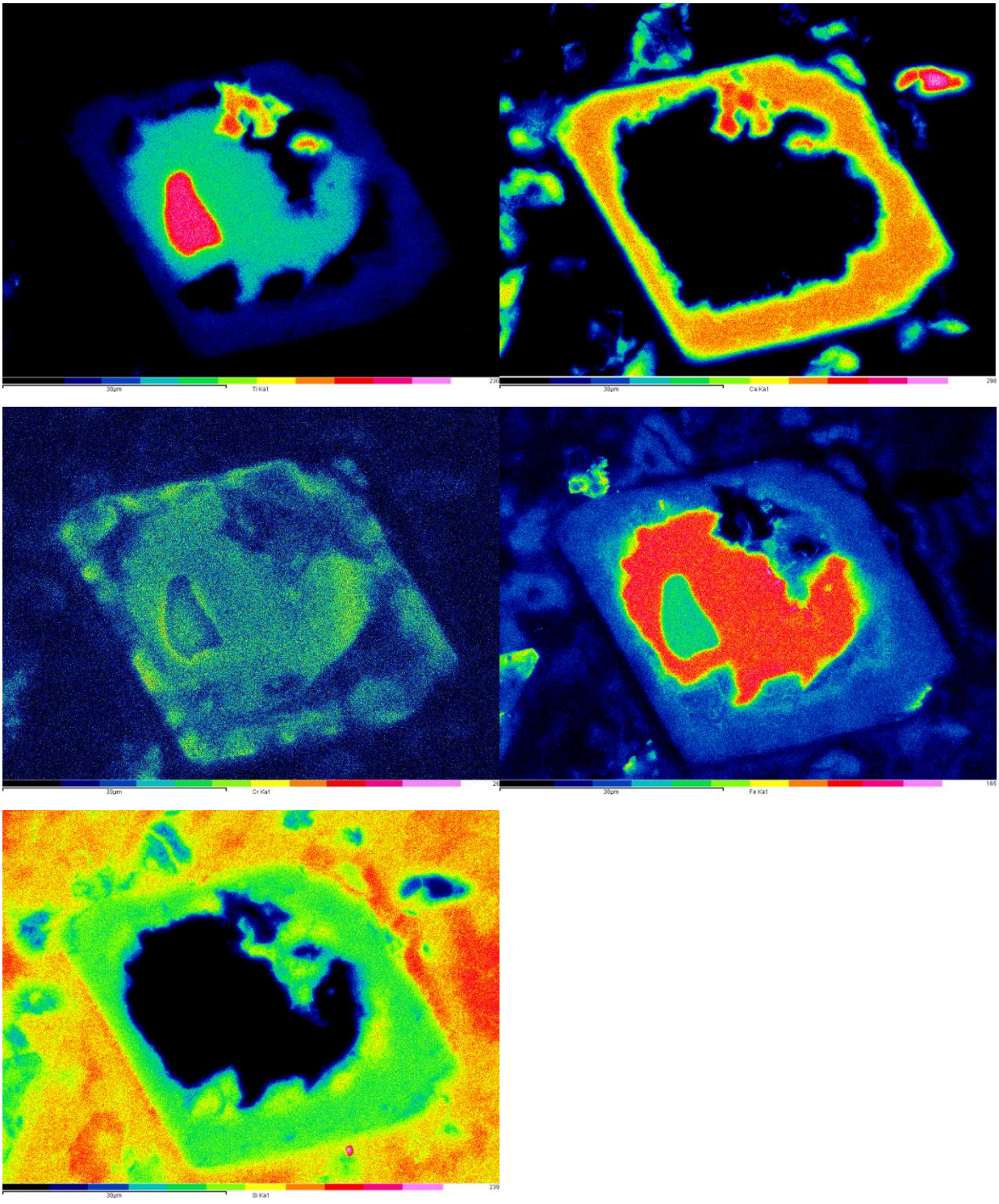

Figure 33 EDS elemental X-ray maps of EGR665 groundmass of the AK15 kimberlite showing Ti (upper left), Ca (upper right), Cr (middle left), Fe (middle right) and Si (bottom left) elemental abundancies

Variation with depth:

AK-15 macrocrysts show no variation with depth and chromite, ilmenite and perovskite are all found as macrocrysts through all depths sampled. Ilmenite macrocrysts are common and typically homogenous however those found in the transitional EGR683 show symplectitic texture with secondary magnetite and perovskite. Furthermore, secondary chromite, and magnetite are present in shallow samples with transitional and deep samples showing chromite perovskite and magnetite, and perovskite, rutile and magnetite respectively. Relic mineralogy is made up of titanite throughout all samples and relic ilmenite present in the deep and shallow samples but not in the transitional sample. The groundmass is homogenous and shows presence of chromite, perovskite rutile and magnetite in all samples.

Geochemical composition of BK01 and AK15 kimberlites

Composition of Chromite

Chromite compositions in all AK15 samples as well as all CKA samples is fairly concentrated towards $MgCr_2O_4$ as can be seen in figure 34 and 35. This indicates that these kimberlites are most similar to the Misery and Leslie kimberlites. These kimberlites appear to be following trend number 1, the Cr-Al trend, grading into more aluminous spinel. Furthermore, these kimberlites show very low Fe^{3+} and Fe^{2+} values which is similar to the Koala and Grizzly kimberlites.

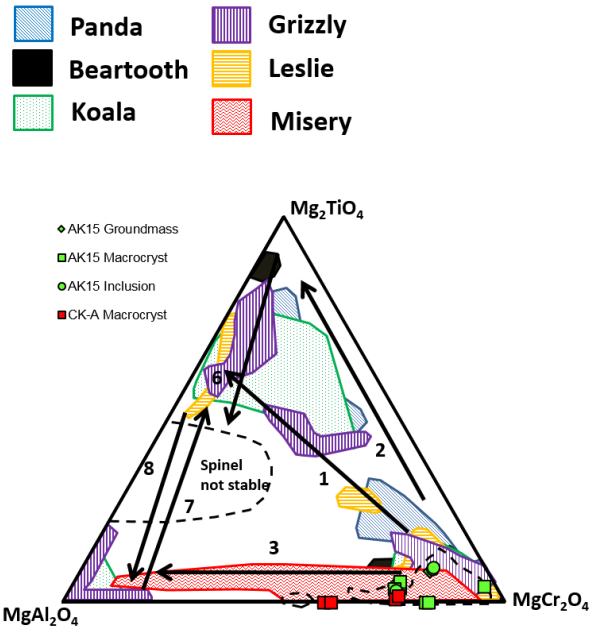

Figure 34 Spinel prism showing different trend lines and Ekati kimberlite zones, After (Kressall, 2016)

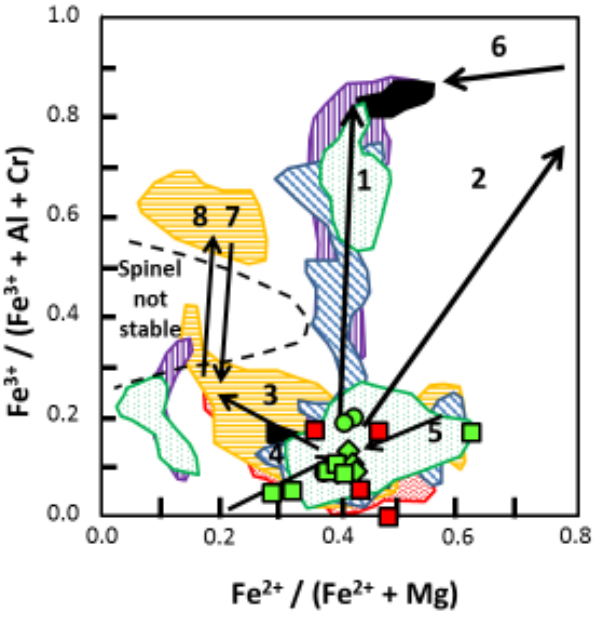

Figure 35. Spinel prism showing different trend lines and Ekati kimberlite zones, After (Kressall, 2016)

Figure 36 and 37 show plots of Cr-no vs Mg-no for both Ekati and Orapa Kimberlites. The data plots in the convergence point of the Cr Al trend and the FeTi trend. AK15 macrocryst, samples appear to follow the Fe-Ti trend fairly closely while CK-A macrocrysts, and AK15 groundmass and inclusions appear to follow the Cr-Al trend.

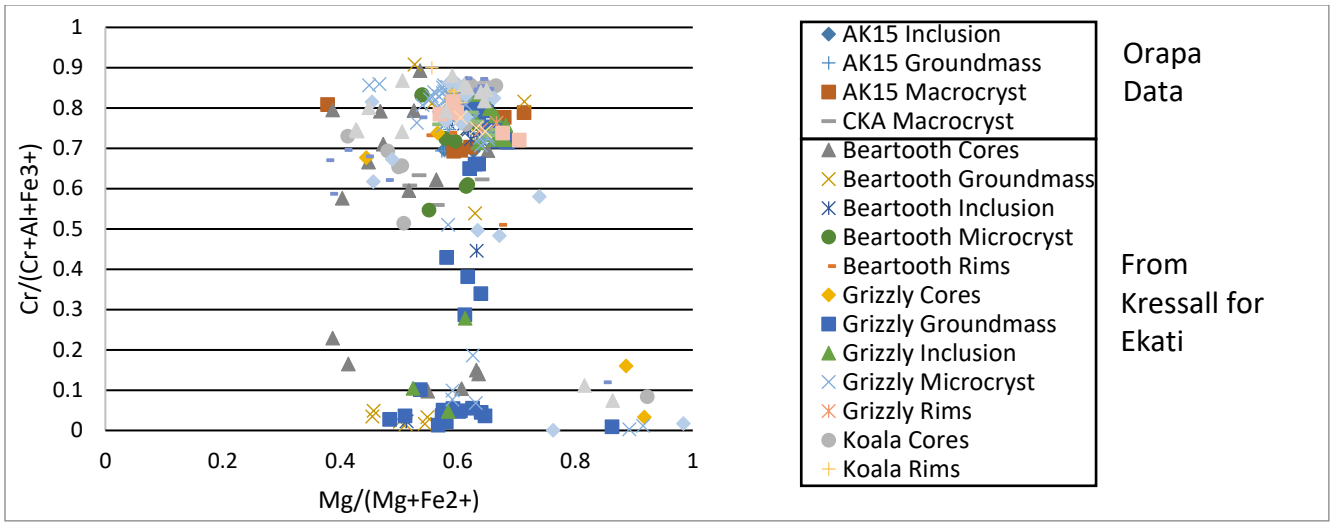

Figure 36. Chromite composition data displaying Cr-no vs Mg-no showing Ekati (from Kressall) kimberlite data as well as Orapa data

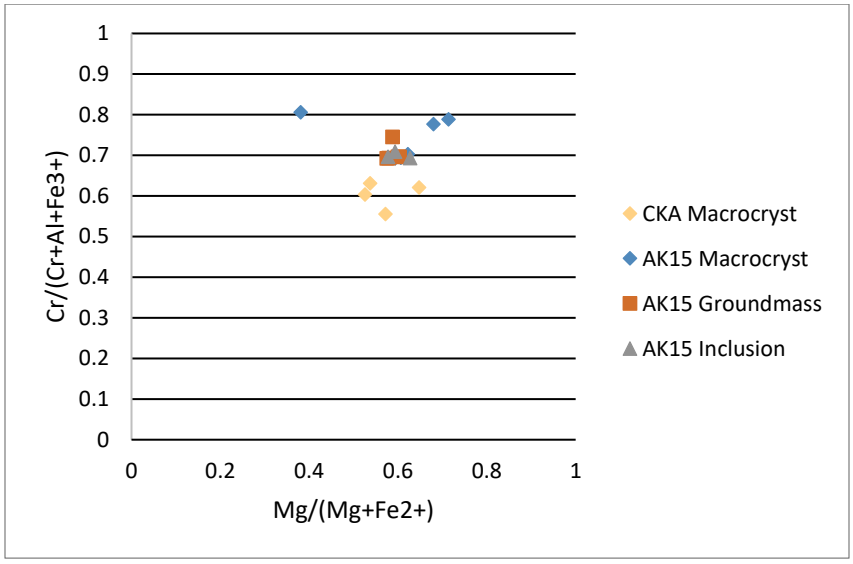

Figure 37. Cr-no vs Mg-no showing only Orapa kimberlite data

According to figure 38 and 39, TiO2 appears to be focused at around 0.2 wt% for both CK-A and AK15 chromite. The limited amount of data limits the ability to see trends however the upper CKA data point at 0.75 wt% TiO2 appear to conform to the top of the TiO2 wt% enrichment trend which can be seen in figure 34.

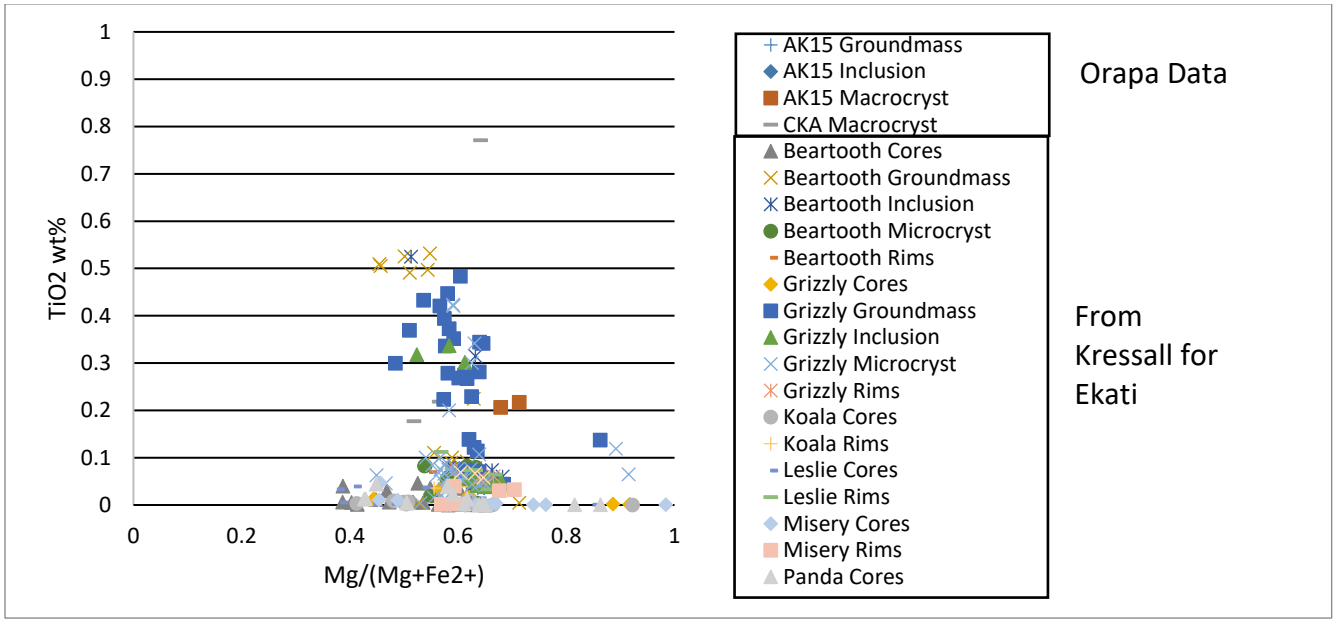

Figure 38. Chromite composition data displaying TiO2 wt% vs Mg-no showing Ekati kimberlite data (from Kressall) as well as Orapa data

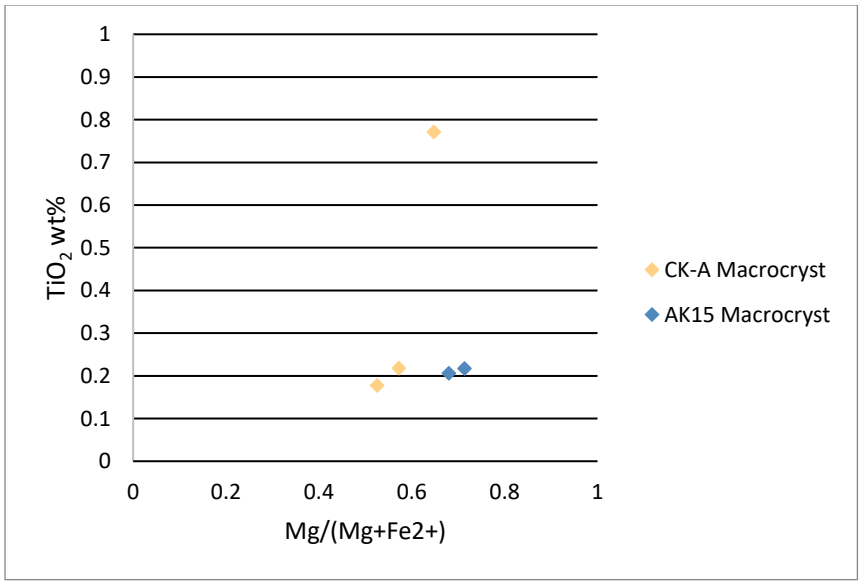

Figure 39 TiO2 wt% vs Mg-no showing Orapa data

As figure 40 and 41 indicate, the Orapa ilmenites found across all facies plot within the kimberlitic ilmenite field. Furthermore, these kimberlites show a very similar compositional trend to that of the ilmenites found in Ekati. There also appears to be little variation between facies and grain types in those facies. However, CKA macrocrysts tend to be the most depleted in Mg with MVK inclusion showing the most Mg enrichment.

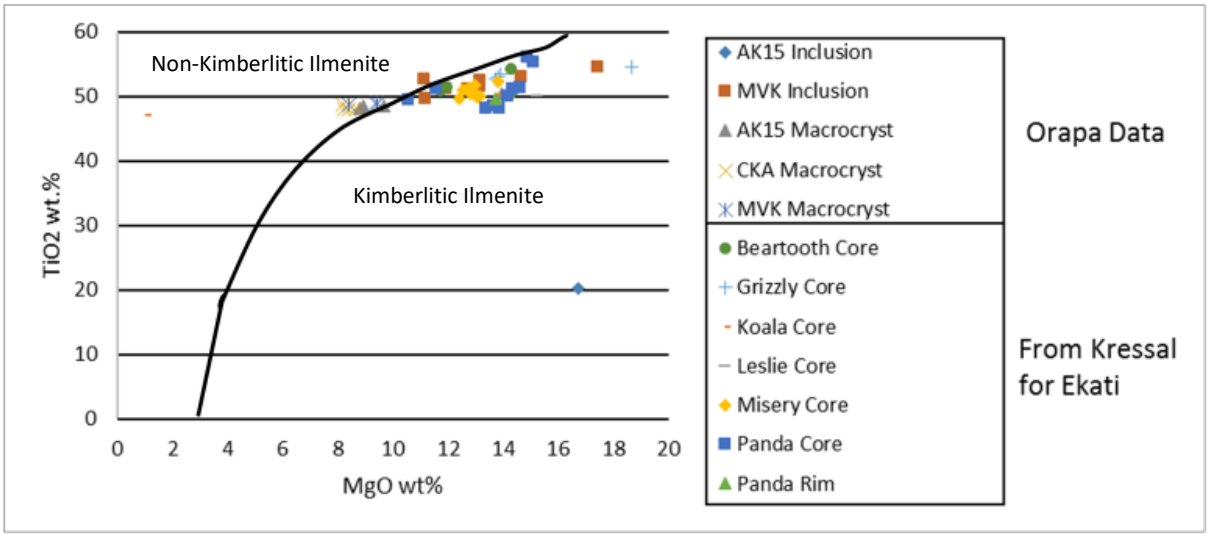

Figure 40. Ilmenite TiO2 wt% vs MgO 2t% for both Ekati and Orapa data

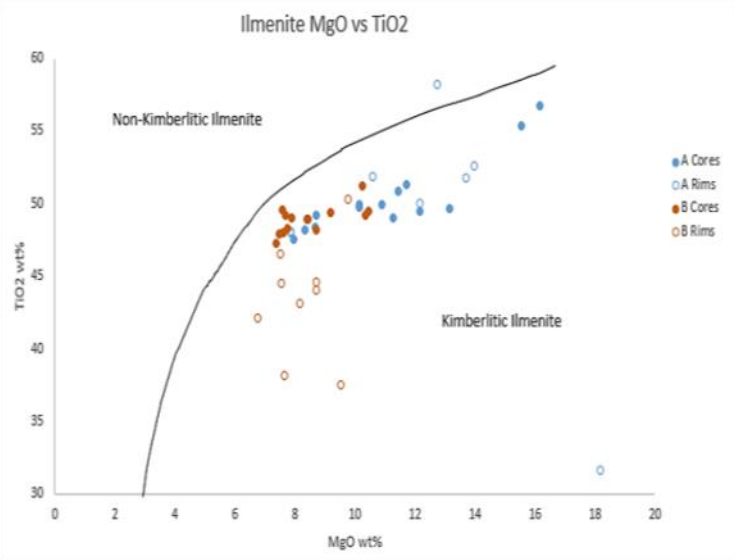

Figure 41 Ilmenite TiO2 wt% vs MgO 2t% for Orapa kimberlite data, figure from Milligan (2014)

Figures 42 and 43 show concentrated Cr values for all kimberlite facies. AK15 Macrocrysts indicate higher Cr proportions, with MVK inclusions also recording high, but more variable data. MVK and CKA macrocrysts show low Cr proportions.

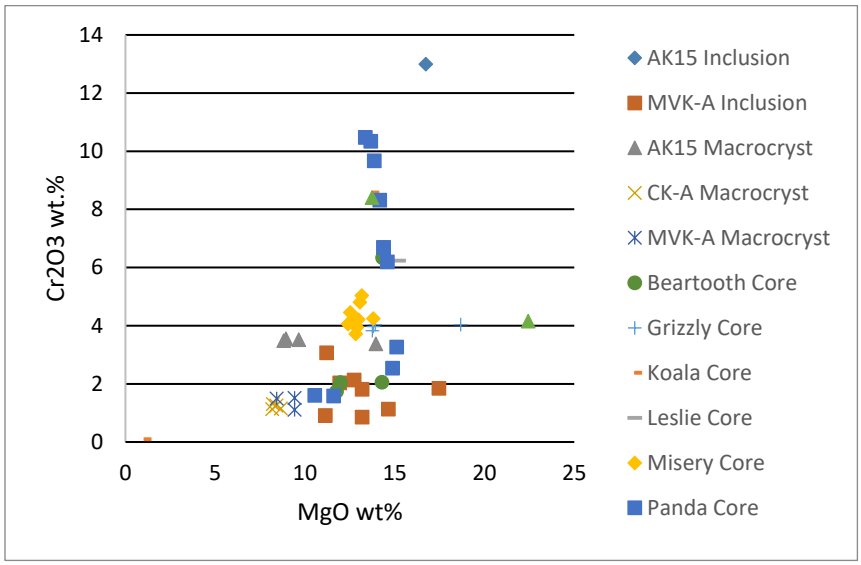

Figure 42 Ilmenite Cr2O3 wt% vs MgO2 wt% for both Ekati and Orapa data

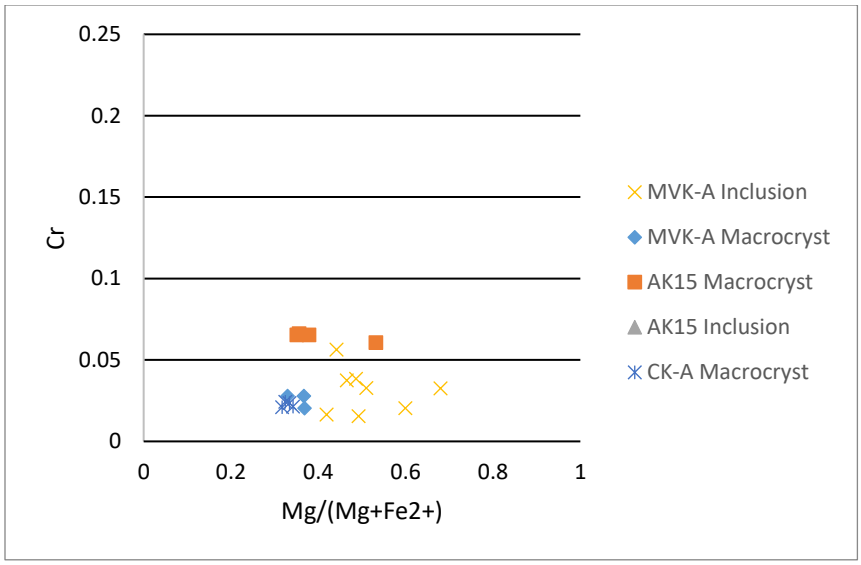

Figure 43. Ilmenite Cr Vs Mg-no for Orapa data

Figure 44 and 45 show that Macrocrysts for all MVK, AK15 and CK-A are enriched in Fe3+ compared to MVK inclusions. The corresponding inclusion data for these kimberlites show that Mg-no decreases dramatically for a comparably small decrease in Fe3+.

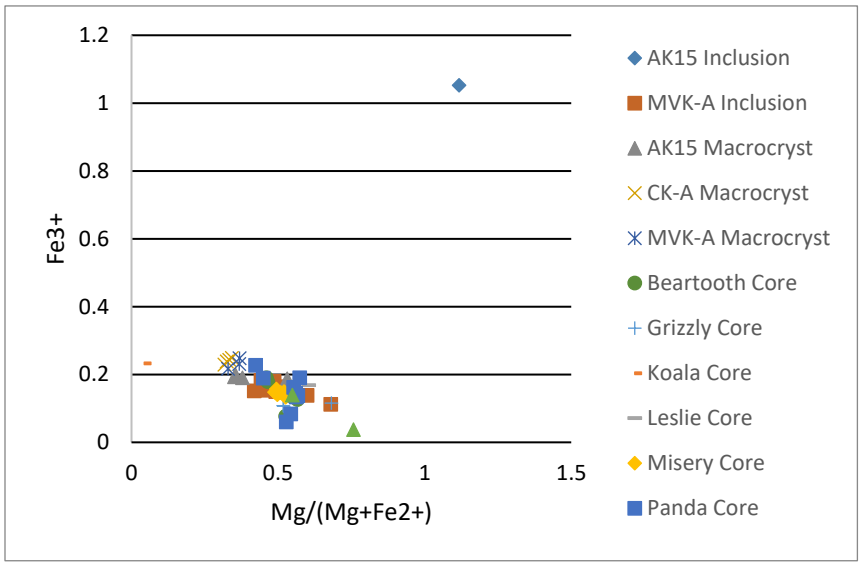

Figure 44 Ilmenite Fe3+ vs Mg-no for both Ekati and Orapa data

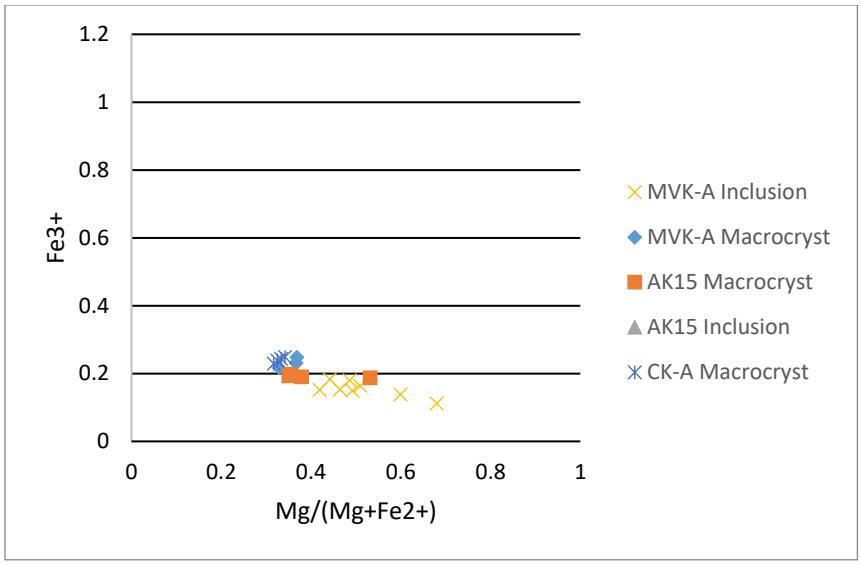

Figure 45 Ilmenite Fe3+ vs Mg-no for Orapa kimberlite data

Figure 46 and 47 show that Mn is quite variable in MVK inclusions while in the other data appears to be quite consistent. This is an indication that MVK inclusions are relatively enriched in Mn.

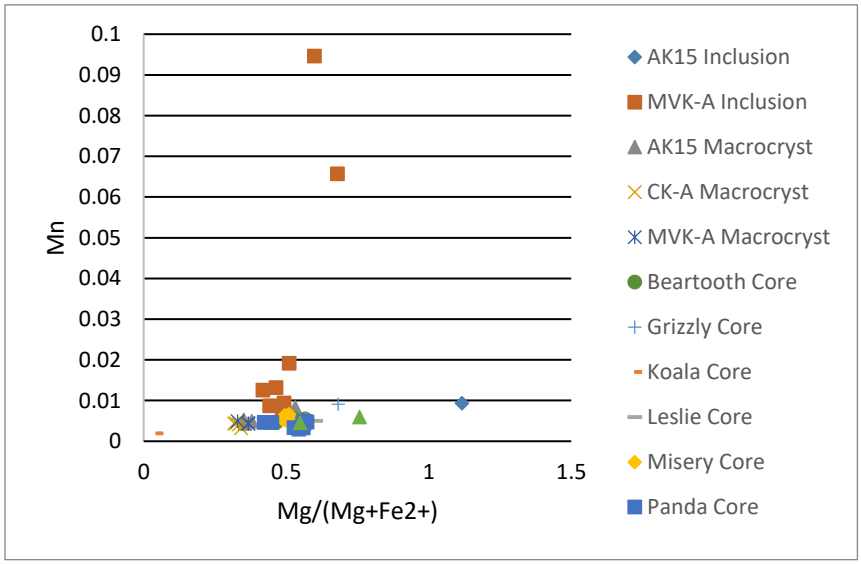

Figure 46. Ilmenite Mn vs Mg-no for Ekati and Orapa data

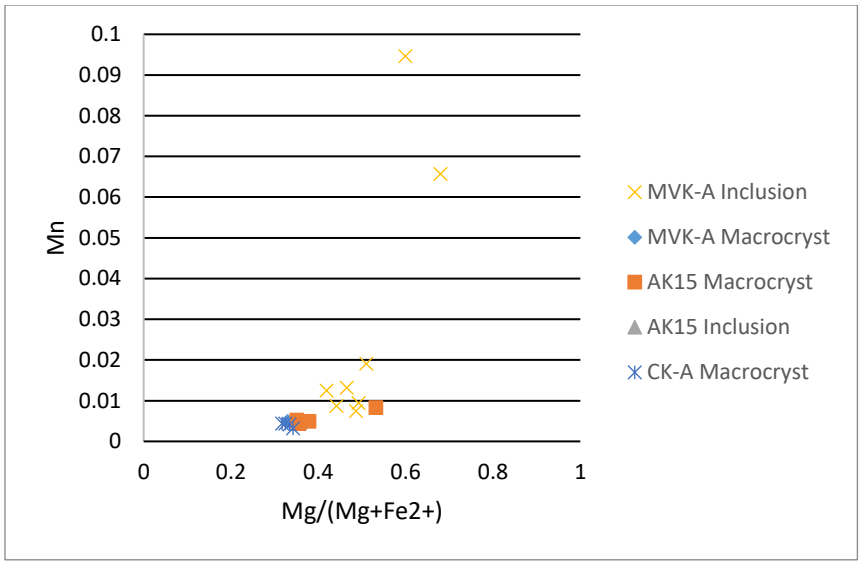

Figure 47. Ilmenite Mn vs Mg-no for Orapa data

Chapter 5: Discussion

Comparison of textural features and implications for crystallization

The BK01 and AK15 samples analyzed show similarities both in mineralogy as well as in the processes which and conditions under which they formed. Table 9 outlines the stable groundmass mineralogy found in each kimberlite facies, as well as oxide minerals found as inclusions in olivine crystals. Furthermore, tables 6, 7, 8 and 9 outline this information in terms of the changes in magmatic conditions throughout the crystallization process. With macrocryst, relic and secondary, and groundmass mineralogy indicating describing the rocks transition through different magmatic conditions with mineralogy changing accordingly. This in turn will alter the stability of different minerals already crystalized resulting in reactions occurring between these pre-existing minerals and the melt, as well as the crystallization of new mineral phases out of the melt. Across all kimberlite facies, Ilmenite macrocrysts are observed which are no longer in stable form. However, the method by which this instability is being adjusted for is not the same across all kimberlite facies. Similar reactions occur with chromite macrocrysts in CK-A and MVK, however this does not occur in CK-B or in AK-15 as in CK-B no chromite macrocrysts are present; all chromite has been completely reacted prior to the crystallization of the complete melt or never formed in the first place. In AK-15 chromite macrocrysts are difficult to distinguish because chromite is stable in the late phase of this kimberlite, therefore

it is stable in the groundmass just as the groundmass formed chromite and would not be actively reacting.

Table 6 Summary of Orapa kimberlite sample macrocryst mineralogy by depth sampled

Depth from (m)	Hole	Kimberlite	Facies	Sample	Mac. Chromite	Mac. Ilmenite	Mac. Per
56.16	NA	AK15	-	EGR665	X	X	X
98.48	NA	AK15	-	EGR683	X	X	X
151.7	NA	AK15	-	EGR705	X	X	X
18.29	H003	BK1	CK-A	EGK637	X	X	
34.53	H002	BK1	CK-A	EGK567		X	
36.7	H002	BK1	CK-A	EGK568		X	
40.78	H002	BK1	CK-A	EGK569	X	X	
42.74	H002	BK1	CK-A	EGK570		X	
NA	H004	BK1	CK-B	EGK619		X	
NA	H004	BK1	CK-B	EGK627		X	
NA	H004	BK1	CK-B	EGK634		X	
45.65	H003	BK1	MVK-A	EGK641	X	X	
50.41	H002	BK1	MVK-A	EGK571		X	
54.33	H002	BK1	MVK-A	EGK572			
124.41	H003	BK1	MVK-A	EGK648		X	

Table 7 Summary of Orapa kimberlite sample secondary (denoting minerals indicating growth after primary crystallization which remain in stable form) mineralogy by depth sampled

Depth from (m)	Hole	Kimberlite	Facies	Sample	Sec. Chr	Sec. Ilm	Sec. Tit	Sec. Per	Sec. Rut	Sec. Mag
56.16	NA	AK15	-	EGR665	X					X
98.48	NA	AK15	-	EGR683	X			X		X
151.7	NA	AK15	-	EGR705					X	X
18.29	H003	BK1	CK-A	EGK637			X			X
34.53	H002	BK1	CK-A	EGK567					X	X
36.7	H002	BK1	CK-A	EGK568					X	X
40.78	H002	BK1	CK-A	EGK569					X	X
42.74	H002	BK1	CK-A	EGK570				X		
NA	H004	BK1	CK-B	EGK619				X		X
NA	H004	BK1	CK-B	EGK627				X		X
NA	H004	BK1	CK-B	EGK634				X		X
45.65	H003	BK1	MVK-A	EGK641				X		X
50.41	H002	BK1	MVK-A	EGK571				X	X	X

54.33	H002	BK1	MVK-A	EGK572						X
124.41	H003	BK1	MVK-A	EGK648				X		X

Table 8 Summary of Orapa kimberlite sample relic (denoting minerals indicating growth after primary crystallization which are no longer in stable form) mineralogy by depth sampled

Depth from (m)	Hole	Kimberlite	Facies	Sample	Rel. Chr	Rel. Ilm	Rel. Tit	Rel. Per	Rel. Rut	Rel. Mag
56.16	NA	AK15	-	EGR665		X	X			
98.48	NA	AK15	-	EGR683			X			
151.7	NA	AK15	-	EGR705		X	X			
18.29	H003	BK1	CK-A	EGK637	X	X			X	
34.53	H002	BK1	CK-A	EGK567						
36.7	H002	BK1	CK-A	EGK568						
40.78	H002	BK1	CK-A	EGK569						
42.74	H002	BK1	CK-A	EGK570			X			
NA	H004	BK1	CK-B	EGK619			X			
NA	H004	BK1	CK-B	EGK627			X			
NA	H004	BK1	CK-B	EGK634						
45.65	H003	BK1	MVK-A	EGK641		X	X		X	
50.41	H002	BK1	MVK-A	EGK571			X			
54.33	H002	BK1	MVK-A	EGK572						
124.41	H003	BK1	MVK-A	EGK648			X			

Table 9 Summary of Orapa kimberlite sample groundmass mineralogy by depth sampled

Depth from (m)	Hole	Kimberlite	Facies	Sample	GM Chr	GM Ilm	GM Tit	GM Per	GM Rut	GM Mag
56.16	NA	AK15	-	EGR665	X			X	X	X
98.48	NA	AK15	-	EGR683	X			X		X
151.7	NA	AK15	-	EGR705	X			X	X	X
18.29	H003	BK1	CK-A	EGK637			X			X
34.53	H002	BK1	CK-A	EGK567					X	X
36.7	H002	BK1	CK-A	EGK568						X
40.78	H002	BK1	CK-A	EGK569						X
42.74	H002	BK1	CK-A	EGK570			X			X
NA	H004	BK1	CK-B	EGK619	X			X		X
NA	H004	BK1	CK-B	EGK627	X			X		X
NA	H004	BK1	CK-B	EGK634				X		X
45.65	H003	BK1	MVK-A	EGK641				X		X
50.41	H002	BK1	MVK-A	EGK571						
54.33	H002	BK1	MVK-A	EGK572						
124.41	H003	BK1	MVK-A	EGK648	X					X

Ilmenite macrocrysts actively reacting in the BK01 and AK15 kimberlites differ in the way they are re-equilibrating with their surroundings. This variation is the result of a different set of changes occurring to stability conditions within the kimberlite bodies. Textures and inferred processes observed in ilmenite grains are similar in CKA-MVK and in AK15-CKB.

In MVK and CKA it is apparent that macrocrysts are undergoing active dissolution. These grains show distinct embayment along grain boundaries. This texture is characterized by bay like sections in the crystal as a result of resorption and is known to be a form of disequilibrium texture (Winter J. D., 2001). In MVK ilmenites are dissolved but show substitution by magnetite throughout, mostly around the margins and occasionally into the

ilmenite. In CKA however, magnetite is crystalizing on top of the ilmenite. Furthermore, in both MVK and CKA titanite is observed crystalizing on top of the grain. This indicates that ilmenite is being dissolved very quickly by whichever medium is reacting with it, be it melt of fluid. Moreover, the medium surrounding the ilmenite grain will be taking in the components of the mineral and over time will become over saturated in titanium and as a result will begin to crystalize the titanite observed in the samples. There is variation in how magnetite behaves in CKA and MVK as in MVK magnetite is forms small margins and rims around ilmenite whereas in CKA magnetite is crystalizing into much more euhedral grains on top of ilmenite. This indicates that in MVK magnetite is simply being substituted while in CKA dissolution is occurring much more quickly. Therefore, the fluid around ilmenite grains in CKA will become enriched in iron much faster than in MVK, resulting in the development of more euhedral magnetite grains.

In contrast to MVK and CKA, in CKB and AK15 Ilmenite macrocrysts have completely reacted. There is not active dissolution occurring between ilmenite macrocrysts and the surrounding rock. Instead, the symplectitic texture observed in the AK15 and CKB ilmenites reflects the instability of ilmenite resulting in the breakdown of the mineral into the perovskite and magnetite. These grid like intergrowths of perovskite and magnetite are developed in response to decreasing pressure and temperature conditions, typically as a do to uplift of the rock package. This process is associated with local diffusive transmission of material between reactants (Winter J. D., 2001).

In CKA and MVK, Chromite behaves similarly to ilmenite in MVK and CKA. Chromite macrocrysts show similar embayed textures to those observed in ilmenite grains, however the reaction products of these grains are different. These grains show similar euhedral grains to the magnetite grains observed in CKA. Therefore, it is expected that in MVK and CKA the substitution by dissolution of chromite to form titanite is occurring. In AK15 however chromite behaves differently, chromite grains show zonation. Typically, a macrocrysts will not be in equilibrium with the melt as it is foreign to it. Therefore, a number of processes may occur which will attempt to re-equilibrate the mineral by some type of reaction. Dissolution may occur through the disintegration of the minerals crystal structure. Reaction will occure when a grain will readjust and change its composition according to that of the melt it is introduced into.

In order for this to happen the mineral phase will need to be stable in the melt. This will result in zoning occurring around the grain. The mineral will readjust to the melt it is introduced to but will remain intact as it is still stable under these conditions, the composition will simply change slightly. AK15 has abundant chromite in the groundmass and it stands to reason that chromite would be a stable phase in this kimberlite. Them mineral is not dissolving it is simply changing the composition of the grain which is manifested as the zoning observed in AK15 chromite grains.

Perovskite is not abundant in all of these kimberlite bodies and is predominantly found as a reaction product. However, it is significant that in MVK, the perovskite's composition shows a very small proportion of rare earth elements and there is relatively high niobium content. Conversely, in AK15, where perovskite is found as large heavily zoned macrocrysts there is a large amount of variation in rare earth element content. These grains show some zones which are significantly enriched in cerium and some that have depleted rare earth element signature only showing small proportions of niobium as well as entire different grains which have a high cerium content. Rare earth elements are commonly associated with mineralization from a fluid as opposed to a melt source. Therefore, the perovskite mineralization with high rare earth element signatures can be attributed to mineralization from a fluid source in presumably later stages of crystallization. In contrast, mineralization with low rare earth element signatures can be attributed to mineralization out of melt and therefore should have predominantly occurred at an earlier stage in crystallization.

Silica Activity and Implication for diamond preservation

Given the nature of these crystallization reactions it is possible to interpret the cooling history of these kimberlite by observing changes in mineral phase interactions within each kimberlite facies. By looking at the variability in abundances of certain minerals as well as the texture and alterations of these minerals developmental constraints can be placed on the magmatic history of the kimberlite samples.

Firstly, as H_2O and CO_2 solubility are associated with changes in the nature of emplacement of kimberlite pipes, if the relative abundance of these volatiles is known or can

be determined a model for emplacement can be deduced. This relationship stems from the degassing mechanisms which are widely accepted as the main driving factor in the movement of kimberlite magma from mantle to crust. Volatile content in kimberlites is controlled by the relative variability of pressure, temperature and silica content within a melt. With higher pressures and temperatures increasing the amount of volatiles contained in a melt. This means that as magma rises and expands adiabatic cooling will ensue and combined with decreasing pressure will result in degassing. (Moussallam, Morizet, Massuyeau, Laumonier, & Gaillard, 2015). Additionally, the amount of silica content is known to influence the nature of degassing in melts. That is to say that within melts containing low amounts of silica degassing will occur abruptly in bulk. This can occur when the melt has a high water content or is enriched in silica. In contrast a CO_2 rich, H_2O poor or silica poor melt will follow a much more gradual, relatively linear, degassing trend. (Mitchell R. , 1973)

Furthermore, the relative abundance of these volatiles in a melt can be determined by observing the dissolution features which appear on chromite grains. In an H_2O scheme it is typical to see chromite with smooth and rounded surface features when in a water under saturated melt while chromite in a water saturated melt will show much more angular features. CO_2 systems tend to show chromite features made up of irregular features such as polyhedrons and knobs. This is consistent with the standard kimberlite model which typically shows an H_2O-CO_2 ratio which is quite low. The same processes which result in these corrosive features in chromite are expected to affect diamonds and as such the features observed on chromites can be used as proxies to model the degree of preservation in diamonds. This is because preservation tends to increase in high free fluid systems.

Another significant relationship affecting kimberlite morphology is that of the perovskite titanite buffer. The two minerals possess very similar chemical formulas, the only difference being the addition of a silica tetrahedral in titanite. Therefore, the relative abundances of these minerals can give indications of the amount of silica activity occurring in the melt, with higher proportions of titanite indicating higher degree of crustal assimilation and a lack of titanite pointing to a lack of crustal assimilation.

With the mineralogical data obtained from SEM analysis it is clear that the degree of crustal assimilation in CK-B is quite low as titanite was only found in the groundmass and not as macrocrysts or as rims around macrocrysts. AK15 shows moderate amount of assimilation with slightly higher amounts of titanite found in the groundmass. Lastly CK-A and MVK show a fairly high amount of crustal assimilation as seen by the presence of large quantities of titanite throughout. Furthermore, in MVK and CK-A grains commonly show zoning of perovskite and titanite, indicating an influx of silica which would crystalize, titanite as well as the halting of titanite crystallization in favour of perovskite crystallization marking the terminus of silicate crystallization. Furthermore, the chromites observed show an angular/stepped nature within MVK and CK-A indicating an aqueus fluid phase. In contrast CK-B and AK15 lack chromite macrocrysts which can be interpreted as evidence of the corrosive nature of the fluids which may have fully dissolved the chromite grains which would typically be expected in rocks of this type. Lastly, the presence of carbonate in such high proportions as well as the wormy textures observed in chromites indicate that all kimberlite facies can be characterized as having low amounts of dissolved CO_2.

Oxide Geothermometers and Oxygen Barometers

Various thermochemical models exist which use variations in composition of solid solution minerals to determine various thermodynamical parameters. Of these models, the most widely used is the system put in place by Buddington & Lindsley in 1964. The basis of this model stems from the exchange equlibrium of Fe^{2+} & Ti between the spinel group solid solution Ulvospinel-Magnetite assemblage and rhombohedral oxide structure Ilmenite-Hematite assemblege. Meaning that the composition of these two different solid solution assemblegas are linked to each other by the thermodynamical conditions under which they form.

Llmenite-magnetite geothermometry

The ILMAT: A Magnetite-Ilmenite Geothermobarometry Program (version 1.20) excel file was used for calcualtions. This worksheet compliles several models for calculating Ulvospinel-Magnetite and Ilmenite-Hematite molar compositions aswell as estimations of fO_2 and temperature. All microporbe data for which both the ilmenite-hematite and ulvospinel-

magnetite grains were present for the same facies and stage in crystalization. Table 10 shows the calculated molar proportions for all micropobe data available. Note that the model put forth by Anderson (1968) results in negative values for ulvospinel composition, therefore these results were omitted from the remainder of the analysis.

Table 10 Molar ilmenite-hematite and ulvospinel-magnetite compositions for MVK inclusions and AK15 Macrocrysts using ILMAT worksheet.

MVK Inclusion				
Calculation Method	Carmichael (1967)	Anderson (1968)	Lindsley & Spencer (1982)	Stormer (1983)
AVG Mol %Ilm	90	84	92	89
AVG Mol % Usp	41	-27	13	10
AK15 Macrocryst				
Calculation Method	Carmichael (1967)	Anderson (1968)	Lindsley & Spencer (1982)	Stormer (1983)
AVG Mol % Ilm	86	83	89	87
AVG Mol % Usp	43	-21	41	63

Ilmenite-hematite and ulvospinel-magnetite compositions for MVK inclusions and AK15 Macrocrysts were plotted according to two graphical models for Fe-Ti oxide geothermometers and oxygen barometers; Andersen and Lindsley (1988) and Ghiorso and Sack (1991) to obtain figures 48 and 49 and table 11. Using this information, table 12 was made up to compile all fugacity and temperature data.

Table 11. Legend used for Andersen and Lindsley (1988) and Ghiorso and Sack (1991) geothermometers and oxygen barometers

Model Used	Carmichael (1967)	Lindsley & Spencer (1982)	Stormer (1983)
MVK Inclusion	**1**	**3**	**4**
AK15 Macrocrysts	**1**	**3**	**4**

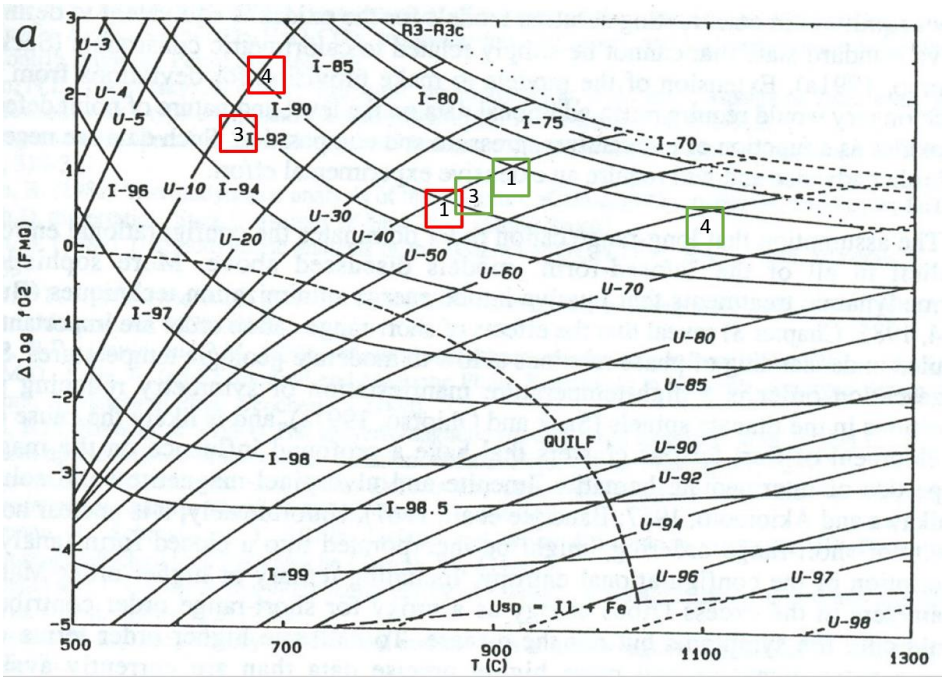

Figure 48. Andersen and Lindsley (1988) graphical geothermometer and oxygen barometer

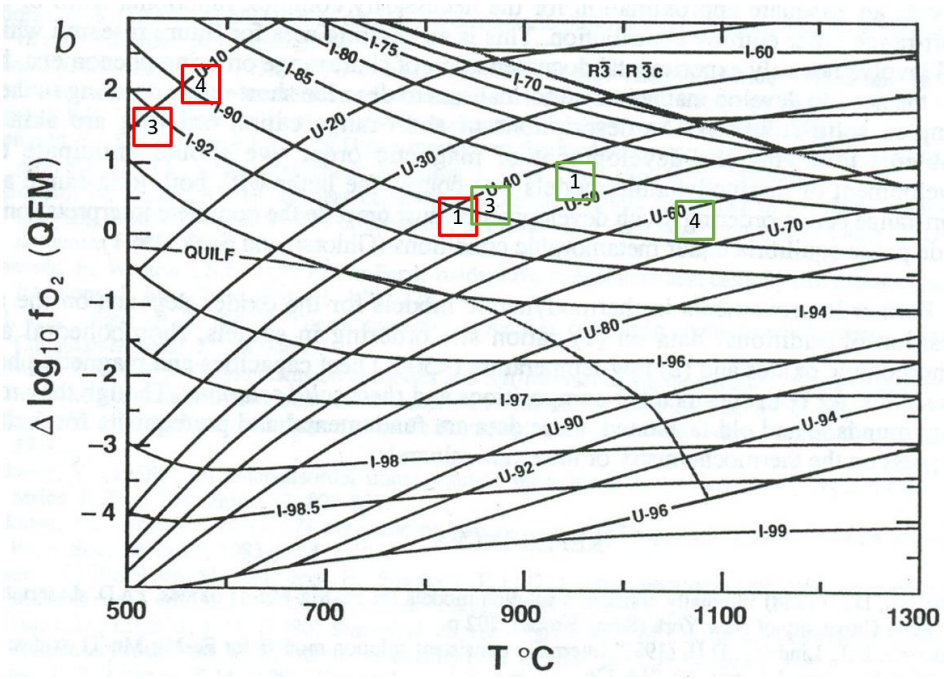

Figure 49. Ghiorso and Sack (1991) geothermometer and oxygen barometer

Table 12. fO2 and temperature data for each kimberlite facies and compositional model used

Grain Type	Geothermometry/ Oxygen barometry model used	Carmichael (1967) Composition Model		Lindsley & Spencer (1982) Composition Model		Stormer (1983) Composition Model	
		$\Delta \log fO_2\ QFM$	T (°C)	$\Delta \log fO_2\ QFM$	T (°C)	$\Delta \log fO_2\ \ QFM$	T (°C)
MVK Inclusion	Andersen and Lindsley (1988)	0.5	875	1.50	625	2.25	675
MVK Inclusion	Ghiorso and Sack (1991)	0.25	825	1.5	525	2	575
AK15 Macrocrysts	Andersen and Lindsley (1988)	1.00	925	0.5	875	0.25	1100
AK15 Macrocrysts	Ghiorso and Sack (1991)	0.75	950	0.25	850	0.25	1075

Table 13 shows average $\Delta \log fO_2$ and Temperature (°C) values for all models used. Temperature values appear to be low in MVK inclusions at 683°C as these minerals would have crystalized during at the same time or before olivine was crystalizing meaning that the values should be above 1200°C. Temperature values for AK15 macrocrysts are more plausible but they are still quite low. $\Delta \log fO_2$ values appear to be adequate as they are relatively low, this indicates that both kimberlite pipes have relatively reducing conditions which is to be expected as both of these kimberlites show diamonds which are well preserved. This would not be the case if conditions were oxidising as diamonds would also oxidize leading to poorer diamond preservation.

Table 13. Averaged fO2 and temperature data for each kimberlite facies

Grain Type	Average $\Delta \log fO_2$QFM	Average Temperature (°C)
MVK Inclusion	1.33	683
AK15 Macrocrysts	0.50	963

Chapter 6: Conclusions

Variations in the amount of crustal assimilation in kimberlite magmas can have significant impacts on their crystallization. Data compiled from microscopic, SEM and EMPA analysis of the BK01 kimberlite composed of coherent kimberlite CK-A and CK-B, and a volcanoclastic phase MVK, as well as coherent kimberlite AK15 indicate that there are variations between the kimberlite facies. These variations although slight show that variations in crustal assimilation between kimberlite bodies led to differences in amounts of volatile content ultimately impacting the diamond preservation potential of the deposits. The coherent CK-B facies which makes up the northern lobe of the BK01 kimberlite complex indicates that a low amount of silica activity as a result of reduced crustal assimilation led to higher critical degassing pressure and temperature conditions. This decreased the free fluid phase of the melt and increased diamond dissolution resulting in the corrosive features which can be observed in the diamonds sourced from these kimberlite facies. This is further supported by geothermometry and oxygen barometry calculations which show that reducing conditions are found in MVK and AK15. Further research on the subject should focus on analyzing larger sample size which would allow for more accurate and more thorough analysis and calculations. Additionally, in order to achieve amore quantitative interpretation of the petrogenesis of these kimberlites a Phase Equilibrium model should be composed. This would allow for the determination of crystallization sequences for all minerals in absolute thermodynamic terms.

References

Barnes, S. J., & Roeder, P. L. (2001). The range of spinel compositions in terrestrial mafic and ultramafic rocks. *Journal of petrology, 42*(12), 2279-2302. Retrieved December 2016

Buddington, A. F., & Lindsley, D. H. (1964). *Iron-Titanium Oxide Minerals and Synthetic Equivalents.* Washington: Carnegie Institution of Washington.

Chinn, I. (2013, January). AK15 Kimberlite notes for Yana.

Chinn, I. (2013, January). BK1 Kimberlite notes for Yana.

Creighton, S., Stachel, T., Matveev, S., Hofer, H., McCammon, C., & Luth, R. (2009). Oxidation of the Kaapvaal lithospheric mantle. *Contributions to Mineral Petrology*, 491-504.

Dreibus, G., Brey, G. P., & Girnis, A. V. (1995). The role of carbon dioxide in the generaton and emplacement of kimberlite magmas: new eperimental data on CO2 solubility. *International Kimberlite Conference*, 80-82.

Fedortchouk, Y., Matveev, S., & Carlson, J. A. (2010, January 2010). H2O and CO2in kimberliticfluid as recorded by diamonds and olivines in severalEkati Diamond Mine kimberlites, Northwest Territories, Canada. (R. Carlson, Ed.) *Earth and Planetary Science Letters, 289*(3-4), 549-559. Retrieved 2016

Field, M., & Scott Smith, B. (1999). Contrasting Geology and Near-Surface Emplacement of Kimberlite Pipes in Southern Africa and Canada. *Proceedings of the 7th International Kimberlite Conference*, 214-237.

Henry, D., & Goodge, J. (2013). *Wavelength-Dispersive X-Ray Spectroscopy (WDS)*. Retrieved from Geochemical Instrumentation and Analysis: http://serc.carleton.edu/research_education/geochemsheets/wds.html

Kopylova, M. (2016, August). Petrography of AK and BK Orapa Kimberlites-2.

Kressall, R. (2016). Dissolution of mantle minerals in kimberlite magmas and modeling of emplacement conditions of kimberlite magma. *Unpublished*.

Lepage, L. D. (2003). ILMAT: an Excel worksheet for ilmenite–magnetite. *Computers & Geosciences*, 673-678.

Lindsley, D. H. (1991). *Oxide minerals: petrologic and magnetic significance.* Stony Brook: Mineralogical Societey of America.

Mitchell, R. (1973). Composition of olivine, silica activity and oxygen fugacity in kimberlite. *Lithos*.

Mitchell, R. H. (1973). Magnesian Ilmenite and its Role in Kimberlite Petrogenesis. *The Journal of Geology, 81*(3), 301-311.

Mitchell, R. H. (1986). *Kimberlites Mineralogy, Geochemistry, and Petrology.* Thunder Bay, Ontario, Canada: Plenum Press. Retrieved 2016

Moussallam, Y., Morizet, Y., & Gaillard, F. (2016). H2O–CO2solubility in low SiO2-melts and the unique mode of kimberlite degassing and emplacement. *Earth and Planetary Science Letters*, 151-160.

Moussallam, Y., Morizet, Y., Massuyeau, M., Laumonier, M., & Gaillard, F. (2015). CO2 solubility in kimberlite melts. *Chemical Geology*, 198-2015.

Railsback, B. (2006). *Bowen's Reaction Series.* Retrieved from Some Fundamentals of Mineralogy and Geochemistry: http://www.gly.uga.edu/railsback/Fundamentals

Roeder, L. P., & Schulze, D. J. (2008). Crystallization of Groundmass Spinel in Kimberlite. *Journal of Petrology*, 1473-1495.

Schluter, T. (2006). *Geological Atlas of Africa.* Nairobi: Springer-Verlag.

Simelane, G. (2012). *105/018/0001 (Orapa BK01) Kimberlite Summary Report.* De Beers Holdings Botswana (Pty) Ltd report.

Skinner, M., & Marsh, J. (2004, June 8). Distinct kimberlite pipe classes with contrasting eruption processes. *Lithos, 76*(1-4), 183-200. Retrieved 2016

Smith, S. (1996). Kimberlites. In M. A. Canada, & R. Mitchell (Ed.), *Undersaturated Alkaline Rocks: Mineralogy, Petrogenesis, and Economic Potential* (Vol. 24, pp. 217-239). Winnipeg, Manitoba, Canada: Mineralogy Association of Canada Short Course Series.

Sparks, S., Baker, L., Brown, R. J., Field, M., Schumacher, J., Stripp, G., & Walters, A. (2006). Dynamical constraints on kimberlite volcanism. *Journal of Volcanology and Geothermal Research*, 18-48.

Swapp, S. (2013). *Geochemical Instrumentation and Analysis*. Retrieved from Scanning Electron Microscopy (SEM): http://serc.carleton.edu/research_education/geochemsheets/techniques/SEM.html

Winter, J. D. (2001). Kimberlites. In J. D. Winter, & N. Folchetti (Ed.), *Principles of Igneous and Metamorphic Petrology* (2nd ed., pp. 425-431). Upper Saddle River, New Jersey, USA: Pearson Hall. Retrieved 2016

Winter, W. F., Henning, A., & Munyawiri, D. (2012). *Overview of the geology of the Orapa BK1 kimberlite.* Unpublished confidential De Beers Exploration Report, GEIC Report Number 146587.

Table 3. Mineralogical data derived from SEM analysis. Minerals classified as either Macrocryst, Relic, Secondary, Groundmass, or as Inclusions on a per site of interest basis by sample ID, Depth and Borehole of origin, as well as Kimberlite and kimberlite facies.

#	Depth from (m)	Depth to (m)	Hole	Sample	Kimberlite	Facies	S.I.	Done	Mac. Chromite	Mac. Ilmenite	Mac. Per	Rel. Chromite	Rel. Ilmenite	Rel. Titanite	Rel. Perovskite	Rel. Rutile	Rel. Magnetite	Sec. Chromite	Sec. Ilmenite	Sec. Titanite	Sec. Perovskite	Sec. Rutile	Sec. Magnetite	GM Chromite	GM Ilmenite	GM Titanite	GM Perovskite	GM Rutile	GM Magnetite	Inc Chromite	Incl Ilmenite	Inc Magnetite	Notes
13	0	0	0	EGR665	AK15	0	1	Done	-	-	-	-	-	-	-	-	-	-	-	-	-	-	-	-	-	-	yes	-	yes	-	-	-	
13	0	0	0	EGR665	AK15	0	2	Done	-	-	yes	-	-	-	-	-	-	-	-	-	-	-	-	-	-	-	yes	yes	yes	-	-	-	
13	0	0	0	EGR665	AK15	0	3	Done	-	-	-	-	-	-	-	-	-	-	-	-	-	-	-	-	-	-	yes	-	-	-	-	-	
13	0	0	0	EGR665	AK15	0	4	Done	-	-	-	-	-	yes	-	-	-	-	-	-	-	-	-	-	-	-	yes	-	yes	-	-	-	
13	0	0	0	EGR665	AK15	0	5	Done	-	-	-	-	-	yes	-	-	-	-	-	-	-	-	yes	-	-	-	yes	-	yes	-	-	-	
13	0	0	0	EGR665	AK15	0	6	Done	-	-	-	-	yes	-	-	-	-	-	-	-	-	-	yes	-	-	-	-	-	-	-	-	-	
13	0	0	0	EGR665	AK15	0	8	Done	-	-	-	-	-	-	-	-	-	-	-	-	-	-	yes	-	-	-	yes	-	-	-	-	-	
13	0	0	0	EGR665	AK15	0	9	Done	-	-	-	-	-	-	-	-	-	-	-	-	-	-	-	yes	-	-	-	-	-	-	-	-	
13	0	0	0	EGR665	AK15	0	10	Done	-	-	-	-	yes	-	-	-	-	yes	-	-	-	-	-	-	-	-	-	-	-	-	-	-	
13	0	0	0	EGR665	AK15	0	11	Done	-	-	-	-	yes	-	-	-	-	-	-	-	-	-	-	yes	-	-	yes	-	yes	-	-	-	
13	0	0	0	EGR665	AK15	0	12	Done	-	-	yes	-	-	-	-	-	-	-	-	-	-	-	-	yes	-	-	yes	-	yes	-	-	-	
13	0	0	0	EGR665	AK15	0	13	Done	yes	-	-	-	-	-	-	-	-	-	-	-	-	-	-	-	-	-	yes	-	yes	-	-	-	
13	0	0	0	EGR665	AK15	0	14	Done	-	yes	-	-	-	-	-	-	-	yes	-	-	-	-	yes	-	-	-	yes	-	-	-	-	-	
13	0	0	0	EGR665	AK15	0	15	Done	-	-	-	-	-	yes	-	-	-	-	-	-	-	-	yes	-	-	-	yes	-	yes	-	-	-	
14	0	0	0	EGR683	AK15	0	3	Done	-	-	-	-	-	-	-	-	-	-	-	-	-	-	-	yes	-	-	yes	-	-	-	-	-	
14	0	0	0	EGR683	AK15	0	4	Done	-	-	-	-	-	-	-	-	-	-	-	-	-	-	yes	yes	-	-	yes	-	-	-	-	-	
14	0	0	0	EGR683	AK15	0	5	Done	-	-	-	-	-	yes	-	-	-	-	-	-	-	-	yes	-	-	-	-	-	-	-	-	-	
14	0	0	0	EGR683	AK15	0	6	Done	yes	-	-	-	-	yes	-	-	-	yes	-	-	-	-	-	-	-	-	yes	-	-	-	-	-	
14	0	0	0	EGR683	AK15	0	7	Done	yes	-	-	-	-	-	-	-	-	-	-	-	-	-	-	yes	-	-	yes	-	-	yes	-	-	
14	0	0	0	EGR683	AK15	0	8	Done	-	-	-	-	-	yes	-	-	-	-	-	-	-	-	yes	-	-	-	-	-	-	-	-	-	
14	0	0	0	EGR683	AK15	0	11	Done	-	-	-	-	-	-	-	-	-	-	-	-	yes	-	yes	-	-	-	yes	-	yes	-	-	-	
14	0	0	0	EGR683	AK15	0	12	Done	-	-	-	-	-	-	-	-	-	-	-	-	yes	-	yes	-	-	-	yes	-	yes	-	-	-	
14	0	0	0	EGR683	AK15	0	13	Done	-	yes	-	-	-	-	-	-	-	-	-	-	yes	-	yes	-	-	-	-	-	-	-	-	-	
14	0	0	0	EGR683	AK15	0	14	Done	-	yes	-	-	-	-	-	-	-	-	-	-	yes	-	yes	-	-	-	-	-	-	-	-	-	
14	0	0	0	EGR683	AK15	0	15	Done	-	-	-	-	-	-	-	-	-	-	-	-	-	-	-	-	-	-	yes	-	yes	-	-	-	
14	0	0	0	EGR683	AK15	0	16	Done	-	-	-	-	-	-	-	-	-	-	-	-	-	-	-	-	-	-	yes	-	-	-	-	-	
14	0	0	0	EGR683	AK15	0	17	Done	-	-	-	-	-	-	-	-	-	-	-	-	-	-	-	-	-	-	yes	-	-	-	-	-	
14	0	0	0	EGR683	AK15	0	18	Done	-	-	-	-	-	-	-	-	-	-	-	-	-	-	-	-	-	-	yes	-	-	-	-	-	
14	0	0	0	EGR683	AK15	0	19	Done	-	yes	-	-	-	-	-	-	-	-	-	-	yes	-	yes	-	-	-	yes	-	-	-	-	-	
14	0	0	0	EGR683	AK15	0	20	Done	-	-	-	-	-	-	-	-	-	-	-	-	-	-	-	-	-	-	yes	-	-	-	-	-	
14	0	0	0	EGR683	AK15	0	22	Done	-	-	-	-	-	-	-	-	-	-	-	-	-	-	-	-	-	-	yes	-	-	-	-	-	
14	0	0	0	EGR683	AK15	0	23	Done	-	-	-	-	-	yes	-	-	-	-	-	-	-	-	-	-	-	-	yes	-	-	-	-	-	
14	0	0	0	EGR683	AK15	0	24	Done	-	-	-	-	-	-	-	-	-	-	-	-	-	-	-	-	-	-	yes	-	-	-	-	-	
14	0	0	0	EGR683	AK15	0	25	Done	-	-	-	-	-	-	-	-	-	-	-	-	-	-	yes	-	-	-	-	-	-	-	-	-	
14	0	0	0	EGR683	AK15	0	26	Done	-	-	-	-	-	-	-	-	-	-	-	-	yes	-	-	-	-	-	-	-	-	-	-	-	
14	0	0	0	EGR683	AK15	0	27	Done	-	-	-	-	-	-	-	-	-	yes	-	-	yes	-	yes	-	-	-	-	-	-	-	-	-	
14	0	0	0	EGR683	AK15	0	28	Done	yes	-	-	-	-	yes	-	-	-	-	-	-	-	-	yes	yes	-	-	-	-	-	-	-	-	
14	0	0	0	EGR683	AK15	0	29	Done	-	-	-	-	-	-	-	-	-	yes	-	-	-	-	-	-	-	-	yes	-	-	-	-	-	
14	0	0	0	EGR683	AK15	0	30	Done	yes	-	-	-	-	-	-	-	-	-	-	-	-	-	-	yes	-	-	yes	-	-	-	-	-	
14	0	0	0	EGR683	AK15	0	31	Done	-	-	-	-	-	-	-	-	-	-	-	-	-	-	-	-	-	-	yes	-	-	-	-	-	
14	0	0	0	EGR683	AK15	0	33	Done	-	-	-	-	-	-	-	-	-	yes	-	-	-	-	-	yes	-	-	yes	-	-	-	-	-	
14	0	0	0	EGR683	AK15	0	35	Done	yes	-	-	-	-	-	-	-	-	-	-	-	-	-	-	yes	-	-	yes	-	-	yes	-	-	
14	0	0	0	EGR683	AK15	0	36	Done	-	yes	-	-	-	-	-	-	-	-	-	-	yes	-	yes	-	-	-	-	-	-	-	-	-	
14	0	0	0	EGR683	AK15	0	9	Done	-	Symplectitic Mgt and Per	-	-	-	yes	-	-	-	-	-	-	-	-	-	-	-	-	yes	-	yes	-	-	-	
14	0	0	0	EGR683	AK15	0	10	Done	-	Symplectitic Mgt and Per	-	-	-	-	-	-	-	-	-	-	yes	-	yes	-	-	-	-	-	-	-	-	-	
14	0	0	0	EGR683	AK15	0	1	Done	yes	-	-	-	-	-	-	-	-	-	-	-	-	-	-	yes	-	-	-	-	-	-	-	-	
14	0	0	0	EGR683	AK15	0	2	Done	-	-	-	-	-	-	-	-	-	-	-	-	-	-	-	yes	-	-	-	-	-	-	-	-	
14	0	0	0	EGR683	AK15	0	3	Done	-	-	-	-	-	-	-	-	-	-	-	-	-	-	-	yes	-	-	-	-	-	-	-	-	
14	0	0	0	EGR683	AK15	0	4	Done	-	-	-	-	-	-	-	-	-	-	-	-	-	-	-	-	-	-	yes	-	-	-	-	-	
14	0	0	0	EGR683	AK15	0	5	Done	-	-	-	-	-	-	-	-	-	-	-	-	-	-	-	-	-	-	yes	-	-	-	-	-	
14	0	0	0	EGR683	AK15	0	6	Done	-	yes	-	-	-	-	-	-	-	-	-	-	-	-	-	yes	-	-	-	-	-	-	-	-	
14	0	0	0	EGR683	AK15	0	7	Done	-	-	-	-	-	-	-	-	-	-	-	-	-	-	-	yes	-	-	-	-	-	-	-	-	
14	0	0	0	EGR683	AK15	0	8	Done	-	yes	-	-	-	-	-	-	-	yes	-	-	-	-	yes	-	-	-	yes	-	-	-	-	-	
14	0	0	0	EGR683	AK15	0	9	Done	-	yes	yes	-	-	-	-	-	-	-	-	-	-	-	-	yes	-	-	-	-	yes	-	-	-	
14	0	0	0	EGR683	AK15	0	10	Done	-	yes	-	-	-	-	-	-	-	-	-	-	-	-	-	-	-	-	-	-	-	-	-	-	
14	0	0	0	EGR683	AK15	0	11	Done	-	-	-	-	-	-	-	-	-	-	-	-	yes	-	yes	-	-	-	-	-	-	-	-	-	
15	0	0	0	EGR705	AK15	0	1	Done	-	-	-	-	-	-	-	-	-	-	-	-	-	-	yes	-	-	-	-	-	yes	-	-	-	
15	0	0	0	EGR705	AK15	0	2	Done	-	-	yes	-	-	-	-	-	-	-	-	-	-	-	-	-	-	-	-	-	-	-	-	-	
15	0	0	0	EGR705	AK15	0	3	Done	-	-	yes	-	-	-	-	-	-	-	-	-	-	-	-	-	-	-	-	-	-	-	-	-	
15	0	0	0	EGR705	AK15	0	4	Done	-	-	-	-	-	-	-	-	-	-	-	-	-	-	yes	-	-	-	-	-	-	-	-	-	
15	0	0	0	EGR705	AK15	0	5	Done	-	-	-	-	-	-	-	-	-	-	-	-	-	-	-	-	-	-	-	-	-	yes	-	-	
15	0	0	0	EGR705	AK15	0	1	Done	-	-	yes	-	-	-	-	-	-	-	-	-	-	-	-	-	-	-	-	-	yes	yes	-	-	
15	0	0	0	EGR705	AK15	0	2	Done	-	-	-	-	-	-	-	-	-	-	-	-	-	-	-	-	-	-	-	-	-	yes	-	-	
15	0	0	0	EGR705	AK15	0	3	Done	-	-	-	-	-	yes	-	-	-	-	-	-	-	-	yes	-	-	-	-	-	-	-	-	-	
15	0	0	0	EGR705	AK15	0	4	Done	-	-	yes	-	-	-	-	-	-	-	-	-	-	yes	-	-	-	-	-	-	-	-	-	-	
15	0	0	0	EGR705	AK15	0	5	Done	-	-	-	-	yes	yes	-	-	-	-	-	-	-	-	yes	-	-	-	-	-	-	-	-	-	
15	0	0	0	EGR705	AK15	0	6	Done	-	-	-	-	-	-	-	-	-	-	-	-	-	yes	yes	-	-	-	-	-	-	-	-	-	
15	0	0	0	EGR705	AK15	0	7	Done	-	-	-	-	-	yes	-	-	-	-	-	-	-	-	yes	-	-	-	-	-	-	yes	-	-	
15	0	0	0	EGR705	AK15	0	8	Done	-	-	-	-	-	yes	-	-	-	-	-	-	-	-	-	-	-	-	-	-	-	-	-	-	
15	0	0	0	EGR705	AK15	0	9	Done	-	-	-	-	-	-	-	-	-	-	-	-	-	-	-	yes	-	-	-	-	yes	-	-	-	
15	0	0	0	EGR705	AK15	0	10	Done	yes	-	-	-	-	-	-	-	-	-	-	-	-	-	-	yes	-	-	-	-	yes	-	-	-	
15	0	0	0	EGR705	AK15	0	11	Done	-	yes	-	-	-	yes	-	-	-	-	-	-	-	-	-	yes	-	-	-	-	-	-	-	-	
15	0	0	0	EGR705	AK15	0	12	Done	-	yes	-	-	-	-	-	-	-	-	-	-	-	-	yes	-	-	-	-	-	-	-	-	-	
15	0	0	0	EGR705	AK15	0	13	Done	-	yes	-	-	-	-	-	-	-	-	-	-	-	-	-	-	-	-	-	-	-	-	-	-	
15	0	0	0	EGR705	AK15	0	14	Done	-	-	yes	-	-	-	-	-	-	-	-	-	-	-	-	-	-	-	-	-	-	-	-	-	
15	0	0	0	EGR705	AK15	0	15	Done	-	-	yes	-	-	yes	-	-	-	-	-	-	-	yes	-	-	-	-	-	-	-	-	-	-	
15	0	0	0	EGR705	AK15	0	16	Done	-	-	-	-	-	-	yes	-	-	-	-	-	-	yes	-	-	-	-	-	-	-	-	-	-	
15	0	0	0	EGR705	AK15	0	17	Done	-	-	yes	-	-	-	-	-	-	-	-	-	-	yes	-	-	-	-	-	-	-	-	-	-	
15	0	0	0	EGR705	AK15	0	18	Done	-	-	-	-	-	-	-	-	-	-	-	-	-	-	-	yes	-	-	yes	-	-	-	-	-	
15	0	0	0	EGR705	AK15	0	19	Done	-	-	-	-	-	-	yes	-	-	-	-	-	-	yes	-	-	-	-	-	-	-	-	-	-	
15	0	0	0	EGR705	AK15	0	20	Done	-	-	-	-	-	-	-	-	-	-	-	-	-	-	-	yes	-	-	-	-	-	-	-	-	
15	0	0	0	EGR705	AK15	0	22	Done	yes	-	yes	-	-	-	-	-	-	-	-	-	-	-	-	-	-	-	-	yes	-	-	-	-	
15	0	0	0	EGR705	AK15	0	23	Done	yes	-	yes	-	-	yes	-	-	-	-	-	-	-	yes	-	-	-	-	-	-	-	-	-	-	
15	0	0	0	EGR705	AK15	0	24	Done	-	-	yes	-	-	yes	-	-	-	-	-	-	-	yes	-	-	-	-	-	-	-	-	-	-	
15	0	0	0	EGR705	AK15	0	25	Done	-	-	yes	-	-	-	-	-	-	-	-	-	-	yes	-	-	-	-	-	-	-	-	-	-	
7	0	0	H004	EGK619	BK1	CK-B	2	Done	-	Symplectitic Mgt and Per	-	-	-	-	-	-	-	-	-	-	yes	-	yes	-	-	-	-	-	-	-	-	-	
7	0	0	H004	EGK619	BK1	CK-B	4	Done	-	Symplectitic Mgt and Per	-	-	-	-	-	-	-	-	-	-	yes	-	yes	-	-	-	-	-	-	-	-	-	
7	0	0	H004	EGK619	BK1	CK-B	6	Done	-	Symplectitic Mgt and Per	-	-	-	yes	-	-	-	-	-	-	yes	-	yes	-	-	-	-	-	-	-	-	-	
7	0	0	H004	EGK619	BK1	CK-B	7	Done	-	Symplectitic Mgt and Per	-	-	-	-	-	-	-	-	-	-	yes	-	yes	-	-	-	-	-	-	-	-	-	
7	0	0	H004	EGK619	BK1	CK-B	9	Done	-	Symplectitic Mgt and Per	-	-	-	yes	-	-	-	-	-	-	yes	-	yes	-	-	-	yes	-	-	-	-	-	
7	0	0	H004	EGK619	BK1	CK-B	10	Done	-	Symplectitic Mgt and Per	-	-	-	-	-	-	-	-	-	-	yes	-	yes	-	-	-	-	-	-	-	-	-	
7	0	0	H004	EGK619	BK1	CK-B	11	Done	-	Symplectitic Mgt and Per	-	-	-	yes	-	-	-	-	-	-	yes	-	yes	-	-	-	-	-	-	-	-	-	
7	0	0	H004	EGK619	BK1	CK-B	12	Done	-	Symplectitic Mgt and Per	-	-	-	yes	-	-	-	-	-	-	-	-	yes	-	-	-	-	-	-	-	-	-	
7	0	0	H004	EGK619	BK1	CK-B	3	Done	-	-	-	-	-	-	-	-	-	-	-	-	yes	-	yes	-	-	-	-	-	-	-	-	-	
7	0	0	H004	EGK619	BK1	CK-B	5	Done	-	-	-	-	-	-	-	-	-	-	-	-	-	-	-	-	-	-	yes	-	yes	-	-	-	
7	0	0	H004	EGK619	BK1	CK-B	8	Done	-	-	-	-	-	-	-	-	-	-	-	-	-	-	-	yes	-	-	-	-	yes	-	-	-	
7	0	0	H004	EGK619	BK1	CK-B	14	Done	-	-	-	-	-	-	-	-	-	-	-	-	-	-	-	yes	-	-	yes	-	yes	-	-	-	
7	0	0	H004	EGK619	BK1	CK-B	15	Done	-	-	-	-	-	yes	-	-	-	-	-	-	-	-	-	-	-	-	-	-	yes	-	-	-	
8	0	0	H004	EGK627	BK1	CK-B	4	Done	-	-	-	-	-	-	-	-	-	-	-	-	-	-	-	-	-	-	-	-	yes	-	-	-	
8	0	0	H004	EGK627	BK1	CK-B	2	Done	-	Symplectitic Mgt and Per	-	-	-	-	-	-	-	-	-	-	yes	-	yes	-	-	-	yes	-	yes	-	-	-	
8	0	0	H004	EGK627	BK1	CK-B	3	Done	-	Symplectitic Mgt and Per	-	-	-	-	-	-	-	-	-	-	yes	-	yes	-	-	-	-	-	-	-	-	-	
8	0	0	H004	EGK627	BK1	CK-B	12	Done	-	-	-	-	-	-	-	-	-	-	-	-	yes	-	yes	-	-	-	yes	-	-	-	-	-	
8	0	0	H004	EGK627	BK1	CK-B	13	Done	-	-	-	-	-	yes	-	-	-	-	-	-	-	-	-	-	-	-	-	-	yes	-	-	-	
8	0	0	H004	EGK627	BK1	CK-B	14	Done	-	-	-	-	-	-	-	-	-	-	-	-	yes	-	yes	-	-	-	yes	-	-	-	-	-	
8	0	0	H004	EGK627	BK1	CK-B	15	Done	-	-	-	-	-	-	-	-	-	-	-	-	-	-	-	yes	-	-	yes	-	yes	-	-	-	
8	0	0	H004	EGK627	BK1	CK-B	5	Done	-	Symplectitic Mgt and Per	-	-	-	-	-	-	-	-	-	-	yes	-	yes	-	-	-	-	-	-	-	-	-	
8	0	0	H004	EGK627	BK1	CK-B	8	Done	-	Symplectitic Mgt and Per	-	-	-	-	-	-	-	-	-	-	yes	-	yes	-	-	-	-	-	-	-	-	-	
8	0	0	H004	EGK627	BK1	CK-B	9	Done	-	Symplectitic Mgt and Per	-	-	-	yes	-	-	-	-	-	-	yes	-	yes	-	-	-	-	-	-	-	-	-	
8	0	0	H004	EGK627	BK1	CK-B	10	Done	-	Symplectitic Mgt and Per	-	-	-	-	-	-	-	-	-	-	yes	-	yes	-	-	-	-	-	-	-	-	-	
8	0	0	H004	EGK627	BK1	CK-B	11	Done	-	Symplectitic Mgt and Per	-	-	-	yes	-	-	-	-	-	-	yes	-	yes	-	-	-	-	-	-	-	-	-	
9	0	0	H004	EGK634	BK1	CK-B	2	Done	-	Symplectitic Mgt and Per	-	-	-	-	-	-	-	-	-	-	yes	-	yes	-	-	-	-	-	yes	-	-	-	
9	0	0	H004	EGK634	BK1	CK-B	3	Done	-	Symplectitic Mgt and Per	-	-	-	-	-	-	-	-	-	-	yes	-	yes	-	-	-	-	-	-	-	-	-	
9	0	0	H004	EGK634	BK1	CK-B	5	Done	-	Symplectitic Mgt and Per	-	-	-	-	-	-	-	-	-	-	yes	-	yes	-	-	-	-	-	-	-	-	-	
9	0	0	H004	EGK634	BK1	CK-B	6	Done	-	Symplectitic Mgt and Per	-	-	-	-	-	-	-	-	-	-	yes	-	yes	-	-	-	-	-	-	-	-	-	
9	0	0	H004	EGK634	BK1	CK-B	7	Done	-	Symplectitic Mgt and Per	-	-	-	-	-	-	-	-	-	-	yes	-	yes	-	-	-	-	-	yes	-	-	-	
9	0	0	H004	EGK634	BK1	CK-B	8	Done	-	-	-	-	-	-	-	-	-	-	-	-	-	-	-	-	-	-	yes	-	yes	-	-	-	
9	0	0	H004	EGK634	BK1	CK-B	9	Done	-	-	-	-	-	-	-	-	-	-	-	-	-	-	-	-	-	-	-	-	yes	-	-	-	
1	34.53	34.7	H002	EGK567	BK1	CK-A	1	Done	-	yes	-	-	-	-	-	-	-	-	-	-	-	yes	yes	-	-	-	-	-	-	-	-	-	
1	34.53	34.7	H002	EGK567	BK1	CK-A	2	Done	-	yes	-	-	-	-	-	-	-	-	-	-	-	-	yes	-	-	-	-	-	-	-	-	-	
1	34.53	34.7	H002	EGK567	BK1	CK-A	3	Done	-	-	-	-	-	-	-	-	-	-	-	-	-	-	-	-	-	-	-	yes	yes	-	-	-	
1	34.53	34.7	H002	EGK567	BK1	CK-A	4	Done	-	yes	-	-	-	-	-	-	-	-	-	-	-	-	yes	-	-	-	-	-	-	-	-	-	
1	34.53	34.7	H002	EGK567	BK1	CK-A	5	Done	-	-	-	-	-	-	-	-	-	-	-	-	-	yes	yes	-	-	-	-	-	-	-	-	-	
1	34.53	34.7	H002	EGK567	BK1	CK-A	6	Done	-	yes	-	-	-	-	-	-	-	-	-	-	-	yes	yes	-	-	-	-	-	-	-	-	-	
1	34.53	34.7	H002	EGK567	BK1	CK-A	7	Done	-	yes	-	-	-	-	-	-	-	-	-	-	-	-	yes	-	-	-	-	-	-	-	-	-	
1	34.53	34.7	H002	EGK567	BK1	CK-A	8	Done	-	-	-	-	-	-	-	-	-	-	-	-	-	-	-	-	-	-	-	yes	yes	-	-	-	
1	34.53	34.7	H002	EGK567	BK1	CK-A	9	Done	-	yes	-	-	-	-	-	-	-	-	-	-	-	yes	yes	-	-	-	-	-	-	-	-	-	
1	34.53	34.7	H002	EGK567	BK1	CK-A	10	Done	-	-	-	-	-	-	-	-	-	-	-	-	-	-	-	-	-	-	-	-	-	-	yes	-	
1	34.53	34.7	H002	EGK567	BK1	CK-A	11	Done	-	-	-	-	-	-	-	-	-	-	-	-	-	yes	yes	-	-	-	-	-	yes	-	-	-	
1	34.53	34.7	H002	EGK567	BK1	CK-A	12	Done	-	-	-	-	-	-	-	-	-	-	-	-	-	-	-	-	-	-	-	-	yes	-	-	-	
1	34.53	34.7	H002	EGK567	BK1	CK-A	13	Done	-	yes	-	-	-	-	-	-	-	-	-	-	-	yes	yes	-	-	-	-	-	-	-	-	-	
1	34.53	34.7	H002	EGK567	BK1	CK-A	14	Done	-	-	-	-	-	-	-	-	-	-	-	-	-	-	yes	-	-	-	-	-	-	-	-	-	
1	34.53	34.7	H002	EGK567	BK1	CK-A	15	Done	-	yes	-	-	-	-	-	-	-	-	-	-	-	-	yes	-	-	-	-	-	-	-	-	-	
1	34.53	34.7	H002	EGK567	BK1	CK-A	16	Done	-	yes	-	-	-	-	-	-	-	-	-	-	-	-	yes	-	-	-	-	-	-	-	-	-	
2	36.7	36.9	H002	EGK568	BK1	CK-A	1	Done	-	yes	-	-	-	-	-	-	-	-	-	-	-	-	yes	-	-	-	-	-	-	-	-	-	
2	36.7	36.9	H002	EGK568	BK1	CK-A	3	Done	-	yes	-	-	-	-	-	-	-	-	-	-	-	-	yes	-	-	-	-	-	-	-	-	-	
2	36.7	36.9	H002	EGK568	BK1	CK-A	4	Done	-	yes	-	-	-	-	-	-	-	-	-	-	-	-	yes	-	-	-	-	-	-	-	-	-	
2	36.7	36.9	H002	EGK568	BK1	CK-A	5	Done	-	-	-	-	-	-	-	-	-	-	-	-	-	-	yes	-	-	-	-	-	-	-	-	-	
2	36.7	36.9	H002	EGK568	BK1	CK-A	6	Done	-	yes	-	-	-	-	-	-	-	-	-	-	-	yes	-	-	-	-	-	-	yes	-	-	-	
2	36.7	36.9	H002	EGK568	BK1	CK-A	7	Done	-	-	-	-	-	-	-	-	-	-	-	-	-	-	-	-	-	-	-	-	yes	-	-	-	
2	36.7	36.9	H002	EGK568	BK1	CK-A	8	Done	-	yes	-	-	-	-	-	-	-	-	-	-	-	-	yes	-	-	-	-	-	-	-	-	-	
2	36.7	36.9	H002	EGK568	BK1	CK-A	9	Done	-	-	-	-	-	-	-	-	-	-	-	-	-	-	yes	-	-	-	-	-	-	-	-	-	
3	40.78	41.01	H002	EGK569	BK1	CK-A	1	Done	-	yes	-	-	-	-	-	-	-	-	-	-	-	yes	yes	-	-	-	-	-	-	-	-	-	
3	40.78	41.01	H002	EGK569	BK1	CK-A	2	Done	-	yes	-	-	-	-	-	-	-	-	-	-	-	yes	yes	-	-	-	-	-	-	-	-	-	
3	40.78	41.01	H002	EGK569	BK1	CK-A	3	Done	-	yes	-	-	-	-	-	-	-	-	-	-	-	-	yes	-	-	-	-	-	-	-	-	-	
3	40.78	41.01	H002	EGK569	BK1	CK-A	4	Done	-	yes	-	-	-	-	-	-	-	-	-	-	-	yes	yes	-	-	-	-	-	-	-	-	-	
3	40.78	41.01	H002	EGK569	BK1	CK-A	6	Done	-	-	-	-	-	-	-	-	-	-	-	-	-	-	-	-	-	-	-	-	yes	-	-	-	
3	40.78	41.01	H002	EGK569	BK1	CK-A	8	Done	yes	-	-	-	-	-	-	-	-	-	-	-	-	-	-	-	-	-	-	-	-	-	-	-	
3	40.78	41.01	H002	EGK569	BK1	CK-A	9	Done	-	yes	-	-	-	-	-	-	-	-	-	-	-	-	yes	-	-	-	-	-	-	-	-	-	
3	40.78	41.01	H002	EGK569	BK1	CK-A	10	Done	-	yes	-	-	-	-	-	-	-	-	-	-	-	yes	-	-	-	-	-	-	yes	-	-	-	
3	40.78	41.01	H002	EGK569	BK1	CK-A	12	Done	-	yes	-	-	-	-	-	-	-	-	-	-	-	-	yes	-	-	-	-	-	yes	-	-	-	
3	40.78	41.01	H002	EGK569	BK1	CK-A	13	Done	-	-	-	-	-	-	-	-	-	-	-	-	-	-	-	-	-	-	-	-	yes	-	-	-	
3	40.78	41.01	H002	EGK569	BK1	CK-A	14	Done	-	yes	-	-	-	-	-	-	-	-	-	-	-	yes	-	-	-	-	-	-	-	-	-	-	
4	42.74	42.96	H002	EGK570	BK1	CK-A	1	Done	-	yes	-	-	-	yes	-	-	-	-	-	-	-	-	-	-	-	-	-	-	-	-	-	-	
4	42.74	42.96	H002	EGK570	BK1	CK-A	2	Done	-	yes	-	-	-	-	-	-	-	-	-	-	yes	-	-	-	-	-	-	-	-	-	-	-	
4	42.74	42.96	H002	EGK570	BK1	CK-A	3	Done	-	-	-	-	-	-	-	-	-	-	-	-	-	-	-	-	-	-	-	-	yes	-	-	-	
4	42.74	42.96	H002	EGK570	BK1	CK-A	4	Done	-	-	-	-	-	-	-	-	-	-	-	-	-	-	-	-	-	-	-	-	yes	-	-	-	
4	42.74	42.96	H002	EGK570	BK1	CK-A	5	Done	-	-	-	-	-	-	-	-	-	-	-	-	-	in Carbonate	-	-	-	-	-	-	-	-	-	-	
4	42.74	42.96	H002	EGK570	BK1	CK-A	6	Done	-	-	-	-	-	-	-	-	-	-	-	-	-	-	-	-	-	yes	-	-	yes	-	-	-	
5	50.41	50.64	H002	EGK571	BK1	MVK-A	3	Done	-	yes	-	-	-	-	-	-	-	-	-	-	-	-	-	-	-	-	-	-	-	-	-	-	
5	50.41	50.64	H002	EGK571	BK1	MVK-A	4	Done	-	yes	-	-	-	-	-	-	-	-	-	-	-	yes	yes	-	-	-	-	-	-	-	-	-	
6	54.33	54.48	H002	EGK572	BK1	MVK-A	2	Done	-	-	-	-	-	-	-	-	-	-	-	-	-	-	yes	-	-	-	-	-	-	-	-	-	
6	54.33	54.48	H002	EGK572	BK1	MVK-A	3	Done	-	-	-	-	-	-	-	-	-	-	-	-	-	-	yes	-	-	-	-	-	-	-	-	-	
10	18.29	18.53	H003	EGK637	BK1	CK-A	1	Done	yes	-	-	-	-	-	-	-	-	-	-	yes	-	-	-	-	-	-	-	-	yes				
10	18.29	18.53	H003	EGK637	BK1	CK-A	2	Done	-	-	-	yes	-	-	-	-	-	-	-	-	-	-	-	-	-	-	-	-	yes				
10	18.29	18.53	H003	EGK637	BK1	CK-A	3	Done	-	yes	-	-	-	-	-	-	-	-	-	-	-	-	-	-	-	-	-	-	-				
10	18.29	18.53	H003	EGK637	BK1	CK-A	4	Done	-	yes	-	-	-	-	-	-	-	-	-	-	-	-	-	-	-	-	-	-	-				
10	18.29	18.53	H003	EGK637	BK1	CK-A	5	Done	-	yes	-	-	-	-	-	-	-	-	-	yes	-	-	yes	-	-	-	-	-	-				
10	18.29	18.53	H003	EGK637	BK1	CK-A	6	Done	-	yes	-	-	-	-	-	-	-	-	-	-	-	-	-	-	-	-	-	-	-				
10	18.29	18.53	H003	EGK637	BK1	CK-A	7	Done	-	yes	-	-	-	-	-	yes	-	-	-	-	-	-	yes	-	-	-	-	-	-				Is atoll rutile in this SI relic or Secondary
10	18.29	18.53	H003	EGK637	BK1	CK-A	8	Done	-	yes	-	-	-	-	-	yes	-	-	-	-	-	-	yes	-	-	-	-	-	-				Is atoll rutile in this SI relic or Secondary
10	18.29	18.53	H003	EGK637	BK1	CK-A	9	Done	-	yes	-	-	-	-	-	yes	-	-	-	yes	-	-	yes	-	-	-	-	-	yes				
10	18.29	18.53	H003	EGK637	BK1	CK-A	10	Done	-	yes	-	-	-	-	-	yes	-	-	-	yes	-	-	yes	-	-	-	-	-	-				
10	18.29	18.53	H003	EGK637	BK1	CK-A	11	Done	-	yes	-	-	-	-	-	yes	-	-	-	yes	-	-	yes	-	-	-	-	-	-				
10	18.29	18.53	H003	EGK637	BK1	CK-A	12	Done	-	yes	-	-	-	-	-	yes	-	-	-	-	-	-	yes	-	-	-	-	-	-				
10	18.29	18.53	H003	EGK637	BK1	CK-A	13	Done	-	yes	-	-	-	-	-	-	-	-	-	yes	-	-	yes	-	-	yes	-	-	-				
10	18.29	18.53	H003	EGK637	BK1	CK-A	14	Done	-	yes	-	-	-	-	-	-	-	-	-	yes	-	-	yes	-	-	-	-	-	-				
10	18.29	18.53	H003	EGK637	BK1	CK-A	15	Done	-	yes	-	-	-	-	-	-	-	-	-	-	-	-	-	-	-	-	-	-	-				
10	18.29	18.53	H003	EGK637	BK1	CK-A	16	Done	-	yes	-	-	-	-	-	yes	-	-	-	-	-	-	-	-	-	-	-	-	-				
10	18.29	18.53	H003	EGK637	BK1	CK-A	17	Done	-	-	-	-	-	-	-	-	-	-	-	yes	-	-	-	-	-	-	-	-	-				
10	18.29	18.53	H003	EGK637	BK1	CK-A	18	Done	-	yes	-	-	-	-	-	yes	-	-	-	yes	-	-	yes	-	-	-	-	-	-				
10	18.29	18.53	H003	EGK637	BK1	CK-A	23	Done	-	-	-	-	-	-	-	-	-	-	-	-	-	-	-	-	-	yes	-	-	yes				
10	18.29	18.53	H003	EGK637	BK1	CK-A	24	Done	-	-	-	-	yes	-	-	yes	-	-	-	-	-	-	yes	-	-	-	-	-	-				
10	18.29	18.53	H003	EGK637	BK1	CK-A	25	Done	-	yes	-	-	-	-	-	-	-	-	-	yes	-	-	yes	-	-	-	-	-	-				
10	18.29	18.53	H003	EGK637	BK1	CK-A	26	Done	-	yes	-	-	-	-	-	yes	-	-	-	yes	-	-	yes	-	-	yes	-	-	-				
10	18.29	18.53	H003	EGK637	BK1	CK-A	27	Done	-	yes	-	-	-	-	-	-	-	-	-	yes	-	-	-	-	-	-	-	-	-				
10	18.29	18.53	H003	EGK637	BK1	CK-A	28	Done	-	-	-	-	-	-	-	-	-	-	-	-	-	-	-	-	-	-	-	-	-		Carbonate		
10	18.29	18.53	H003	EGK637	BK1	CK-A	29	Done	-	yes	-	-	-	-	-	-	-	-	-	yes	-	-	yes	-	-	-	-	-	-				
11	45.65	45.85	H003	EGK641	BK1	MVK-A	2	Done	yes	yes	-	-	-	-	-	-	-	-	-	-	-	-	-	-	-	-	-	-	-				
11	45.65	45.85	H003	EGK641	BK1	MVK-A	3	Done	yes	-	-	-	-	-	-	-	-	-	-	-	-	-	-	-	-	-	-	-	-				
11	45.65	45.85	H003	EGK641	BK1	MVK-A	4	Done	yes	-	-	-	-	-	-	-	-	-	-	yes	-	-	-	-	-	-	-	-	-				
11	45.65	45.85	H003	EGK641	BK1	MVK-A	5	Done	yes	-	-	-	-	-	-	-	-	-	-	yes	-	-	-	-	-	-	-	-	-				
11	45.65	45.85	H003	EGK641	BK1	MVK-A	6	Done	-	yes	-	-	-	-	-	-	-	-	-	yes	-	-	yes	-	-	yes	-	-	-				
11	45.65	45.85	H003	EGK641	BK1	MVK-A	7	Done	-	-	-	-	-	-	-	-	-	-	-	-	-	-	yes	-	-	-	-	-	yes				
11	45.65	45.85	H003	EGK641	BK1	MVK-A	9	Done	-	-	-	-	-	-	-	-	-	-	-	yes	-	-	-	-	-	-	-	-	yes				
11	45.65	45.85	H003	EGK641	BK1	MVK-A	10	Done	-	yes	-	-	-	-	-	-	-	-	-	-	-	-	-	-	-	-	-	-	-				
11	45.65	45.85	H003	EGK641	BK1	MVK-A	11	Done	-	yes	-	-	-	-	-	-	-	-	-	yes	-	-	yes	-	-	-	-	-	-				
11	45.65	45.85	H003	EGK641	BK1	MVK-A	12	Done	-	-	-	-	-	-	-	-	-	-	-	-	-	-	yes	-	-	-	-	-	yes				
11	45.65	45.85	H003	EGK641	BK1	MVK-A	13	Done	-	yes	-	-	-	-	-	-	-	-	-	yes	-	-	-	-	-	-	-	-	-				
11	45.65	45.85	H003	EGK641	BK1	MVK-A	14	Done	-	yes	-	-	-	-	-	-	-	-	-	yes	-	-	-	-	-	-	-	-	-				
11	45.65	45.85	H003	EGK641	BK1	MVK-A	15	Done	-	-	-	-	-	-	-	-	-	-	-	-	-	-	-	-	-	-	yes	-	yes				
11	45.65	45.85	H003	EGK641	BK1	MVK-A	16	Done	-	-	-	-	-	yes	-	-	-	-	-	-	yes	-	-	-	-	-	-	-	-				
11	45.65	45.85	H003	EGK641	BK1	MVK-A	17	Done	-	-	-	-	-	-	-	yes	-	-	-	-	-	-	-	-	-	-	yes	-	yes				
11	45.65	45.85	H003	EGK641	BK1	MVK-A	18	Done	-	yes	-	-	-	-	-	-	-	-	-	-	-	-	-	-	-	-	-	-	-				
11	45.65	45.85	H003	EGK641	BK1	MVK-A	19	Done	-	-	-	-	yes	-	-	-	-	-	-	-	-	-	-	-	-	-	yes	-	-				
11	45.65	45.85	H003	EGK641	BK1	MVK-A	20	Done	-	-	-	-	-	-	-	-	-	-	-	-	-	-	-	-	-	-	yes	-	-				
11	45.65	45.85	H003	EGK641	BK1	MVK-A	21	Done	-	-	-	-	-	yes	-	-	-	-	-	-	-	-	-	-	-	-	-	-	-				
11	45.65	45.85	H003	EGK641	BK1	MVK-A	22	Done	-	-	-	-	-	yes	-	-	-	-	-	-	-	-	yes	-	-	-	-	-	-				
11	45.65	45.85	H003	EGK641	BK1	MVK-A	23	Done	-	-	-	-	yes	yes	-	-	-	-	-	-	-	-	-	-	-	-	-	-	-				
11	45.65	45.85	H003	EGK641	BK1	MVK-A	24	Done	-	-	-	-	-	-	-	yes	-	-	-	-	-	-	yes	-	-	-	-	-	-				
11	45.65	45.85	H003	EGK641	BK1	MVK-A	25	Done	-	-	-	-	-	-	-	-	-	-	-	-	-	-	-	-	-	-	-	-	-		olivine	olivine	
11	45.65	45.85	H003	EGK641	BK1	MVK-A	26	Done	-	yes	-	-	-	yes	-	-	-	-	-	-	-	-	yes	-	-	-	-	-	-				
11	45.65	45.85	H003	EGK641	BK1	MVK-A	27	Done	-	-	-	-	-	-	-	yes	-	-	-	-	-	-	yes	-	-	-	-	-	-				
11	45.65	45.85	H003	EGK641	BK1	MVK-A	28	Done	-	-	-	-	-	-	-	-	-	-	-	-	-	-	-	-	-	-	-	-	-		olivine		
11	45.65	45.85	H003	EGK641	BK1	MVK-A	29	Done	-	-	-	-	-	-	-	-	-	-	-	-	-	-	-	-	-	-	-	-	-		olivine		
11	45.65	45.85	H003	EGK641	BK1	MVK-A	30	Done	yes	yes	-	-	-	-	-	-	-	-	-	-	-	-	-	-	-	-	-	-	-				
11	45.65	45.85	H003	EGK641	BK1	MVK-A	32	Done	-	-	-	-	-	-	-	-	-	-	-	yes	-	-	-	-	-	-	-	-	-				
11	45.65	45.85	H003	EGK641	BK1	MVK-A	33	Done	yes	-	-	-	yes	yes	-	yes	-	-	-	yes	-	-	yes	-	-	-	-	-	-				
11	45.65	45.85	H003	EGK641	BK1	MVK-A	34	Done	-	-	-	-	yes	yes	-	-	-	-	-	-	-	-	yes	-	-	-	-	-	-				
11	45.65	45.85	H003	EGK641	BK1	MVK-A	35	Done	-	yes	-	-	-	-	-	-	-	-	-	-	-	-	-	-	-	-	-	-	-				
11	45.65	45.85	H003	EGK641	BK1	MVK-A	36	Done	-	yes	-	-	-	-	-	-	-	-	-	yes	-	-	yes	-	-	-	-	-	-				
11	45.65	45.85	H003	EGK641	BK1	MVK-A	38	Done	-	-	-	-	-	yes	-	-	-	-	-	-	-	-	-	-	-	-	yes	-	-				
11	45.65	45.85	H003	EGK641	BK1	MVK-A	39	Done	-	-	-	-	-	-	-	-	-	-	-	-	-	-	-	-	-	-	-	-	yes				
11	45.65	45.85	H003	EGK641	BK1	MVK-A	40	Done	-	-	-	-	-	-	-	yes	-	-	-	-	-	-	-	-	-	-	yes	-	-				
11	45.65	45.85	H003	EGK641	BK1	MVK-A	41	Done	-	yes	-	-	-	-	-	-	-	-	-	-	-	-	-	-	-	-	-	-	-				
11	45.65	45.85	H003	EGK641	BK1	MVK-A	42	Done	-	-	-	-	-	-	-	-	-	-	-	-	-	-	yes	-	-	-	-	-	-				
11	45.65	45.85	H003	EGK641	BK1	MVK-A	43	Done	-	-	-	-	-	yes	-	-	-	-	-	-	-	-	yes	-	-	-	-	-	-				
11	45.65	45.85	H003	EGK641	BK1	MVK-A	44	Done	-	yes	-	-	-	-	-	-	-	-	-	-	-	-	-	-	-	-	-	-	-				
11	45.65	45.85	H003	EGK641	BK1	MVK-A	45	Done	-	yes	-	-	-	-	-	-	-	-	-	-	-	-	-	-	-	-	-	-	-				
11	45.65	45.85	H003	EGK641	BK1	MVK-A	46	Done	-	-	-	-	-	-	-	-	-	-	-	-	-	-	-	-	-	-	-	-	yes				
11	45.65	45.85	H003	EGK641	BK1	MVK-A	48	Done	-	yes	-	-	-	yes	-	-	-	-	-	-	-	-	-	-	-	-	-	-	-				
11	45.65	45.85	H003	EGK641	BK1	MVK-A	49	Done	-	yes	-	-	-	-	-	-	-	-	-	-	-	-	yes	-	-	-	-	-	-				
11	45.65	45.85	H003	EGK641	BK1	MVK-A	37	Done	-	Symplectitic Mgt and Ilm	-	-	-	-	-	-	-	-	-	-	-	-	-	-	-	-	-	-	-				
12	124.41	124.65	H003	EGK648	BK1	MVK-A	1	Done	-	yes	-	-	-	yes	-	-	-	-	-	-	yes	-	-	-	-	-	-	-	-	-	-	-	
12	124.41	124.65	H003	EGK648	BK1	MVK-A	2	Done	-	yes	-	-	-	-	-	-	-	-	-	-	-	-	yes	-	-	-	-	-	yes	-	-	-	
12	124.41	124.65	H003	EGK648	BK1	MVK-A	3	Done	-	-	-	-	-	-	-	-	-	-	-	-	-	-	yes	-	-	-	-	-	-	-	-	-	
12	124.41	124.65	H003	EGK648	BK1	MVK-A	4	Done	-	yes	-	-	-	-	-	-	-	-	-	-	-	-	-	-	-	-	-	-	-	-	-	-	
12	124.41	124.65	H003	EGK648	BK1	MVK-A	5	Done	-	yes	-	-	-	-	-	-	-	-	-	-	yes	-	yes	-	-	-	-	-	-	-	-	-	
12	124.41	124.65	H003	EGK648	BK1	MVK-A	6	Done	-	yes	-	-	-	-	-	-	-	-	-	-	yes	-	yes	-	-	-	-	-	-	-	-	-	
12	124.41	124.65	H003	EGK648	BK1	MVK-A	7	Done	-	yes	-	-	-	-	-	-	-	-	-	-	-	-	-	-	-	-	-	-	-	-	-	-	
12	124.41	124.65	H003	EGK648	BK1	MVK-A	8	Done	-	yes	-	-	-	-	-	-	-	-	-	-	-	-	-	-	-	-	-	-	-	-	-	-	
12	124.41	124.65	H003	EGK648	BK1	MVK-A	9	Done	-	yes	-	-	-	-	-	-	-	-	-	-	-	-	-	-	-	-	-	-	-	-	-	-	
12	124.41	124.65	H003	EGK648	BK1	MVK-A	10	Done	-	-	-	-	-	-	-	-	-	-	-	-	-	-	-	yes	-	-	-	-	yes	-	-	-	
12	124.41	124.65	H003	EGK648	BK1	MVK-A	11	Done	-	-	-	-	-	-	-	-	-	-	-	-	-	-	yes	-	-	-	-	-	-	-	-	-	

Table 4. EMPA data normalized to chromite and adjusted to include proportions of both 3+ and 2+ oxidation states of iron

No.	Sample	Kimberlite	Facies	Grain Type	Label	Fe3+	Mg	Al	Si	Ca	Ti	V	Cr	Mn	Fe2+	Na	K	Ni	Total	MgO	Al2O3	SiO2	CaO	TiO2	V2O3	Cr2O3	MnO	FeO	Na2O	K2O	NiO	Fe2O3	Nb2O5	Ta2O5	ZnO	CoO	Total
7	EGR683	AK15	-	Groundmass	AK15 Groundmass	0.166457	0.637841	0.398638	0.003733	0.002122	0.065911	0.003982	1.30216	0.003382	0.42093	0.001636	0	0.00543	3.012222	13.181	10.42	0.115	0.061	2.699	0.153	50.748	0.123	15.18291	0.026		0.208	6.672351	0.009		0.05		99.64826
8	EGR683	AK15	-	Groundmass	AK15 Groundmass	0.170665	0.635946	0.394156	0.005187	0.001573	0.068496	0.004839	1.296343	0.006576	0.424161	0	0	0.004749	3.01269	13.077	10.252	0.159	0.045	2.791	0.185	50.272	0.238	15.21578	0		0.181	6.803624	0.011		0.007		99.2374
9	EGR683	AK15	-	Groundmass	AK15 Groundmass	0.231344	0.644599	0.211308	0.002536	0.003325	0.135963	0.01236	1.303205	0.012803	0.455779	0.001682	0	0.004965	3.01987	12.958	5.373	0.076	0.093	5.416	0.462	49.406	0.453	15.85987	0.026		0.185	8.946107	0		0.072		99.32598
10	EGR683	AK15	-	Groundmass	AK15 Groundmass	0.192599	0.631526	0.359246	0.003325	0.002857	0.095947	0.004751	1.254167	0.005716	0.461734	0.000574	0	0.00331	3.015753	12.868	9.259	0.101	0.081	3.874	0.18	48.194	0.205	16.36698	0.009		0.125	7.586863	0.035		0.06		98.94485
13	EGR683	AK15	-	Groundmass	AK15 Groundmass	0.165194	0.615179	0.398879	0.004543	0.003256	0.077127	0.003957	1.275762	0.007917	0.458597	0	0	0.002471	3.012881	12.627	10.356	0.139	0.093	3.137	0.151	49.384	0.286	16.43267	0		0.094	6.578148	0.023		0.063		99.36382
32	EGR705	AK15	-	Inclusion	AK15 Inclusion	0.168678	0.661359	0.4071	0.005089	0.000769	0.058113	0.004263	1.304322	0.002376	0.394265	0	0	0.005535	3.01187	13.6	10.589	0.156	0.022	2.368	0.163	50.583	0.086	14.14734	0		0.211	6.726317	0		0.042		98.69366
34	EGR705	AK15	-	Inclusion	AK15 Inclusion	0.342374	0.658959	0.182153	0.002223	0.007608	0.135968	0.004762	1.206136	0.008853	0.483341	0	0	0.002962	3.035338	13.322	4.658	0.067	0.214	5.447	0.179	45.986	0.315	16.67282	0		0.111	13.12465	0.003		0.046		100.1455
60	EGR705	AK15	-	Inclusion	AK15 Inclusion	0.321168	0.668334	0.177977	0.006275	0.0008	0.144944	0.009845	1.219153	0.01606	0.459853	0.002499	0	0.004447	3.031355	13.217	4.452	0.185	0.022	5.68	0.362	45.469	0.559	15.5598	0.038		0.163	12.07672	0		0.029		97.81252
5	EGR683	AK15	-	Macrocryst	AK15 Macrocryst	0.104879	0.675778	0.340469	0.002304	0.000313	0.005028	0.005098	1.54925	0.000687	0.319461	0	0	0.002296	3.005563	13.972	8.904	0.071	0.009	0.206	0.196	60.408	0.025	11.61936	0		0.088	4.239213	0.001		0.018		99.75657
6	EGR683	AK15	-	Macrocryst	AK15 Macrocryst	0.094411	0.705291	0.32723	0.002037	0.000243	0.005279	0.005237	1.574776	0.001698	0.284006	0.001943	0	0.002314	3.004466	14.632	8.587	0.063	0.007	0.217	0.202	61.613	0.062	10.37882	0.031		0.089	3.834184	0.005		0.021		99.742
11	EGR683	AK15	-	Macrocryst	AK15 Macrocryst	0.168838	0.659163	0.385902	0.003844	0.000969	0.065805	0.003652	1.312475	0.00435	0.400962	0.000689	0	0.005377	3.012025	13.689	10.137	0.119	0.028	2.708	0.141	51.403	0.159	14.52976	0.011		0.207	6.799195	0		0.031		99.96196
12	EGR683	AK15	-	Macrocryst	AK15 Macrocryst	0.191247	0.653581	0.360119	0.001861	0.009164	0.095683	0.004345	1.257533	0.010922	0.42742	0	0	0.002914	3.01479	13.43	9.36	0.057	0.262	3.896	0.166	48.732	0.395	15.2814	0		0.111	7.598629	0.018		0.07		99.37703
35	EGR705	AK15	-	Macrocryst	AK15 Macrocryst	0.163604	0.624517	0.411437	0.003594	0.004691	0.064748	0.003772	1.295107	0.005258	0.428953	0.001837	0	0.004599	3.012118	12.821	10.684	0.11	0.134	2.634	0.144	50.142	0.19	15.3764	0.029		0.175	6.517334	0.011		0.036		99.00373
36	EGR705	AK15	-	Macrocryst	AK15 Macrocryst	0.315103	0.409879	0.042743	0.000388	0.000869	0.067853	0.005482	1.512987	0.003851	0.673332	0.003895	0	0.002551	3.038932	7.801	1.029	0.011	0.023	2.559	0.194	54.306	0.129	21.94382	0.057		0.09	11.41214	0		0.145		99.69996
14	EGK569	BK1	CK-A	Macrocryst	CK-A Macrocryst	0.109699	0.568494	0.765446	0	3.39E-05	0.005195	0.004115	1.10937	0.00432	0.437412	0.000921	0	0.002497	3.007502	12.038	20.502	0	0.001	0.218	0.162	44.302	0.161	16.28408	0.015		0.098	4.538456	0.018		0.277		98.61454
15	EGK569	BK1	CK-A	Macrocryst	CK-A Macrocryst	0.301496	0.519819	0.776775	0	0.000797	0.004308	0.004098	1.204195	0.003535	0.482881	0	0	0.002186	3.000091	10.778	20.372	0	0.023	0.177	0.158	47.087	0.129	17.84372	0		0.084	0.061432	0.042		0.294		97.04915
22	EGK637	BK1	CK-A	Macrocryst Core	CK-A Macrocryst	0.348187	0.598783	0.410908	0	0.000598	0.019028	0.007023	1.255812	0.003946	0.334622	0.04783	0	0.002981	3.029718	12.244	10.628	0	0.017	0.771	0.267	48.428	0.142	11.66604	0.752		0.113	13.49003	0		0.184		98.70207
23	EGK637	BK1	CK-A	Macrocryst Rim	CK-A Macrocryst	0.335089	0.531817	0.384426	0.002225	0.004767	0.032853	0.006421	1.240525	0.003826	0.463669	0.023821	0	0.004018	3.033457	10.424	9.531	0.065	0.13	1.276	0.234	45.856	0.132	15.52166	0.359		0.146	12.46583	0		0.128		96.26849

Table 5. EMPA data normalized to ilmenite and adjusted to include proportions of both 3+ and 2+ oxidation states of iron

No.	Sample	Kimberlite	Facies	Grain Type	Label	Fe3+	Mg	Al	Si	Ca	Ti	V	Cr	Mn	Fe2+	Na	K	Ni	Total	MgO	Al2O3	SiO2	CaO	TiO2	V2O3	Cr2O3	MnO	FeO	Na2O	K2O	NiO	Fe2O3	Nb2O5	Ta2O5	ZnO	CoO	ZrO2	Total
19	EGR677	AK15	-	Macrocryst	AK15 Macrocryst	0.19290184	0.31206455	0.00405962	0.00049886	0.00063632	0.862158	0	0.0654229	0.00527167	0.57738741	0.00262533	0	0.00173854	2.02476504	8.812	0.145	0.021	0.025	48.242	0	3.484	0.262	28.1284465	0.057	0.091	10.4435012	0.278	0	0.001	99.9899477
20	EGR677	AK15	-	Macrocryst	AK15 Macrocryst	0.19073897	0.33900737	0.00199782	9.4173E-05	0.00070632	0.86135422	0	0.06545323	0.0049255	0.55606225	0.0017346	0	0.00166622	2.02374068	9.659	0.072	0.004	0.028	48.631	0	3.517	0.247	27.3436538	0.038	0.088	10.4232675	0.388	0	0.019	100.457921
18	EGR677	AK15	-	Macrocryst	AK15 Macrocryst	0.19798971	0.31430074	0.00352948	9.4322E-05	0.00022739	0.86263763	0	0.06615262	0.00439398	0.5690911	0.00507482	0	0.00182056	2.02531235	8.941	0.127	0.004	0.009	48.627	0	3.549	0.22	27.9055248	0.111	0.096	10.7890285	0.224	0	0	100.602553
21	EGR677	AK15	-	Macrocryst	AK15 Macrocryst	0.1875609	0.47412938	0.00292842	0.00022796	0.00095255	0.86425015	0	0.06076167	0.00832174	0.41805424	0.00066296	0	0.00108165	2.01893162	13.952	0.109	0.01	0.039	50.395	0	3.372	0.431	21.243196	0.015	0.059	10.5915824	0.397	0	0.03	100.643778
17	EGK569	BK1	CK-A	Macrocryst	CK-A Macrocryst	0.24340013	0.29761037	0.00966697	0	0.00056042	0.85758458	0	0.02347297	0.00414828	0.59435806	0.00207432	0	0.00110898	2.03398508	8.397	0.345	0	0.022	47.947	0	1.249	0.206	28.6800236	0.045	0.058	13.0521923	0.187	0.009	0	100.197216
25	EGK636	BK1	CK-A	Macrocryst Rim	CK-A Macrocryst	0.24912225	0.3051828	0.00627732	0	0.00020291	0.85829773	0	0.02142553	0.00320805	0.58743851	0.00257022	0	0.00100901	2.03473432	8.648	0.225	0	0.008	48.195	0	1.145	0.16	28.4407728	0.056	0.053	13.4036418	0.171	0	0	100.505415
16	EGK569	BK1	CK-A	Macrocryst	CK-A Macrocryst	0.23854184	0.2904038	0.00912197	0.00014245	0.00063596	0.85897225	0	0.02437893	0.00440397	0.60432229	0.00105874	0	0.00152752	2.03350973	8.205	0.326	0.006	0.025	48.091	0	1.299	0.219	29.225808	0.023	0.08	12.8201702	0.201	0	0.031	100.551978
24	EGK636	BK1	CK-A	Macrocryst Core	CK-A Macrocryst	0.2293635	0.2869577	0.00585903	0	0.00060586	0.86519509	0	0.02100809	0.00437035	0.6173894	0.00036545	0	0.00125059	2.0323699	8.17	0.211	0	0.024	48.812	0	1.128	0.219	30.1353266	0.008	0.066	12.4417518	0.258	0	0.006	101.479078
51	EGK571	BK1	MVK-A	Inclusion	MVK-A Inclusion	0.15380859	0.41603717	0.00586949	0.00261868	0.00165341	0.90099312	0	0.03746354	0.01316957	0.47888543	0.0049866	0	0.00073335	2.01621896	11.936	0.213	0.112	0.066	51.222	0	2.027	0.665	23.8627527	0.11	0.039	8.51727803	0	0.018	0	98.7880307
64	EGK571	BK1	MVK-A	Inclusion	MVK-A Inclusion	0.1123874	0.58448236	0.00320265	0.00235808	0.00255063	0.92360406	0	0.03262903	0.06570158	0.27487807	0.00204651	0	0.0034136	2.00725396	17.458	0.121	0.105	0.106	54.666	0	1.838	3.454	14.3612288	0.047	0.189	6.5252993	0.029	0.013	0	98.9125281
48	EGK571	BK1	MVK-A	Inclusion	MVK-A Inclusion	0.13866272	0.49965741	0.00288691	0.0027471	0.0020849	0.91328566	0	0.02033994	0.09460389	0.3339473	0	0	0.0027064	2.01092223	14.641	0.107	0.12	0.085	53.029	0	1.124	4.879	17.039713	0	0.147	7.86276644	0.092	0.038	0	99.1644794
65	EGK571	BK1	MVK-A	Inclusion	MVK-A Inclusion	0.16402016	0.45073943	0.01454587	0.00167465	0.00498966	0.89139887	0	0.03282241	0.01911973	0.43333789	0.00298005	0	0.00070108	2.01632979	13.18	0.538	0.073	0.203	51.65	0	1.81	0.984	21.9694672	0.067	0.038	9.2410516	0.105	0	0	99.8585188
58	EGK641	BK1	MVK-A	Inclusion	MVK-A Inclusion	0.18295771	0.38739036	0.02532826	0.00069624	0.00079572	0.86656376	0	0.05630225	0.00866887	0.48964126	0	0	0.0021651	2.02050953	11.197	0.926	0.03	0.032	49.632	0	3.069	0.441	24.458077	0	0.116	10.1560851	0.017	0	0	100.074162
57	EGK641	BK1	MVK-A	Inclusion	MVK-A Inclusion	0.14934432	0.44989633	0.01421965	0.00141943	0.00282094	0.90633782	0	0.01550935	0.0094048	0.46390516	0.0003995	0	0.00200693	2.01526422	13.182	0.527	0.062	0.115	52.622	0	0.857	0.485	23.6260878	0.009	0.109	8.45245027	0.111	0.002	0	100.159538
38	EGK572	BK1	MVK-A	Inclusion	MVK-A Inclusion	0.18022382	0.43366084	0.01470258	0.00121094	0.00115058	0.88144093	0	0.03852354	0.00741189	0.458714	0.00066448	0	0.00148837	2.01919197	12.732	0.546	0.053	0.047	51.28	0	2.133	0.383	23.2854111	0.015	0.081	10.1668269	0.037	0	0	100.759238
63	EGK571	BK1	MVK-A	Inclusion	MVK-A Inclusion	0.15126642	0.38093647	0.01128443	0.00045922	0.00113167	0.90991497	0	0.01648026	0.01250501	0.52902069	0.00258204	0	0.00156096	2.01715077	11.129	0.417	0.02	0.046	52.676	0	0.908	0.643	26.8551326	0.058	0.085	8.53352532	0.054	0	0	101.424658
44	EGK571	BK1	MVK-A	Macrocryst Core	MVK-A Macrocryst	0.2166346	0.2965922	0.00827579	0.00014186	0.00065863	0.86778119	0	0.02784669	0.00490623	0.60381577	0.00169608	0	0.00127396	2.02962299	8.415	0.297	0.006	0.026	48.788	0	1.49	0.245	29.4353157	0.037	0.067	11.7360885	0.245	0	0	100.787404
42	EGK572	BK1	MVK-A	Macrocryst	MVK-A Macrocryst	0.24768225	0.32887884	0.00529667	0.00088947	0.00072731	0.85773948	0	0.02044554	0.0043022	0.56409355	0.00226915	0	0.00118596	2.03351041	9.425	0.192	0.038	0.029	48.709	0	1.105	0.217	27.6266764	0.05	0.063	13.4804286	0.219	0	0.001	101.155105
45	EGK571	BK1	MVK-A	Macrocryst Rim	MVK-A Macrocryst	0.23091042	0.32719966	0.00941697	0.00100168	0.00019968	0.86192115	0	0.02791584	0.00441972	0.56437674	0.00167113	0	0.0015737	2.03060668	9.422	0.343	0.043	0.008	49.182	0	1.516	0.224	27.8545316	0.037	0.084	12.6648953	0.144	0	0	101.522427

Table 6. Geothermometry data for MVK inclusion and AK15 Macrocryst samples calculated from EMPA data usi
ILMAT: A Magnetite-Ilmenite Geothermobarometry Program (version 1.20)

	MVK inclusion	MVK inclusion	MVK inclusion	MVK inclusion
Sample ID	EGK641	EGK571	EGK572	EGK641
Sample No.	62	46	40	58
Wt% Oxides	**Magnetite**	**Magnetite**	**Magnetite**	**Ilmenite**
SiO2	0.05	15.908	8.416	0.03
TiO2	8.992	1.98	2.009	49.632
Al2O3	1.02	0.302	0.148	0.926
Fe2O3(T)				
FeO(T)	73.453	59.445	68.027	33.597
MnO	0.546	0.28	0.386	0.441
MgO	9.924	13.049	5.947	11.197
CaO	0.087	0.398	0.309	0.032
Na2O	0.039	0.168	0.135	0
K2O				
Cr2O3	1.274	0.075	0.069	3.069
BaO				
ZnO	0	0	0	0
V2O3	0	0.122	0.181	0
NiO	0.246	0.064	0.042	0.116
Nb2O3	0	0.011	0.039	0.017
Sum:	95.631	91.802	85.708	**99.057**
Carmichael (1967)	**Recalculated Iron and Total**			
Fe2O3 wt. %	55.0	30.8	41.1	10.4
FeO wt. %	24.0	31.7	31.1	24.2
Total:	101.1	94.9	89.8	100.1
cations	**Cation prop. (Carmichael 1967)**			
Si	0.0017	0.5429	0.3285	0.0007
Ti	0.2360	0.0508	0.0590	0.8668
Al	0.0419	0.0121	0.0068	0.0253
Fe+3	1.4432	0.7913	1.2067	0.1817
Fe+2	0.7001	0.9053	1.0139	0.4705
Mn	0.0161	0.0081	0.0128	0.0087
Mg	0.5162	0.6639	0.3460	0.3875
Ca	0.0033	0.0146	0.0129	0.0008
Na	0.0026	0.0111	0.0102	0.0000
K	0.0000	0.0000	0.0000	0.0000
Cr	0.0351	0.0020	0.0021	0.0563
Ba	0.0000	0.0000	0.0000	0.0000
Zn	0.0000	0.0000	0.0000	0.0000
V	0.0000	0.0033	0.0057	0.0000
Ni	0.0069	0.0018	0.0013	0.0022
Nb	0.0000	0.0002	0.0008	0.0002
Total:	3.0034	3.0074	3.0066	2.0007
Calc. Methods:	**Mol % Usp**	**Mol % Usp**	**Mol % Usp**	**Mol % Ilm**
Carmichael (1967)	23.78%	59.37%	38.75%	86.75%
Lindsley & Spencer (1982)	24.45%	6.32%	6.74%	90.56%
Stormer (1983)	16.26%	6.92%	6.72%	87.54%